Dissertation an der Fakultät für Biologie
der Ludwig-Maximilians-Universität München

The role of the protease Ddi2 in brown adipose tissue thermogenesis and ferroptosis

Anahita Ofoghi

München 2025

The role of the protease Ddi2 in brown adipose tissue thermogenesis and ferroptosis

Dissertation zur Erlangung des Akademischen Grades

Doktor der Naturwissenschaften

an der Fakultät für Biologie

der Ludwig-Maximilians-Universität München

vorgelegt von

Anahita Ofoghi

aus

Teheran, Iran

Jahr

2025

Diese Dissertation wurde angefertigt
Unter der Leitung Prof. Dr. Wolfgang Enard
an der Fakultät für Biologie der Ludwig-Maximilians-Universität München

Erstgutachter:	Prof. Dr. Wolfgang Enard
Zweitgutachter:	Prof. Dr. Alexander Bartelt
Tag der Abgabe:	23.04.2025
Tag der mündlichen Prüfung:	27.10.2025

Table of Contents

Abstract

Adipose tissue is mainly divided into two subgroups: white (WAT) and brown (BAT) adipose tissue. When WAT mass increases, it can lead to obesity and related metabolic diseases such as diabetes and atherosclerosis. On the other hand, BAT contributes to energy expenditure and heat production through the process of non-shivering thermogenesis (NST). An important aspect of brown adipocyte functionality involves maintaining proper homeostasis under high metabolic rates and thermogenic conditions. As a result of enhanced protein turnover, unfolded and misfolded proteins accumulate inside the cell, which requires an adaptive response from the proteasome to clean the cell and maintain proper proteostasis. An ER-membrane protein transcription factor nuclear factor erythroid-2,like-1 (Nfe2l1 or Nrf1) is a key regulator of proteasome activity in BAT.

In my thesis, I investigated the role of DNA-damage inducible 1 homolog 2 (Ddi2) in proteolytic cleavage of Nfe2l1 in context of brown adipose tissue thermogenesis and ferroptosis. Nfe2l1 posttranslational modification comprises of retrotranslocation from the ER lumen to the cytosolic face, deglycosylation of glycan residues by Ngly1, and proteolytic cleavage by Ddi2. Ddi2 is an aspartic protease that permits the translocation of Nfe2l1 to the nucleus and activation of proteasome subunit genes. I initially demonstrated that Ddi2 is induced by cold, abundant in BAT and vital for Nfe2l1 cleavage. Notably, the absence of Ddi2 perturbed proteasomal activity and the ubiquitin-proteasome system (UPS), culminating in the hyperubiquitylation of cellular proteins. To my surprise, this observation was dispensable for Nfe2l1-dependant regeneration of proteasome subunits, as cells successfully promote expression of *Psm* genes. Silencing *Ddi2* and the aberrant UPS functionality did not impede adipocyte processes such as adipocytes differentiation, lipogenesis, and mitochondrial function. Moreover, the phenotype of *Ddi2* knockout (KO) mice failed to manifest any alterations in energy balance and BAT activation. The results from the first stage of my project raised the question of whether BAT activates other compensatory mechanisms or if the uncleaved Nfe2l1 is sufficiently active on its own. Additionally, I investigated whether Ddi2/Nfe2l1 pathway protects from oxidative stress and production of reactive oxygen species (ROS). To this aim, I studied ferroptosis as a non-apoptotic oxidative form of cell death, which is mediated by iron-dependent lipid peroxidation. Lack of Ddi2 sensitizes cells to ferroptosis and causes UPS remodeling in these cells. Therefore, this study offers a promising framework for proteostatic regulation by Ddi2-proteasome pathway. Ddi2 is a novel player in regulating UPS and can be used as a promising target in therapy to improve anti-cancer drugs.

Zusammenfassung

Adipöses Gewebe wird hauptsächlich in zwei Untergruppen unterteilt: weißes (WAT) und braunes (BAT) adipöses Gewebe. Wenn die WAT-Masse zunimmt, kann dies zu Fettleibigkeit und damit verbundenen Stoffwechselerkrankungen wie Diabetes und Atherosklerose führen. Andererseits trägt BAT durch den Prozess der nicht zitternden Thermogenese (NST) zum Energieverbrauch und zur Wärmeproduktion bei. Ein wichtiger Aspekt der Funktionalität brauner Adipozyten besteht darin, unter hohen Stoffwechselraten und thermogenen Bedingungen eine ordnungsgemäße Homöostase aufrechtzuerhalten. Infolge eines erhöhten Proteinumsatzes in diesem Zustand, sammeln sich ungefaltete und fehlgefaltete Proteine in der Zelle an, was eine adaptive Reaktion des Proteasoms erfordert, um die Zelle zu reinigen und eine ordnungsgemäße Proteostase aufrechtzuerhalten. Ein ER-Membranprotein-Transkriptionsfaktor, der nukleare Faktor Erythroid-2-ähnlich-1 (Nfe2l1 oder Nrf1), ist ein wichtiger Regulator der Proteasom-Aktivität im BAT.

In meiner Dissertation habe ich die Rolle des DNA-Schadens-induzierbaren 1 Homolog 2 (Ddi2) bei der proteolytischen Spaltung von Nfe2l1 im Kontext der Thermogenese und Ferroptose im braunen Fettgewebe untersucht. Die posttranslationale Modifikation von Nfe2l1 umfasst die Retrotranslokation vom ER-Lumen zur zytosolischen Oberfläche, die Deglykosylierung des Glykanrests durch das Ngly1 und die proteolytische Spaltung durch Ddi2. Ddi2 ist eine Aspartat Protease, die die Translokation von Nfe2l1 in den Zellkern und die Aktivierung der Gene der Proteasom-Untereinheit ermöglicht. Ich konnte zunächst zeigen, dass die Ddi2 durch Kälte induziert wird, im BAT reichlich vorhanden ist und für die Spaltung von Nfe2l1 von entscheidender Bedeutung ist. Bemerkenswerterweise führte das Fehlen von Ddi2 zu einer Beeinträchtigung der Proteasom-Aktivität und des Ubiquitin-Proteasom-Systems (UPS), was zur Hyperubiquitinierung von zellulären Proteinen führte. Interessanterweise, war diese Beobachtung unabhängig von der Nfe2l1-abhängigen Regeneration der Proteasom-Untereinheiten, da die Zellen erfolgreich die Expression von Psms fördern konnten. Die Inaktivierung von Ddi2 im Adipöses und die abweichende UPS-Funktionalität beeinträchtigten Prozesse wie die Differenzierung von Adipozyten, die Lipogenese und die mitochondriale Funktion nicht. Darüber hinaus zeigte der Phänotyp von *Ddi2*-Knockout (KO)-Mäusen keine Veränderungen im Energiehaushalt und in der BAT-Aktivierung. Die Ergebnisse der ersten Phase meines Projekts warfen die Frage auf, ob BAT andere kompensatorische Mechanismen aktiviert oder ob ungespaltenes Nfe2l1 alleine ausreichend aktiv ist. Zusätzlich untersuchte ich, ob der Ddi2/Nfe2l1-Weg vor oxidativem Stress und der Produktion von reaktiven Sauerstoffspezies (ROS) schützt. Zu diesem Zweck habe ich die Ferroptose als eine nicht-apoptotische oxidative Form

des Zelltods untersucht, die durch eisenabhängige Lipidperoxidation vermittelt wird. Das Fehlen von Ddi2 sensibilisiert die Zellen für Ferroptose und verursacht eine Umgestaltung des UPS in diesen Zellen. Daher bietet diese Studie einen vielversprechenden Rahmen für die proteostatische Regulation durch den Ddi2-Proteasom-Weg. Ddi2 ist ein neuer Akteur bei der Regulierung des UPS und kann als vielverheißendes Zielmolekül in der Therapie zur Verbesserung von Krebsmedikamenten genutzt werden.

List of Figures

List of Tables

Abbreviations

a.u.	Arbitrary units
Adipoq	Adiponectin
AMC	7-Amino-4-Methylcoumarin
AMP	Adenosine monophosphate
ANOVA	Analysis of variance
APC	Adipose progenitor cell
ARE	Antioxidant response element
ATF3	Activating Transcription Factor 3
ATF6	Activating transcription factor 6
ATP	Adenosine triphosphate
BAT	Brown adipose tissue
BiP	Binding immunoglobulin protein
BSA	Bovine serum albumin
bZip	Basic leucine zipper
cAMP	cyclic adenosine monophosphate
CCS	Cosmic calf serum
CNC	Cap ’n’ Collar
CS	Calf serum
CT	Computed tomography
CVD	Cardiovascular diseases
Ddi2	DNA-damage inducible 1 homolog 2
Ddit3	DNA-damage inducible transcript 3
Dex	Dexamethasone
DiGly	Diglycine
DME	Drug-metabolizing enzyme
DMEM	Dulbecco Modified Eagle Medium
DMSO	Dimethyl Sulfoxide
DNA	Deoxyribonucleic acid
DUB	Deubiquitinating enzymes
e.g.	exempli gratia
ECAR	Extracellular acidification rate
ER	Endoplasmic reticulum ERAD
ERAD	ER-associated degradation
et al.	*et alii*
ETC	Electron transport chain

EtOH	Ethanol
$FADH_2$	Flavin adenine dinucleotide
Fabp4	Fatty acid binding protein 4
FBS	Fetal bovine serum
FCCP	*N*-[4-(Trifluoromethoxy)phenyl]carbonohydrazonoyldicyanide
FDG	Fluoro-deoxyglucose
Fer-1	Ferrostatin
FFA	Free fatty acid
FGF21	Fibroblast growth factor-21
Fig.	Figure
GLM	Generalized linear model
GLUT4	Glucose transporter type 4
GO	Gene ontology
GPX	GSH peroxidase
GSH	Glutathione
GST	Glutathione S-transferase
HDD	Helical domain
HEPES	2-[4-(2-Hydroxyethyl)piperazin-1-yl]ethane-1-sulfonic acid
HMOX1	Heme oxygenase-1
HSF1	Heat-Shock Transcription Factor 1
IBMX	3-Isobutyl-1-Methylxanthine
IMM	Inner mitochondrial membrane
Indo	Indomethacin
KD	Knock down
Keap1	Kelch-like ECH associating protein 1
KEGG	Kyoto encyclopedia of genes and genomes
KO	Knock out
MeOH	Methanol
MRI	Magnetic resonance imaging
MSC	Mesenchymal stromal cells
NaCl	Sodium chloride
NAD	Nicotinamide adenine dinucleotide
NADH	Nicotinamide adenine dinucleotide (NAD) + hydrogen (H)
NaOH	Sodium hydroxide
Nfe2l1 (Nrf1)	Nuclear factor erythroid 2-like 1
NFV	Nelfinavir

Ngly1	N-glycanase 1
NGM	Normal growth medium
Nqo1	NAD(P)H:quinoneoxidoreductase 1
NST	Non-shivering thermogenesis
NTD	N-terminal domain
O_2	Oxygen
OCR	Oxygen consumption rate
OXPHOS	Oxidative phosphorylation
p97	Valosin-containing protein (VCP)
PAGE	Polyacrylamid gel electrophoresis
PCA	Principle component analysis
PCR	Polymerase chain reaction
PET	Positron emission tomography
Pgc1α	Peroxisome proliferator receptor-γ, co-activator 1-α
PKA	Protein kinase A
PL-OH	Lipid alcohols
PL-OOH	Lipid peroxides
PMF	Proton motive force
PPAR	Peroxisome proliferator-activated receptor
Prdx	Peroxiredoxin
PTM	Post translational modifications
PS	Penicillin-Streptomycin
PSM	Proteasome subunit genes
RER	Respiratory exchange ratio
RNA	Ribonucleic acid
ROS	Reactive oxygen species
Rosi	Rosiglitazone
Rot/AA	Rotenone and Antimycin A
RT	Room temperature
RTA	Radical-trapping antioxidant
RT-qPCR	Reverse transcriptase qPCR
RVP	Retroviral protease-like domain
SDC	Sodium deoxycholate
SDH	Succinate dehydrogenase
SDS	Sodium dodecyl sulfate

SDS-PAGE	Sodium dodecyl sulfate polyacrylamide gel electrophoresis
SEM	Standard error of the mean
siRNA	Small interfering RNA
SNS	Sympathetic nervous system
SOD	Superoxide dismutase
ST	Shivering thermogenesis
SygRNA	Synthetic guide RNA
T2DM	Type 2 diabetes mellitus
T3	Triiodothyronine
TCA	Tricarboxylic acid cycle
TG	Triglycerides
TRIS	Tris(hydroxymethyl)aminomethane
UBL	Ubiquitin-like domain
UCP1	Uncoupling protein 1
UIM	Ubiquitin-interacting motif
UPR	Unfolded protein response
UPS	Ubiquitin-proteasome system
VCP	Valosin-containing protein
WT	Wild-type

1. Introduction

1.1 Obesity

Obesity is primarily defined as a body mass index ≥ 30 kg/m^2 (1), and is mainly characterized by accumulation dysfunctional adipose tissue (AT) (2). However, lipid distribution seems to underline the development of metabolic diseases in obese people, more than BMI and total fat mass (3). Obesity further contributes to the development of insulin resistance, activation of the sympathetic nervous system, endothelial dysfunction, and increased vascular resistance, all of which increase the risk of cardiovascular diseases (4). Moreover, obesity significantly increases the chance of developing hypertension, stroke, metabolic dysfunction-associated fatty liver disease (MAFLD), cancer, dementia, and obstructive sleep apnea (5-10). Obesity is mainly caused by the expansion of the adipose tissue, and is associated with dysregulated adipokine secretion, mitochondrial dysfunction, and glucose/lipid metabolism (11-13). Expansion of adipose tissue in obesity is also accompanied by inflammatory changes that is characterized by an increase in circulating cytokines, chemokines, tumor necrosis factor 1 alpha (TNF-α), interleukins, and interferons, or by the infiltration of new inflammatory cells such as macrophages (2). This impairment caused by genetic, environmental, and behavioral factors is mechanistically linked to various metabolic diseases (14). Therefore, the treatment of obesity through therapeutic interventions emphasizes the need for pharmacological strategies that promote energy balance and decreasing intracellular lipids accumulation (15).

1.2 Adipose tissue heterogeneity and function

Adipose tissue is a remarkably heterogeneous and active organ (16). Cellular subpopulations, heterogeneity, and homeostasis of different AT depots are related to the development of various diseases such as obesity, type 2 diabetes mellitus (T2DM), inflammation, and cardiovascular diseases (CVD) (2). Based on morphology, AT can be broadly classified into white adipose tissue (WAT), brown adipose tissue (BAT), and beige subsets (17). WAT can be found in various locations, which constitutes a new classification including: Subcutaneous (located under the skin), epicardial, perivascular, and visceral (or omental) fat depots (18). BAT was initially thought to be only present in small rodents such as mice, rats, and hamsters (19). While a significant amount of the tissue is present in newborns, the identification and roles of thermogenic BAT in human adults seem difficult. However, via simultaneous examinations with fluoro-deoxyglucose (FDG)-positron

emission tomography (PET) and X-ray computed tomography (CT), which detect symmetrical FDG uptake in the shoulder and thoracic spine regions, the existence of BAT in adults was identified (20) (Fig. 1).

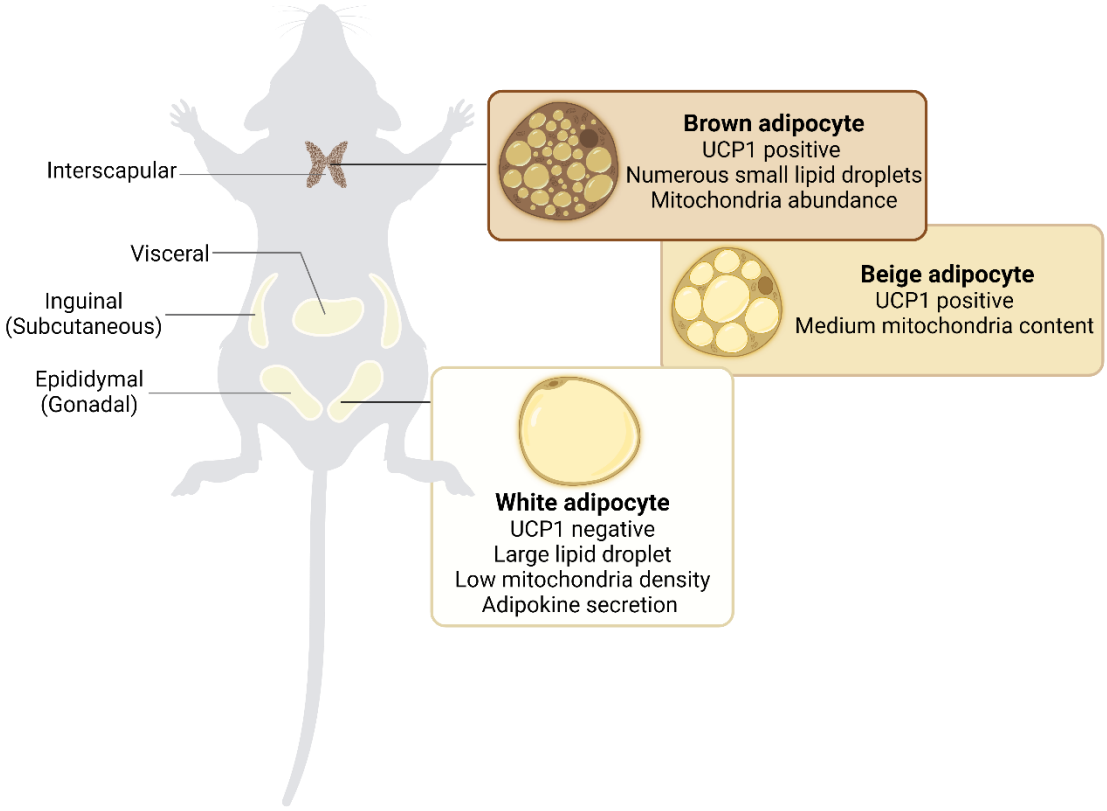

Figure 1: Major adipose tissue depots in mice. Brown and white (visceral and subcutaneous) adipose tissue depots in mice (left). "Browning" of adipocytes as a reversible transdifferentiation of the adipose tissue (right). Development of beige adipocytes in white adipose tissue to make brown adipocytes. Created with Biorender.com.

Endotherms, including humans, are generally well adapted to warm climates on earth by dissipating heat in various forms (e.g., high sweat rate and high surface to volume ratio) (21). However, they are required to evolve compensatory mechanisms to adapt to colder conditions (22). When exposed to cold, mammals rely on an increase in thermogenic rate to produce heat via activation of shivering (ST) or non-shivering (NST) thermogenesis processes. Cold-induced involuntary muscle contractions and activation of BAT play the main role in shivering and non-shivering thermogenesis, respectively (21). During NST, BAT produces heat via the dissipation of chemical energy from nutrients via a unique mitochondrial protein named uncoupling protein 1 (UCP1). UCP1 uncouples mitochondrial oxidative stress phosphorylation to dissipate the electrochemical gradient as a form of heat but not ATP synthesis. Therefore, β-adrenergic mediated activation of BAT has a beneficial metabolic effect on controlling whole-body energy balance, obesity,

insulin resistance, and atherosclerosis (23-27). Beige or brite adipocytes are the third type of fat cells, which are inducible and generated in WAT depots (28). During the process of “browning” and in response to stimuli such as cold acclimation, beige adipocytes express thermogenic marker UCP1 and exert adaptive thermogenic function (29) (Fig. 1). While only about one third of AT is comprised of adipocytes, other cell types such as fibroblasts, macrophages, endothelial cells, stromal cells, and immune cells can be found inside AT (15). AT is also known as an endocrine organ that secretes adipokines, growth factors, cytokines and chemokines within particular depots. Adipokines that are largely produced by adipocytes include leptin, adiponectin, resistin, omentin, and fibroblast growth factor 21 (FGF21) (30). AT naturally expands either by the volume of the pre-existing adipocytes (hypertrophy) or by generating new small adipocytes (hyperplasia) (Fig. 2).

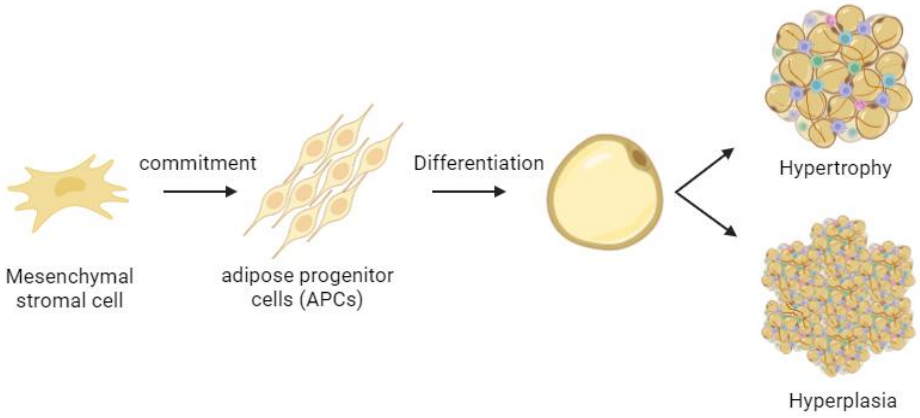

Figure 2: Hyperplasia and hypertrophy in adipose tissue. Pluripotent mesenchymal stromal cells (MSC) undergo commitment to differentiate into adipose progenitor cells (APCs). APCs then differentiate into mature adipocytes. Expansion of mature adipocytes occurs through increase in the volume of pre-existing adipocytes (Hypertrophy) or generation of new small adipocytes (hyperplasia). Created with Biorender.com.

Various molecular signaling pathways dictate the differentiation of mesenchymal stem cells to mature WAT, BAT, beige AT, or skeletal muscle cells (31). An *in vivo* study of brown adipocyte precursors by electron microscopy in interscapular BAT of adult mice identified four stages in the differentiation of interstitial stem cells to mature brown adipocytes: (1) interstitial cells, (2) protoadipocytes, (3) preadipocytes, and (4) mature brown adipocytes (32). Interstitial stem cells and protoadipocytes are mainly characterized by lack of lipid droplets and having a few tiny lipid droplets, respectively. Preadipocytes or adipoblasts contain many mitochondria, well-developed smooth endoplasmic reticulum, and lipid droplets. An abundance in mitochondria with very dense cristae and

lipid droplets in numerous small vacuoles (multilocularity) characterizes mature adipocytes (32). In contrast to BAT, white adipocytes contain few mitochondria and a unique lipid vacuole (unilocularity) in their relatively little cytoplasm (33).

1.2.1 β-Adrenergic signaling in adipose tissue

BAT is a highly vascularized thermogenic organ that consumes triglyceride-derived fatty acids and glucose to produce heat (34).The natural potent activator of BAT is cold which increases sympathetic outflow to β-adrenergic receptors (35) (Fig. 3). In case of high-energy demand, through the process of lipolysis, triacylglycerols (TAGs) break down into fatty acids (FAs) and glycerol inside lipid droplets. Therefore FAs either undergo oxidation in the form of ATP or function as fuel for activation of NST (36). BAT use these fatty acids, which leads to proton ions escalation in the mitochondrial intermembrane space required for subsequent UCP1 activity (37). Norepinephrine (NE) is a catecholamine that promotes lipolysis in adipocytes. In response to cold stimulation, NE is released from neuronal terminals that innervate adipocytes through β-adrenergic receptors (βARs) to increase intracellular levels of cyclic-AMP (cAMP) (38). Activation of thermogenesis, lipolysis and induction of hypertrophy in BAT requires an increase in cAMP levels (39). Although FAs are vital substrate for cellular energy, they can have a deleterious effect through a condition called lipotoxicity (40). The buildup of toxic lipid metabolites can lead to numerous disorders such as inflammation, insulin resistance, and apoptosis (41, 42).

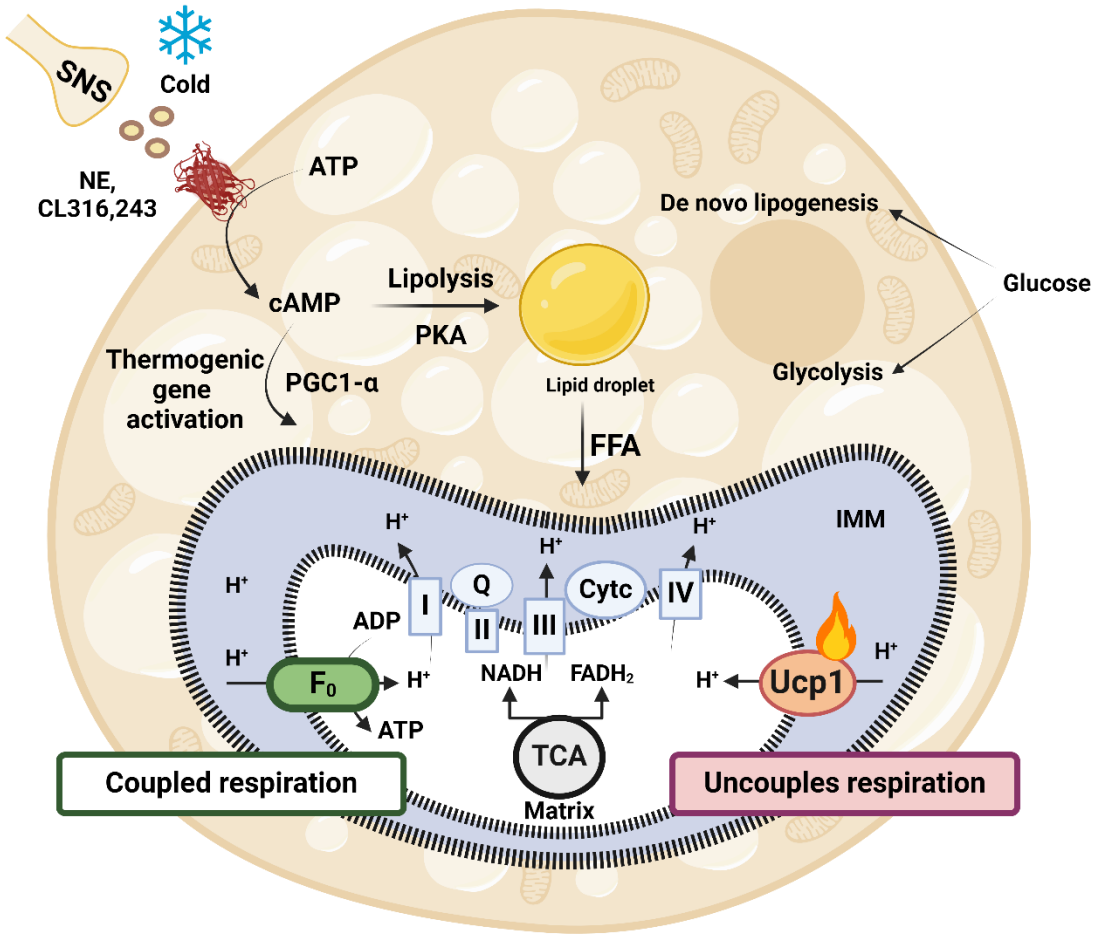

Figure 3: Brown adipose tissue activation. Stimulation of through β-adrenergic receptors (βARs) in brown adipocytes by sympathetic nervous system (SNS). SNS releases norepinephrine (NE) which bind to the receptors and induces increase in cAMP level, and activates protein kinase A (PKA). PKA increases lipolysis to hydrolysis triacylglycerides to free fatty acids (FFA). FFA enters mitochondria and will be used in the electron transport chain (ETC) consisting of I, II, III, IV, ETC multi-subunit complexes I through IV; Q, coenzyme Q; Cyt c, cytochrome c. In mitochondria, proton motive force (PMF) created by the ETC system is used to produce ATP through processed called "Coupled respiration" (left). Cells increase generation of NADH and $FADH_2$ by oxidation of substrate in the tricarboxylic acid cycle (TCA) to re-establish the electrochemical proton gradient across the inner mitochondrial membrane (IMM). In brown adipocytes, the protons bound to UCP1 (right). This UCP1-mediated proton leak results in heat production, but not ATP synthesize. This processed called "uncoupled respiration". Created with Biorender.com.

The thermogenesis specialty of BAT is due to the high number of mitochondria and the presence of a unique protein, UCP1, located in the inner mitochondrial membrane (IMM) lipid bilayer (Fig. 3). Ucp1 uncouples the electron transport chain (ETC) from ATP synthesis, which allows the generation of energy in the form of heat from the oxidation of substrates (43, 44). In mammals, the oxidation pathways of substrates (like glucose, FAs, and amino acids) converge on the TCA cycle, which generates reduced electron carriers including NADH and $FADH_2$ in the mitochondria. These electron carriers then

donate their electrons to the four multi-subunit complexes (I-IV) of the ETC located in the inner mitochondrial membrane (IMM) along with two mobile electron carriers: coenzyme Q and cytochrome c (45). Followed by the transferring of electrons through the ETC, the pumping of protons into the intermembrane space creates an electrochemical proton gradient called the proton motive force (PMF). These protons translocate into the mitochondrial matrix through the F0 component which leads to biosynthesis of ATP from ADP and inorganic phosphate (46). Therefore, the rate of substrate oxidation is dependent on the availability of ADP. If there are any fluctuations in the coupling between ATP production and electron flow through ETC results in production of reactive oxygen species (ROS) (47). In an alternative pathway, called uncoupled respiration, the main outcome is heat, but not ATP production. In this process, protons pass from intermembrane space into the matrix through the membrane-bound UCP1, which causes a drop in PMF and heat production. Therefore, dissipation of PMF by UCP1 reduces mitochondrial ROS production, and provides a remarkable capacity for the oxidation of substrates in BAT mitochondria (48). Various elements including the sympathetic nervous system, hormones such as catecholamines and thyroid hormone, and environmental cues like cold exposure tightly regulate the thermogenesis of BAT mitochondria (49, 50).

1.2.2 Adipose tissue and protein quality control

AT plays a vital role in maintaining metabolic homeostasis under normal conditions (51). The endoplasmic reticulum (ER) plays the key role in protein and lipid metabolism, secretory and membrane protein synthesis and folding, calcium homeostasis, etc. (52). Perturbation in any of these processes will cause impairment in ER homeostasis (53). Any condition that blocks ER function may result in ER stress which is triggered by the uncontrollable accumulation of unfolded or misfolded proteins inside, or outside, the ER (e.g. in the nucleus or cytosol) (54). The ER's failure to cope with the excess protein load or the challenges of proteostasis will cause a wide range of consequences such as inhibition of synaptic function, alteration of calcium homeostasis, insulin resistance, and inflammation (55). Activation of several mechanisms such as unfolded protein response (UPR), ER-associated degradation (ERAD), and autophagy helps to maintain protein quality control in cells (55). UPR is responsible for restoring ER homeostasis (adaptive UPR) or promoting cell death (maladaptive/unchecked UPR) (56, 57). The inhibition of protein translation and enhancement of the folding capacity of the ER is one crucial step in UPR activation (55). Another major pathway in UPR processes is the attachment of unfolded proteins to the ER chaperone BiP (also known as GRP78). Because of this binding, BiP releases from three UPR sensors anchored in the ER membrane: protein

kinase R-like ER kinase (PERK, encoded by EIF2AK3), inositol-requiring enzyme 1-alpha (IRE1α, a serine/threonine protein kinase/endoribonuclease encoded by ERN1), and activating transcription factor-6 (ATF6) (58). Consequently, an orchestrated downstream signaling cascade modulates the transcription of genes involved in promoting protein folding via UPR (59). Mitochondrial unfolded protein response (UPR^{mt}) refers to the accumulation of misfolded proteins within the mitochondria and impaired OXPHOS capacity. Therefore, UPR^{mt} has beneficial effect on maintaining mitochondrial proteostasis via the expression of genes such as proteases, chaperones, and mitokines (60). While coordinated activation of mitochondrial function is required for lipid breakdown and oxidative phosphorylation (OXPHOS), any malfunction in mitochondrial oxidative capacity that occurs in metabolic disorders results in the accumulation of lipids in AT, skeletal muscle and liver (61). There are multiple layers of mitochondrial protein quality control to improve overall metabolism and energy homeostasis, namely: UPR^{mt}, antioxidants, mitochondrial fusion and fission followed by non-functional mitochondria degradation or mitophagy (62).

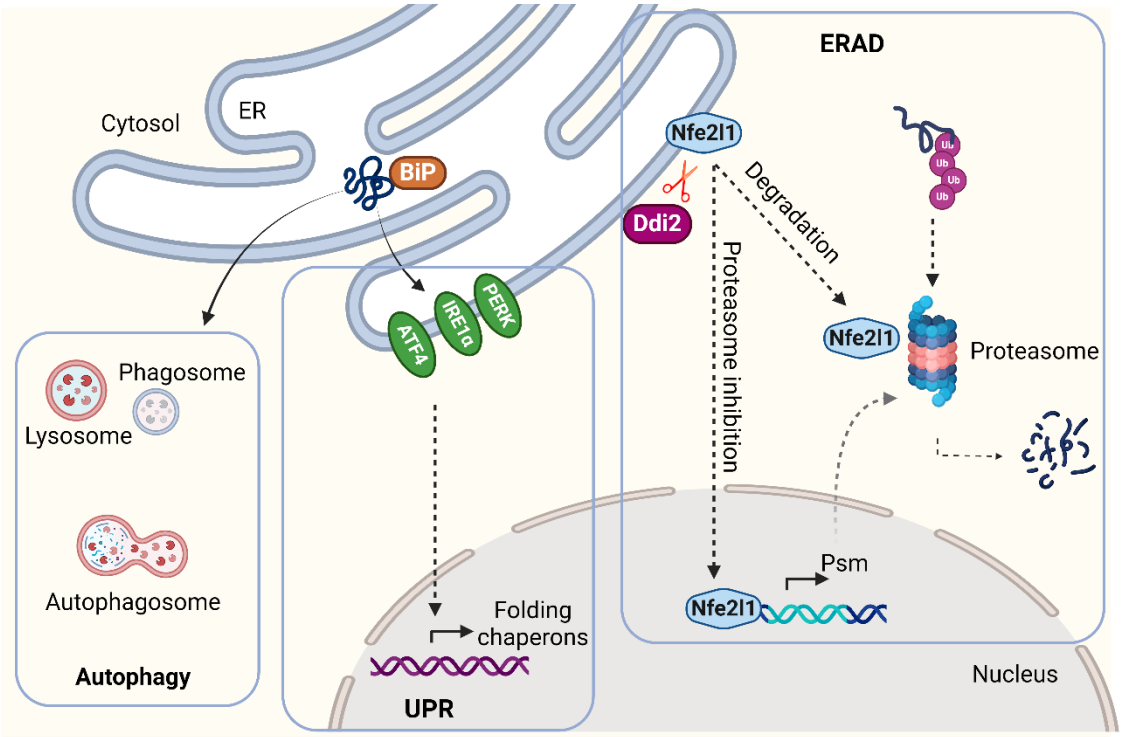

Figure 4: Major protein quality control pathways. The UPR is one of the responsible cellular mechanisms for maintaining proper proteostasis. Unfolded proteins bind to chaperon proteins and UPR sensors in ERAD, misfolded proteins undergo ubiquitination degradation via proteasome. Upon proteasome inhibition and proteostatic stress, transcription factor NFE2L1 escapes degradation and get cleaves by protease Ddi2 and translocate to the nucleus to promote transcription of proteasome subunits. In autophagy, redundant intracellular parts and organelles are degraded inside the autolysosomes. Created with Biorender.com.

Unlike UPR, which relies on “repairing”, activation of an alternative process termed ERAD leads to degradation of these accumulated proteins to avoid ER stress. When UPR fails, activation of ERAD eliminates proteins through the ubiquitin proteasome system (UPS). The intimate and dynamic coordination of UPR and ERAD is crucial for the disposal of misfolded proteins and simultaneous loss of both pathways leads to decreased cell survival to during acute stress (63). In ERAD, misfolded proteins are shuttled from the ER lumen to the cytosol and undergo ubiquitination and degradation by the proteasome. An ER-anchored transcription factor called Nfe2l1 plays a crucial role in securing an adaptive increase in proteasomal activity by increasing the expression of proteasome subunits (64). Moreover, the role of Nfe2l1 in the activation of the canonical mitochondrial UPR pathway through alterations in the in expression of UPR^{mt}-associated genes such as ATF4 and 5, CHOP, and their target genes GRP75 (or HSPA9) and FGF21 has been reported (65). Lastly, during autophagy, double membrane structures engulf cytoplasmic cellular parts and then fuse to lysosomes to form autophagosomes in which digestion occurs (55).

1.2.3 Adipose tissue and antioxidant defense

ROS are highly reactive compounds that play a role in signaling and cell homeostasis by regulating cell proliferation, differentiation, and survival (66). Although ROS are by-product of a normal metabolism, they play a role as a casual factor in a number of diseases such as inflammation, aging, atherosclerosis, carcinogenesis, etc. (67). The imbalance between reactive oxygen or nitrogen species (ROS and RNS) levels and the antioxidant defense system is termed as oxidative stress (68). During oxidative stress, increase in ROS production leads to several events such as oxidation of proteins, inhibition of enzymes, DNA damage, and lipid peroxidation, which collectively can activate programmed cell death (69). Therefore, it is vital to eliminate the toxicity of ROS by enzymatic reactions involved in antioxidant defense. Various levels of antioxidant defense in mammalian cells protect biological macromolecules from oxidative stress, including: molecules (e.g., glutathione (GSH), ascorbic acid) and enzymes (e.g., catalase, GSH peroxidase (GPX), superoxide dismutase (SOD)) (68).

As a high metabolically active tissue, mitochondrial and cytoplasmic processes such as lipolysis leads to generation of ROS and RNS in AT (70). However, in intense metabolic conditions, such as obesity and human diabetes, the antioxidant defense is incapable to re-establish the redox homeostasis (71). Acute β-adrenergic-stimulated activation of BAT thermogenesis is paralleled by enhanced levels of mitochondrial superoxide, hydrogen peroxide, and lipid hydroperoxide in the tissue (72). Activation of the Nfe2l2-an-

tioxidant response element signaling is considered a major mechanism of cellular defense against ROS (73). Activation of Nfe2l2 reduces lipolysis in AT, and knockdown of this gene reduces H_2O_2-induced lipid accumulation (74). It has been shown that another member of the Nfe family, Nfe2l1, also binds to the promoter regions through the antioxidant response elements (ARE) and regulates the expression of genes involved in ROS, inflammation, and cell differentiation (17). To protect cells against ROS, Nfe2l1 regulate genes encoding enzymes related to glutathione (GSH) biosynthesis, as a major antioxidant in the cell (75). Moreover, expression regulation of some other antioxidant genes including NAD(P)H dehydrogenase, ferritin-H, quinone 1 (NQO1), metallothionein (MT)-1 and -2 in fibroblasts and hepatocyte is mediated by Nfe2l1 (76-79).

1.3 Nuclear factor erythroid 2 like (Nfe2l) gene family

The transcription factor nuclear factor erythroid-2, like-1 (Nfe2l1, also referred to as TCF11 or Nrf1) is the main regulator of maintaining proper proteostasis and cellular integrity by upregulating the expression of genes encoding proteasome subunits (64). Nfe2l1 belongs to the CNC (Cap 'n' Collar) family of basic leucine zipper proteins with structurally related proteins that mediate transcriptional regulation via ARE (80, 81). Members of the CNC-bZIP family including Nfe2l1, Nfe2l2, Nfe2l3, p45NFE2, Bach1, and Bach2 (82-85) (Fig. 5). Loss of function in Nfe2l2 plays a vital role in susceptibility to oxidative stress-induced damage in knockout mice (86). It is well established that Nfe2l2 function is regulated through interaction with the actin binding protein Kelch-like ECH associating protein 1 (Keap1) and is subject to rapid degradation in the cytoplasm of cells. Upon receiving signals such as reactive oxygen species (ROS), Nfe2l2 dissociates from Keap1, translocate to the nucleus, and transactivates its target genes (87). A set of drug-metabolizing enzymes (DMEs) such as NAD(P)H:quinoneoxidoreductase 1 (NQO1) and glutathione S-transferase (GST), heme oxygenase-1 (HMOX1), and peroxiredoxin 6 (Prdx6) are among these protective antioxidant genes (88-90).

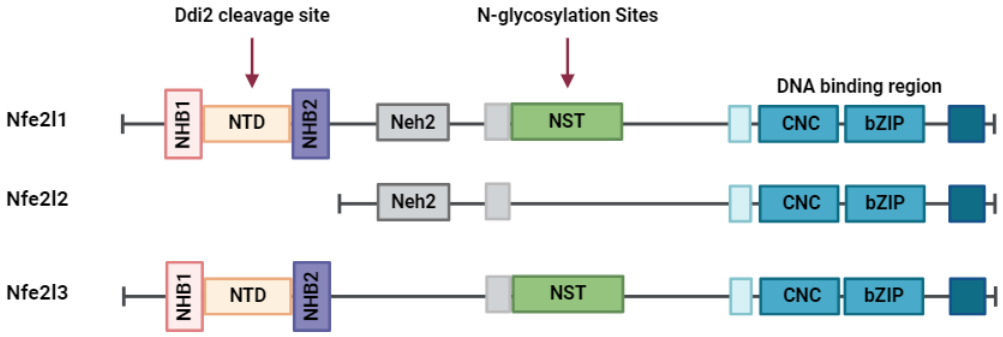

Figure 5: Major members of the CNC-bZIP transcription factor family. The schematic of the structural domains of Nfe2l1, Nfe2l2, and Nfe2l3 transcription factors. The NHB1 peptide within Nfe2l1 and Nfe2l3 N-terminal domain (NTD) is a signal that enables these proteins to anchor within the endoplasmic reticulum (ER) membrane. Both CNC and bZIP regions enable heterodimerization with a small Maf protein and other bZIP proteins prior to binding to antioxidant response element (ARE) in promoter regions of target gene sequence. NST (Asn/Ser/Thr-rich) is a potential N-glycosylation sites. Neh2 domain within Nfe2l2 sequence is a functional domain near N terminus that interacts with Keap1. Both Nfe2l1 and Nfe2l3 have Ddi2 cleavage proteolytic site in their structure. Created with Biorender.com.

Nfe2l1 shares structural similarities with Nfe2l2 and is indispensable for viability during mouse embryonic development (91) (Fig. 5). Simultaneous loss of Nfe2l1 and Nfe2l2 leads to early embryonic lethality (92). Nfe2l1 is essential for cell survival of fibroblasts in mice in response to oxidative stress. Lower levels of glutathione has been detected in

Nfe2l1 null embryos, leading to enhanced sensitivity to the toxicity of oxidative compounds. Indeed, Nfe2l1 activates expression of glutamyl-cysteine ligase genes (*Gclc* and *Gclm*) via AREs in their promoter region (76, 78). While both Nfe2l1 and Nfe2l2 contain CNC and bZIP domain, Nfe2l1 also contains a functional Neh2 domain near N terminus that interacts with Keap1 (93). The N terminus region mediates the cytoplasmic localization of the protein. While Nfe2l1 is anchored in the endoplasmic reticulum membrane, deletion of this N-terminal hydrophobic transmembrane domain leads to nuclear accumulation of the protein (94). Under normal conditions, Nfe2l1 activity is suppressed by ER-associated degradation (ERAD) and its components ubiquitin ligase Hrd1 and β-TrCP complexes (95). When proteostasis is challenged, accumulation of ubiquitinated proteins exceeds the capacity of available proteasomes. To this end, Nfe2l1 undergoes several post-translational modification steps to play a crucial role to prevent ER stress, cellular dysfunction and proteotoxicity (96). Nfe2l1 is retrotranslocated to the cytosol face of ER by the p97/VCP ATPase complex, accompanied by deglycosylation by N-glycanase 1 (NGLY1, also known as PNGase) (97) and proteolytic cleavage by the protease DNA damage-inducible 1 homolog 2 (DDI2) (98). This process forms the cleaved active form of Nfe2l1 with a molecular weight of 95 kDa, from full-length inactive 120 kDa, which then translocate to the nucleus and promotes proteasome gene expression by binding to antioxidant response elements in the promoter regions (64) (Fig. 6).

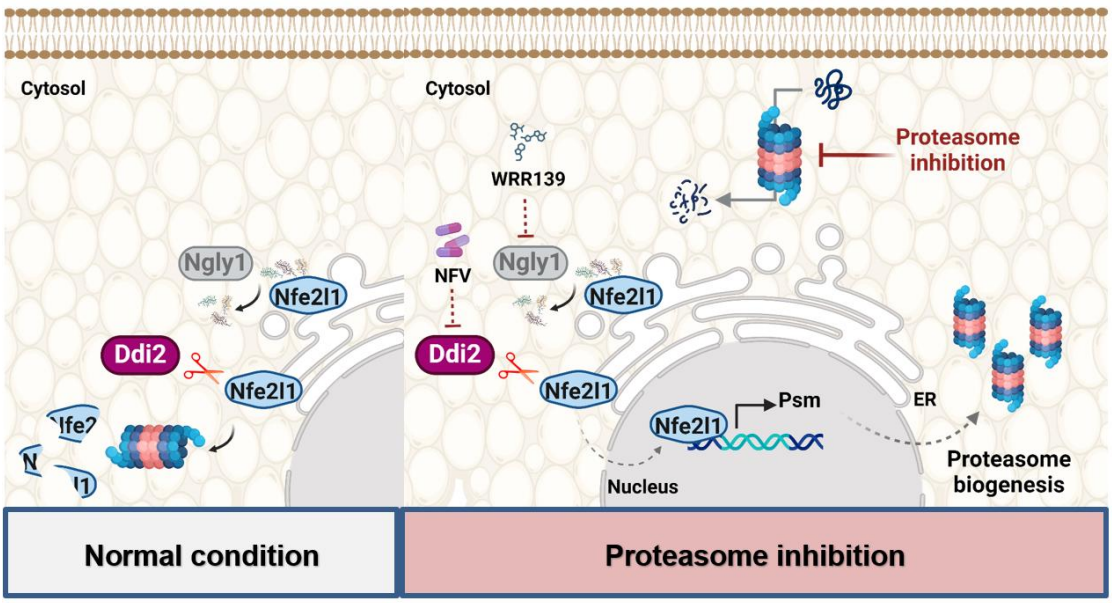

Figure 6: Activation of Nfe2l1 and "bounce-back" response. Endoplasmic reticulum (ER)-resident nuclear factor erythroid-derived 2-related factor 1 (Nfe2l1/Nrf1) undergoes constant degradation via ER-associated degradation (ERAD) machinery under basal conditions in cell. Upon proteasome inhibition, Nfe2l1 skips the degradation and translocate to the cytosol face of ER. After post-translational modification by Ngly1 and Ddi2, active form of Nfe2l1 enters the nucleus and promotes the expression of proteasome subunits genes (*Psm*). WRR139 and Nelfinavir (NFV) are chemical compounds targeting and inhibiting Ngly1 and Ddi2 activities, respectively. Created with Biorender.com.

The nuclear factor (erythroid 2)-like (Nrf3) or Nfe2l3, is the sixth member of NRF family (99). Tissue localization of Nfe2l3 is mostly in placental tissue, which differs from ubiquitous expression pattern of Nfe2l1 and Nfe2l2 (84, 100). The under-studied physiological function of Nfe2l3 is due to the absence of abnormalities in Nfe2l3-deficient mice under physiological conditions (101, 102). However, recent research has attracted more attention to the intriguing function of Nfe2l3 in cancer malignancy (103, 104). Although the activation of Nfe2l3 involves similar processing steps as those of Nfe2l1, involving deglycosylation by the enzyme Ngly1 and proteolytic cleavage by Ddi2, it does not affect expression of proteasome subunit genes (105). Upon activation, Nfe2l3 translocate to the nucleus and increases gene expression of POMP and CPEB3, thereby stimulating 20S proteasome assembly (106). However, studies focused on the complementary crosstalk between Nfe2l1 and Nfe2l3 in colon cancer cells suggest that Nfe2l3 suppresses translation of Nfe2l1 in HCT116 cells to maintain basal proteasome activity (107).

1.4 Ngly1/Ddi2-mediated PTM of Nfe2l1

N-glycanase 1 (PNGase Caenorhabditis elegans yeast orthologue, NGLY1 in humans, Ngly1 in mice) is the enzyme responsible for maturation of proteins in cytosol by removing N-glycans from intact glycoproteins (97, 108-110). A correlated activity of Ngly1 and Ddi2 is required for proper processing of Nfe2l1 in case of proteasome inhibitors toxicity in cells (111). N-glycosylation of Nfe2l1 occurs within the Asn/Ser/Thr-rich (NST) glycodomain in protein architecture, which includes eight potential N-glycosylation sites (Fig. 5). Transcriptional activation of Nfe2l1 happens through conversion of asparagine (Asn) to aspartic acid (Asp) residues to create a functional transactivating domain in Nfe2l1 structure (97, 112). While *Ngly1*$^{-/-}$ mice with a C57BL/6 background are embryonically lethal, its deficiency can lead to disorders related to endoplasmic reticulum associated degradation pathways such as neurological dysfunction, movement disorder, seizures, liver disease, etc. (113).

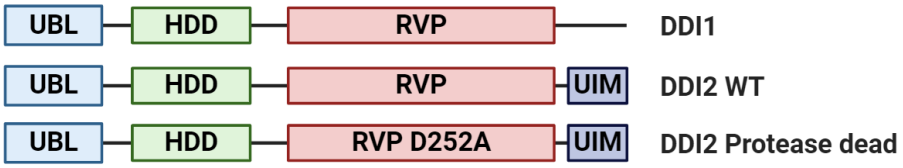

Figure 7: Domain organization of, DDI1, wild type DDI2, and protease dead (D252) mutant DDI2. UBL: ubiquitin-like domain; HDD; helical domain; UIM: ubiquitin-interacting motif; RVP: retroviral protease-like domain. Created with Biorender.com.

Ddi2 is the aspartic protease responsible for cleavage and subsequent activation of Nfe2l1 into the full-length cytosolic form (98, 114). Moreover, proteolytic activity of Ddi2 is required for cleavage-dependent activation of other proteins in the cells such as nuclear translocation of Nfe2l1 (99), the scaffolding protein angiomotin (AMOT) related to vertebrate embryonic angiogenesis (115). Another role of Ddi2, together with Ddi1, is acting as proteasomal shuttle proteins, which is necessary for the maintenance of genomic stability in response to DNA replication stress. In this process, DDI2 is responsible for removal of Replication Termination Factor 2 (RTF2), a key component in mammalian replisome, from stalled fork which otherwise will lead to incomplete replication, sensitivity to replication drugs, and chromosome instability (116). DDI2 is a highly conserved aspartic protease in eukaryotes containing a HIV retroviral protease-like (RVP) domain (Fig. 7). Two genes encoding Ddi1-like proteins in human genome: 396-amino-acid DDI2 homolog 1 (hDDI1), which seems to be descendant of yDdi1 (yeast Ddi1), and the 399-amino-acid Ddi2 homolog 2 (hDDI2) (117). Ddi2 contains a ubiquitin-like domain (UBL) at the N-terminal and RVP domain near C-terminal in its structure (117). In 2014, Radhakrishnan et al. showed that cleavage of Nfe2l1 occurs between Trp103 and Leu104

that is exactly the cleavage motif of retroviral aspartyl proteases (118). Silencing *Ddi2* with siRNA decreases the full-length form of Nfe2l1. Ddi2, lacking the UBL domain partially restores the effect of *Ddi2* knockdown. However, replacing aspartic acid 252 in the active site of protein with asparagine (D252N) to make protease-dead Ddi2 (mutant form of protein) that lacks UBL domain, did not exhibit the same effect (98). Disruption in NFE2L1/DDI2 pathways diminish proteasome activity in serious disorders such as in Multiple myeloma (MM) (119) colorectal cancer (CRC) tumorigenesis (120), neurodegenerative disorders, and muscle dysfunction (121). Furthermore, DDI2 is also considered as a target of miR-3607 to inhibit tumorigenesis of colorectal cancer (CRC) (120).

1.5 Nfe2l1 and proteotoxic stress

The UPS machinery controls protein turnover via degrading ERAD substrate that translocate to the cytosol. Coordinated activity of several components of UPS including ubiquitin, 26S proteasome, ubiquitinating and deubiquitinating enzymes (DUB) are required for maintaining proper cellular proteostasis which otherwise will lead to various diseases (122).

1.5.1 Ubiquitin biology

Ubiquitination was introduced as a complex PTM of proteins in 1980, which plays an important role in DNA damage, protein localization, cell cycle regulation, apoptosis, autophagy, cancer, neurodegenerative diseases, and many more pathways. Ubiquitination is a cascade of enzymatic reactions that link ubiquitin molecules to target proteins. Ubiquitin (Ub) is a highly conserved small protein with 76 amino acids in all eukaryotic cells, which can bind to lysine (Lys) residue of protein targets. Based on lysine residues in the ubiquitin molecule, ubiquitin chain can be divided to different isoform including K6, K11, K27, K29, K33, K48, and K63. Different ubiquitin chains can be formed linking ubiquitin moieties through one of lysine residues or the N-terminal methionine residue (M1). Different ubiquitin chains play different functions in cell such as degradation by proteasome (Lys48 and Lys11) and various signaling pathways such as DNA replication, endocytic trafficking, and autophagy-lysosome pathway (Lys63) (122-124). Maintaining a stable state of intracellular ubiquitin requires dynamic production and degradation of ubiquitin molecules. Basal level of ubiquitin is mediated by proper synthesis of ubiquitin by genes including UbC, UbB, UbA52, and UbA80. On the other hand, DUBs maintain the ubiquitin homeostasis by releasing ubiquitin units from ubiquitinated proteins in cells, which is then degraded by lysosomes or proteasomes to recover ubiquitin level (125) (Fig. 8). It has been shown that Nfe2l1 along with other transcription factors such as Nfe2l2, SP1, and

Heat-Shock Transcription Factor 1 (HSF1) regulate transcription of UbC for encoding polyubiquitin under cell stress conditions (126-128).

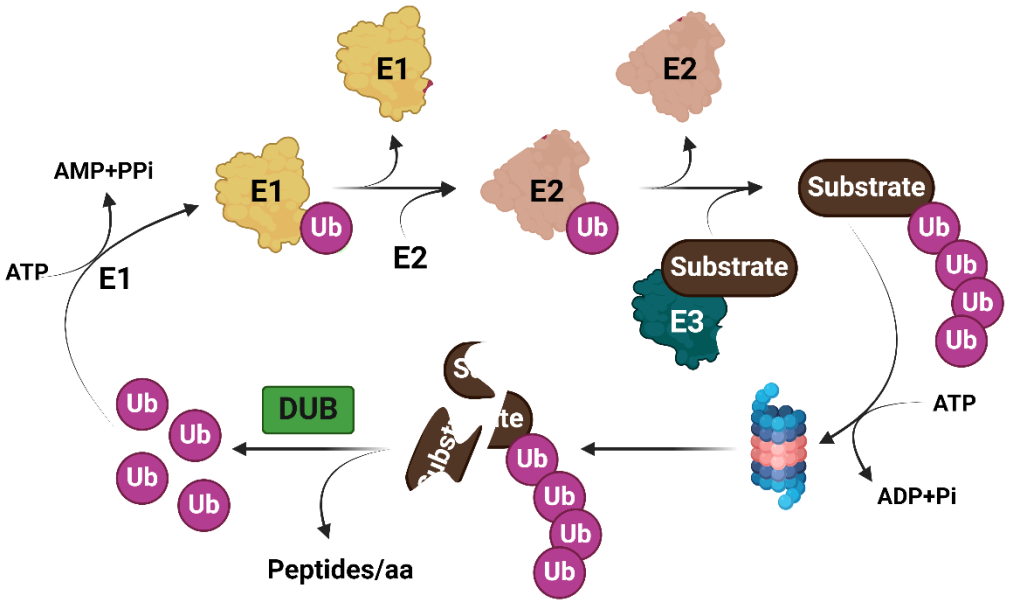

Figure 8: Ubiquitination of proteins. Three enzymes are involved in addition of ubiquitin chains to lysine residues of proteins targeted for degradation. In the first step, ubiquitin is activated by E1 (ubiquitin-activating) enzyme and then transferred to E2 (ubiquitin carrier protein) enzyme. In the last step, E3 ligases mediate the covalent attachment of ubiquitin to the target substrate. Substrates tagged with one (monoubiquitinated) or several (polyubiquitinated chain) ubiquitins are delivered to proteasome for degradation. Deubiquitinating enzymes (DUB) removes ubiquitin from protein targets and release free ubiquitin for recycling. Created with Biorender.com.

1.5.2 Mechanisms of UPS

Eukaryotic cells have developed ubiquitin-26S proteasome as a defense mechanism to recognize and control the accumulation of unfolded or misfolded proteins' toxicity. Attachment of ubiquitin chains plays a selective label role in targeting proteins to the 26S proteasome for degradation. This binding is modulated by three types of ubiquitinases in the cell: E1 ubiquitin-activating enzymes, E2 ubiquitin-conjugating enzymes and E3 ubiquitin–ligase enzymes (31, 32) (Fig. 8). In a simplified model, the E1 enzyme generates a thioester bond between the C-terminal of ubiquitin and a Cys residue in its catalytic active site by hydrolyzing ATP. When ubiquitin is activated, it forms a thioester bond with an E2 enzyme. Next, the charged E2 enzyme transfers the activated ubiquitin to the target proteins through the activity of ubiquitin ligase or E3 (122). Recruited E3 ligases further mediate the degradation of ubiquitin-labeled proteins through 26S proteasome function. The proteasome contains multimeric assemblies: the 'barrel-shaped' 28-subunit core particle (CP, also called 20S) and the regulatory particles 19S particle (also known as RP or PA700). The 19S regulates the delivery of substrates to the 20S particle

in an ATP-dependent manner. 26S or 30S proteasome structures are made by association of 20S with one or two 19S particles, respectively (129) (Fig. 9).

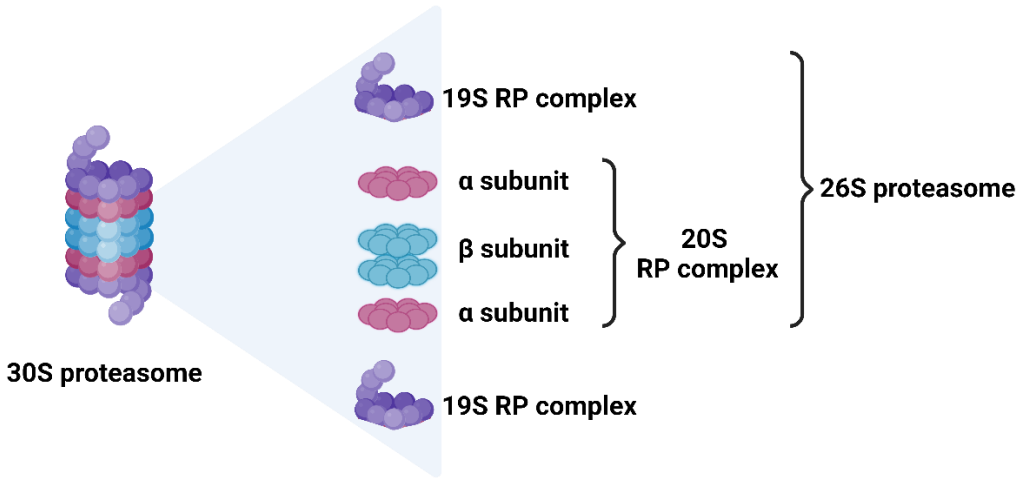

Figure 9: Schematic representation of proteasome complexity. Proteasome exists in various forms within the cell. 20S consists of four rings (2 external α subunits and 2 internal β subunits) in a stack. The 19S regulatory particle caps the core 20S complex to produce 26s proteasome core complex (2) with proteolytic activity. 30S proteasome containing 20S particle plus two 19S regulatory particle complexes. Created with Biorender.com.

The initial reversible binding between proteins and 26S proteasome complex is independent of ATP hydrolysis and can be disrupted by other Ub binding domains or high salt concentrations. In contrast, degradation of protein requires an ATP-dependent tight-binding step (130). 20S proteasome has a cylindrical structure that consists of four stacked rings. Outer rings in this structure contain seven α subunits while the two inner β rings contain seven different β subunits, which three of them harbor active sites. Based on their specificity toward peptide substrates these actives sites are classified to: Trypsin-like, chymotrypsin-like, and caspase like sites (131). Targeting multiple subunits of the proteasome can be used for treating several related disorders such as anti-cancer drugs. Bortezomib (BTZ, velcade), Carfilzomib (CFZ, kyprolis), Ixazomib (IXZ, ninlaro), and epoxomicin are among commercially available proteasome inhibitors (132, 133). The reversible binding of these chemical compounds to β5 subunits of 19S RP inhibits the chymotrypsin-like enzymatic activity and therefore lead to accumulation of ubiquitinated proteins and apoptosis cell death (133-135). Cells require an adaptive mechanism to increase proteasome abundance under either chemical-inhibition of proteasome or physiological demands. Higher eukaryotes activate the transcription factor Nfe2l1 in a complex feedback loop, which then stimulates production of new 26S proteasomes (136).

1.6 Nfe2l1 and ferroptosis

Regulated cell death is initiated by intracellular and extracellular perturbations that trigger tightly orchestrated molecular programs (137, 138). Ferroptosis is a form of non-apoptotic cell death mediated by iron-dependent lipid peroxidation and loss of plasma membrane integrity (139, 140). Recent studies have implicated ferroptosis in several pathologies, such as neurodegeneration and cancer (141). Execution of ferroptosis is tightly linked to lipid and glutathione metabolism. Intracellular iron, which is abundantly available in two forms of reduced ferrous (Fe^{2+}) and oxidized ferric (Fe^{3+}), can lead to generation of phospholipid peroxides. Fe^{2+} forms the labile iron pool (LIP) through a Fenton reaction can generate reactive oxygen species (Fig. 10). The produced ROS then initiates autoxidation of phospholipids in membrane (142). The glutathione redox system is also essential to prevent ferroptosis. Glutamate-cysteine ligases are responsible for catalyzing intracellular GSH synthesis. In this model, cysteine is taken up cysteine through the cystine/glutamate antiporter (xCT) system which can be inhibited by erastin to induce ferroptosis (143). Glutathione peroxidase 4 (GPX4) is a critical enzyme protecting from lipid reactive oxygen species (ROS) formation and, thus, from ferroptosis by most prominently uses glutathione for its antioxidative activity (144). GSH depletion triggers ferroptosis similar to other type of cell death such as apoptosis, necrosis, and autophagy (145). GPX4, dependent or independent of GSH depletion, can be inactivated through genetic interventions or pharmacological ferroptosis-inducing compounds (FINs) (e.g., RSL3, FIN56, ML162, ML210 or FINO2) (146). While depletion of the reduced glutathione pool predisposes cells to ferroptosis, the compound RAS synthetic lethal 3 (RSL3) directly inhibits GPX4 (147-149). GPX4 catalyzes the reduction of phospholipid hydroperoxides (PLOOH) into corresponding phospholipid alcohols (150). Therefore, inactivation of GPX4 leads to the accumulation of PLOOH, and inducing cell membrane damage and death (151). Thus, oxidative stress is sensed and mitigated by GPX4 and its inactivation leads to lipid peroxidation and cell death in cells and mouse models (152). High-throughput screenings identified two potent ferroptosis inhibitor ferrostatin-1 (Fer-1) and liproxstatin-1 (Lip-1). Fer-1 was one of the first synthetic radical-trapping antioxidants (RTAs) to block ferroptosis by preventing accumulation of lipid hydroperoxide in HT-1080 cells (142).

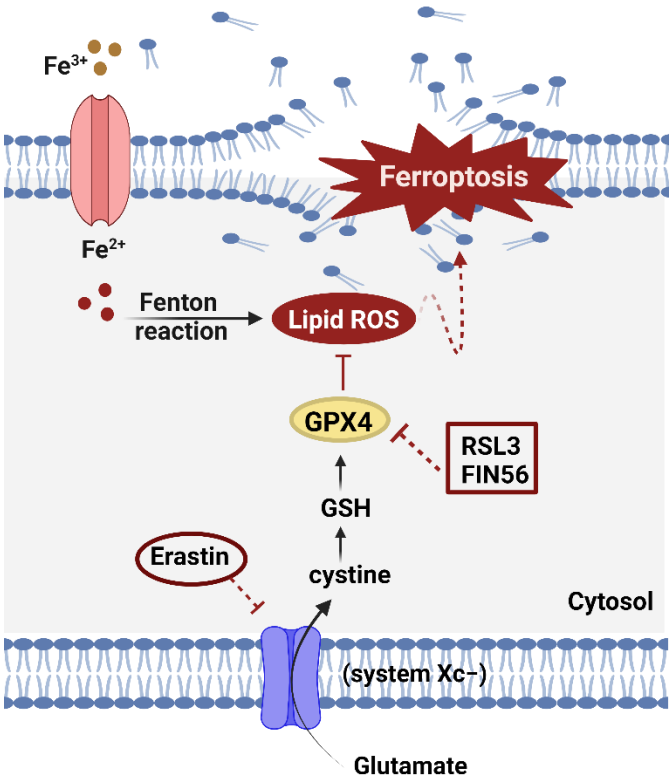

Figure 10: the mechanism of ferroptosis pathway. Fe^{3+} transports into the cell and Fe^{2+} promotes accumulation of lipid peroxides through Fenton reaction and lipid oxidation. Cystine is used to synthesize glutathione (GSH) inside the cell. GPX4 uses glutathione as a reduction cofactor to reduce toxic lipid peroxides (PL-OOH) to non-toxic lipid alcohols (PL-OH). Created with Biorender.com.

Nfe2l1, independent of Nfe2l2, maintains the expression of GPX4 as the key protein against lipid peroxidation (153). Ngly1-mediated activation of Nfe2l1 decreases ferroptosis sensitivity (153). Expression of ROS scavengers such as peroxiredoxins (PRDX) and superoxide dismutase (SOD) which contribute to decreased lipid peroxidation and ferroptosis is dependent on Nfe2l1. STAT3 signaling, which negatively regulates ferroptosis in multiple diseases like ulcerative colitis, pancreatic and gastric cancer, induces Nfe2l1 activation and GPX4 expression (17). Interestingly, ferroptosis is linked to adaptive changes in protein homeostasis, as ferroptosis initiation is associated with diminished proteasomal activity and restoration of proteasomal activity and protects cells from ferroptotic cell death (154).

1.7 Scientific aims

AT possesses a remarkable capacity for energy storage and expenditure through the activity of WAT and BAT, respectively. The imbalance between these two opposing functions leads to disrupted cellular homeostasis and therefore metabolic diseases. The regulation of UPS plays a fundamental role in maintaining cellular and protein homeostasis (proteostasis). Transcription factor Nfe2l1 is a crucial regulator of UPS in case of genetic or environmental stressors such as inflammation, proteotoxicity, or oxidative stress and cell death. Nfe2l1 undergoes multiple posttranslational modification steps for activation and translocation to the nucleus to increase proteasome biosynthesis and function. Ddi2 is the protease responsible for cleavage and processing of Nfe2l1. However, the specific Ddi2 mode of function in Nfe2l1 processing and physiological relevance of Ddi2 ablation in cell or animal models has not been elaborated yet.

In this study, I investigated:

1. The role of Ddi2 proteolytic activity in Nfe2l1 cleavage and activation in BAT thermogenesis.
2. The significance of Ddi2/Nfe2l1 pathway in UPS regulation and protection against oxidative stress and ferroptosis cell death.

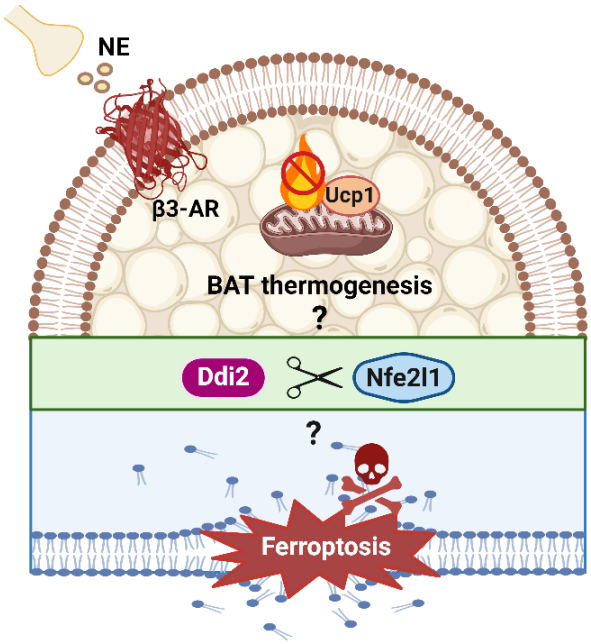

Figure 11: Project overview: Investigating the role of protease Ddi2 in regulation of ubiquitin proteasome system in adipose tissue thermogenesis and ferroptosis cell death. Ddi2 cleavage and activation of Nfe2l1 in *in vitro* cell models and BAT-specific phenotype. Additionally, the adaptation of UPS system in ferroptosis cell death mediated by Ddi2/Nfe2l1 pathway. Created with Biorender.com.

2. Material und Methods

2.1 Mouse experiments

All mouse experimental procedures were approved by the animal welfare committees of the government of Upper Bavaria, Germany (ROB-55.2-2532.Vet_02-20-32) and by the Harvard T.H. Chan School of Public Health (HSPH) Institutional Animal Care and Use Committee. All animals had ad libitum access to chow diet (sniff) and water and were housed at room temperature (22°C) with a 12-h light-dark cycle. Thermoneutrality acclimatization performed by keeping mice at 30°C for 7 days. For short-term cold exposure and long-term adaptation mice were kept at 4°C for 24h and 7 days, respectively. Mice were killed by cervical dislocation and tissues were snap-frozen in liquid nitrogen and stored at -80°C for experiments indicated. Mice carrying floxed alleles of *Ddi2* were generated by the Hotamisligil Lab, Harvard T.H. Chan School of Public Health, Boston, USA, from *Ddi2*$^{tm1a(EUCOMM)Hmgu}$ (https://www.mousephenotype.org/data/genes/MGI:1917244). For that, C57BL/6N-A/a ES cells were injected into blastocysts, giving rise to chimeric mice, of which males were continuously bred until germ line transmission was successful in producing founders carrying the *Ddi2*^{tm1a} allele. Mouse experiments with the floxed *Ddi2*^{tm1a} mice transgenic for Ucp1-Cre were performed in collaboration by the Hotamisligil Lab, Harvard T.H. Chan School of Public Health, Boston, USA. For indirect calorimetry experiments, CL (Tocris) 0.5 mg/kg in saline IP were injected to mice for measuring BAT activity. The Sable Systems PromethionCore® was used to determine indirect calorimetry parameters. Harvested tissues were snap-frozen in liquid nitrogen and then stored at -80°C.

2.2 Cell culture and treatments

Multiple immortalized human and mouse cells lines were used in this study. WT-1 brown, and 3T3L1 white immortalized preadipocytes cells were kept inside the incubators to reach 80% confluency in T75 flasks and they were seeded at 6, 24, and 96-well cell culture plates as indicated in various experiments. For ferroptosis experiments, 300,000, 100,000, and 30,000 parental WT and *DDI2* KO EA.hy926 cells were seeded at 6, 24, and 96-well cell culture plates, respectively. Knockout of *Ddi2* in human EA.hy926 cells were described previously (155). Cells were cultured in DMEM Glutamax (Gibco), supplemented with 10 % v/v fetal bovine serum (FBS, Sigma) and 1 % v/v Penicillin-Streptomycin (PS, Sigma). Cells were incubated at 37°C, 5 % v/v CO_2 and were passaged two to three times a week. Primary GPX4 mutant fibroblasts derived from a patient with Sedaghatian-type Spondylometaphyseal Dysplasia (SSMD) (a homozygous mutation

c.647G>A in exon 6 of GPX4) and control cells were provided by Sanath K. Ramesh (curegpx4.org). As GPX4 mutant cells undergo cell death under normal conditions, these cells were incubated in DMEM GlutaMax (Gibco) supplemented with 10 % v/v FBS and 1 % v/v PS, supplemented with 10 µM ferrostatin-1 at 37°C, 5 % v/v CO_2. For treatments, different concentrations of RSL3 (SelleckChem), FIN56 (SelleckChem), and ferrostatin-1 (SelleckChem) were used as indicated. Inhibition of proteasome was performed using bortezomib (BTZ) (SelleckChem), and Epoxomicin (SelleckChem). Nelfinavir mesylate (NFV) (Sigma), and WRR139 (Sigma) were used for chemical inhibition of Ddi2 and Ngly1, respectively.

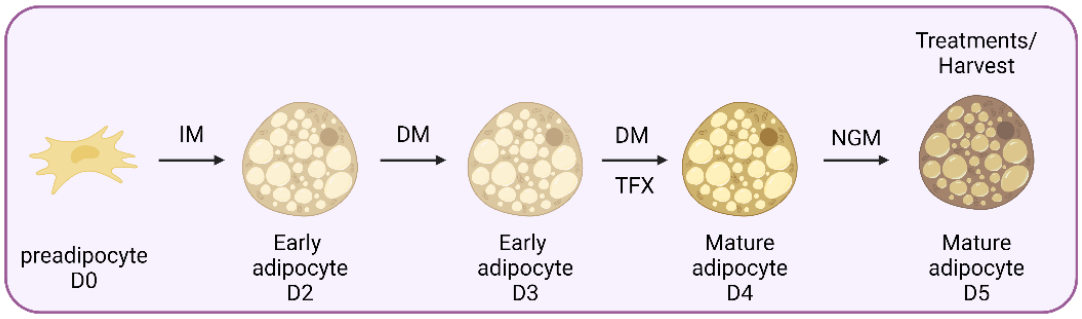

Figure 12: Differentiation and transfection protocol of immortalized brown preadipocytes WT-1. Cells were transfected with siRNA on day 3 of the differentiation protocol. Treatments were performed as indicated time points for each experiment before harvest on day 5. Created with Biorender.com.

To differentiate immortalized preadipocytes to mature adipocytes, cells were kept in normal growth medium (NGM) at 37°C, 5 % v/v CO_2 as shown in Fig. 12. When cells reach ~ 80 % confluency, induction medium (IM) (for specific content, see table 1) was added to the flask. This step is called day 0. On day 2 the medium was exchanged by differentiation medium (DM). Reverse transfection was carried out on day 3 of differentiation protocol. After 24 h, normal medium was added to each well and based on each experiment's treatments and harvest of cells after washing cells with DPBS were performed before day 5.

Table 1. Overview of all growth, induction, and differentiation medium ingredients. Abbreviations: FBS: Fetal Bovine Serum (Sigma), CS: Calf serum (Sigma), CCS: Cosmic calf serum (GE Healthcare Life Sciences), PS: Penicillin-Streptomycin (Sigma), T3: Triiodothyronine (Sigma), IBMX: 3-Isobutyl-1-Methylxanthine (Sigma), Indo: Indomethacin, Rosi: Rosiglitazone (Cayman Chemicals), Dex: Dexamethasone (Sigma), DMEM: Dulbecco's Modified Eagle Medium (Gibco).

Cell line	Growth Medium (GM)	Induction Medium (IM)	Differentiation Medium (DM)
WT-1	DMEM + 10 % FBS + 1 % PS	DMEM + 10 % FBS + 1 % PS + 850 nM insulin (Sigma) + 1 µM Rosi + 1 nM T3 + 500 µM IBMX + 1 µM Dex + 125 µM Indo	DMEM + 10 % FBS + 1 % PS + 1 µM Rosi + 1 nM T3
3T3L1	DMEM + 10 % CS + 1 % PS	DMEM + 10 % CCS + 1 % PS + 850 nM insulin + 1 µM Rosi + 500 µM IBMX + 1 µM Dex	DMEM + 10 % CCS + 1 % PS + 850 nM insulin + 1 µM Rosi + 500 µM IBMX + 1 µM Dex

2.3 Reverse transfection

In vitro knockdown experiments were performed by reverse transfection of 30nM SMARTpool siRNA (Dharmacon) in Lipofectamin RNAiMAX (Thermo). In the first step, for each 24-well plates 0.5 µM of siRNA and 1.5 µM of RNAiMAX were diluted in 50 µM Opti-MEM in different tube and left in room temperature for 5 minutes. After the incubation time, two tubes were mixed and further incubated at room temperature for 20 minytes. This transfection mixture (TFX) was then added to each well and cells suspension were transferred to the TFX. To prepare cell suspension, the adherent cells were collected by adding 2 ml trypsin, incubation at incubator at 37°C and 5% CO2 for 5 min, and then neutralizing trypsin by adding normal growth medium to the flask. After centrifugation, cell pellets were diluted in differentiation medium and were mixed with transfection mixture by gentle shaking. The transfected plate was kept in the incubator for 24 hours and the next day (D4) the medium was removed, and new normal growth medium were added to the cells. Differentiation protocol lasted for 5 days therefore treatments as indicted in each experiment were performed before harvesting the cells. For transfection of plasmids constructs (including Empty vector, DDI2 WT, DDI D252, NFE2L1 WT, NFE2L1-8ND), 250 ng of each plasmid, 1.5 µl of TransIT-X2® Transfection Reagent,

and 100 µL of Opti-MEM were all mixed in one tube. After 10 min incubation, cells were added to the medium followed by similar procedure as siRNA transfection.

2.4 Extraction and purification of plasmid DNA

To increase the amount of plasmid DNA, normal bacterial transformation was performed. To this aim, One Shot™ TOP10 chemically competent *E. coli* (Thermo Fisher Scientific) was thawed on ice. 1 µL of the target plasmid (10ng) was added into the vial of Shot™ cells and mixed gently. The mix was incubated on ice for 30 minutes. The mixture was heat-shocked for 45 seconds at 42°C without shaking and then directly placed on ice for 2 minutes. Next, 250 µL of pre-warmed Super Optimal broth with Catabolic repression growth medium (Thermo Fisher Scientific) was added to each vial followed by horizontal shake at 37°C. After 1 h, 30 µL of the mixture is plated onto the agar plate containing ampicillin by four quadrants streak method and kept at 37°C to grow. The day after a single colony was selected and added to 5 Ml of LB medium containing 100 µg/mL ampicillin whilst shaking 37°C for 8 h to further grow. Next, for large overnight culture, 100 µL of the medium containing bacteria was added to 400 mL of LB medium and incubated for 12-16 h on shaker incubator at 37°C. NucleoBond® Xtra EF purification system (Macherey-Nagel) protocol was used to extract the plasmid from the medium based on manufacturer's protocol. The final concentration of diluted plasmid was measured using spectrophotometry (NanoDrop, Thermo Fisher Scientific).

2.5 Aquabluer

Cell viability was assessed by AquaBluer MultiTarget Pharmaceuticals) by changing the medium of cells to 1:100 of AquaBluer in phenol red-free DMEM GlutaMax when cells are ready for harvest. Cell plates were incubated for 4 h at 37°C incubator for change of Aquabluer color. Using a Spark Reader (Tecan) fluorescence was measured at emission of 590 nm with an excitation of 540 nm.

2.6 Protein extraction and immunoblotting

Cells were lysed in Radio-Immunoprecipitation (RIPA) buffer (150 mM NaCl (Merck), 5 mM EDTA, 50 mM Tris (Merck) pH 8, 1 % v/v IGEPAL CA-630, 0.5 % w/v sodium deoxycholate (Sigma), 0.1 % w/v SDS (Roth)). To inhibit degradation of proteins and endogenous proteases Lysates, 10 ml of lysis buffer was one supplemented with cOmplete protease inhibitor cocktail tablet (Roche) and PhosStop (Roche). Lysates were centrifuged for 15 min (4°C, 21,000 *g*) and the supernatant was separated for subsequent protein quantification. To extract proteins from tissue samples, 200 TRIzol lysis reagents

(Thermo) was added to 2 mL safe lock tubes (Eppendorf) containing organs. One metal bead (Quiagen) was added to each tube to ensure sufficient homogenization of the cells. Tubes containing cells or tissues were further mechanically disrupted for 3 min in TissueLyser II (30 Hz; Qiagen). The concentration of proteins in supernatant of cells and tissues was determined by Pierce BCA Protein Assay (Thermo) according to the manual. Proteins were denatured for 5 min at 95°C in Bolt LDS Sample buffer (Thermo) with 5 % v/v 2-mercaptoethanol (Sigma). 30 µg of proteins were loaded in Bolt 4-12 % Bis-Tris gels (Thermo), followed by transferring onto a 0.2 µm Polyvinylidenfluorid (PVDF) membrane. The setting for the transfer were 25 Volts, 1.3 Amperes for 7 min. Membranes were blocked in TBS-T (200 mM Tris (Merck), 1.36 mM NaCl (Merck), 0.1 % Tween-20 (Sigma)) containing 5 % w/v milk powder for 1 h at room temperature after staining in Ponceau S solution. Incubation by primary antibodies (Table 2) was performed overnight at 4°C in 5 % milk, followed by washing membranes 3 times for 10 min with TBS-T and incubation with horseradish-peroxidase (HPR) linked secondary antibodies for 1 h at room temperature. SuperSignal West Pico PLUS (Thermo) as a substrate for the horseradish-peroxidase was used for developing blots in a ChemiDoc MP imager (Bio-Rad).

Table 2. List of all antibodies used for immunoblotting

Antibody	Company (Cat. No.)	Dilution
DDI2	Abcam (ab197081)	1:1000
NFE2L1	Cell Signaling Technologies (D5B10)	1:500
β-TUBULIN	Cell Signaling Technologies (2146)	1:1000
UBIQUITIN (P4D1)	Cell Signaling Technologies (3936)	1:1000
20S Proteasome α subunit	Abcam (ab22674)	1:1000
Anti-Lamin B1	Abcam (ab229025)	1:1000
Anti-rabbit IgG, HRP-linked	Cell Signaling Technologies (7074)	1:10000
Anti-mouse IgG, HRP-linked	Cell Signaling Technologies (7076)	1:10000
GAPDH	Cell Signaling Technologies (D16H11)	1:1000

2.7 Proteasome activity assay

Cells lysis was performed in lysis buffer (40 mM Tris (Merck) pH 7.2, 50 nM NaCl (Merck), 5 mM MgCl2(6H2O) (Merck), 10 % v/v glycerol (Sigma), 2 mM ATP (Sigma), 2 mM 2-mercaptoethanol (Sigma). Samples were kept on ice. Mechanical lysis occurred by TissueLyser II (Qiagen) for 3 min, 30 Hz. Next, samples were centrifuged (15 min, 4°C, 21,000 g) and the supernatant was used for the assay. Proteasome Activity Fluorometric Assay II kit (UBPBio, J41110) was used to measure three different catalytic activities of proteasome as manufacturer's protocol. The emission was measured over the course of 15 minutes in 60 seconds intervals at 460 nM in the plate reader (Tecan). BCA Protein Assay (Bio-Rad Protein Assay Kit II) was used to normalize the activity of subunits to protein levels.

2.8 Native PAGE

Cells were lysed in lysis buffer (50 mM Tris/HCl pH 7.5, 2 mM DTT, 10 % v/v glycerol (Sigma), 5 mM MgCl2 (Merck), 0.05 % v/v Digitonin, 2 mM ATP (Sigma)) containing phosphatase inhibitor (PhosStop, Roche), as described previously (156). Samples were kept on ice for 20 min followed by mechanical lysis by TissueLyser II (3 min, 30 Hz; Qiagen) and centrifugation for 15 min (4°C, 21,000 *g*). Concentration of proteins was determined with Bio-Rad Protein Assay Kit II. 15 µg of protein were loaded in NuPAGE 3-8 % Tris-Acetate gels (Thermo) and the gel let run for 4 h at constant voltage of 150 V. Gels were incubated for 30 min at 37°C in an activity buffer (1 mM MgCl2 (Merck), 50 mM Tris (Merck), 1 mM DTT) with 0.05 mM substrate Suc-Leu-Leu-Val-Tyr-AMC. ChemiDoc MP (Bio-Rad) was used to measure fluorescent signals. Afterwards, to prepare samples for blotting, gel was incubated in a solubilization buffer (2 % w/v SDS, 1.5 % v/v 2-Mercaptoethanol (Sigma), 66 mM Na_2CO_3) for 15 min. Samples were transferred to a PVDF membrane at 40 mA through tank transfer. The membrane was kept for 1 h in the ROTI-block, followed by overnight incubation in primary antibody (1:1000). The day after, the membrane was incubated for 3 h in the secondary antibody (1:10,000) at room temperature and developed as previously described in chapter 2.6 (Protein extraction and immunoblotting).

2.9 NFE2L1 reporter assay

HEK293a cells were used to stably express short half-life firefly luciferase driven by upstream activator sequence (UAS) promoter and a chimeric NFE2L1. In this model, the DNA-binding domain of NFE2L1 was replaced by the UAS-targeting Gal4 DNA-binding

domain (157). The assay measures nuclear translocation and its transactivation by binding of NFE2L1-UAS to the luciferase promoter (157). 50,000 cells were seeded in 96-well plates and treated with indicated chemical compounds. Cell lysis and luciferase emission was measured by Dual-Glo Luciferase Assay System (Promega) according to the manufacturer's instructions.

2.10 Gene expression analysis

RNA extraction was performed using Nucleospin RNA kit (Macherey Nagel), based on manufacturer's instruction. Concentration of RNAs were measured with a NanoDrop spectrophotometer (Implen). To prepare complementary DNA (cDNA), 500 ng of measured RNA were added to 2 µL of Maxima^{TM} H Master Mix 5x and the total volume was adjusted to 10 µL with H_2O. Biometra TRIO thermal cycler (Analytic Jena) setting for cDNA synthesis was: 10 min at 25°C, 15 min at 50°C, 5 min at 85°C, followed by final cool down to 4°C.

The cDNA was diluted at the ratio of 1:40 in aqua ad injectabilia, and 4 µL of cDNA, 5 µL of PowerUp^{TM} SYBR Green Master Mix (Thermo), and 1 µL of 5 µM primer stock (Table 3) were used to measure Relative gene expression. Cycle thresholds (Ct) of gees were measured using a Quant-Studio 5 Real-time PCR system (Thermo). Relative gene expression was normalized to TATA-box binding protein (*TBP*) levels by ddCt-method.

Table 3: RTqPCR primers.

Gene	Forward Primer (5')	Reverse Primer (5')
NFE2L1 (Hs)	AGTGGAGACTTAACCAAAGAGGAC	CTCCTTCTGGCGGTGACTAT
Nfe2l1 (Mm)	TTGGCTCTACCAACCTAGCAG	CCAGCATAGCTCGTCTAACAG
Nfe2l2 (Mm)	CTCCGTGGAGTCTTCCATTTAC	GCACTATCTAGCTCCTCCATTTC
Nfe2l3 (Mm)	TGAGCCAAGCTATAAGCCATGA	AATGGTTCTTGTGCCTGGAA
DDI2 (Hs)	TGCATGTAGTGTGTGTGTACTGC	CCAGTGAGGTAGATTCTTTACCACTT
Ddi2 (Mm)	ACGGGCATCCTGTGAAAG	CACAGGCCTGGCTCTAATAG
TBP (Hs)	CCCATGACTCCCATGACC	TTTACAACCAAGATTCACTGTGG

Tbp (Mm)	AGAACAATCCAGACTAGCAGCA	GGGAACTTCACATCACAGCTC
Nqo1	AGCGTTCGGTATTACGATCC	AGTACAATCAGGGCTCTTCTCG
Hmox1	AGGGTCAGGTGTCCAGAGAA	CTTCCAGGGCCGTGTAGATA
Psma1	TGCGTGCGTTTTTGATTT TAGAC	CCCTCAGGGCAGGATTCATC
Psma2	TGGCTGTGTTCCGACTTTC	AAGCTTACCAGATGGGCTGA
Psmb1	TTCCACTGCTGCTTACCGAG	CGTTGAAGGCATAAGGCGAAAA
Psmb2	CCCAGACTATGTCCTCGTCG	CCGTGTGAAGTTAGCTGCTG
Psmb4	ACTGGCCACTGGTTATGGTG	CAGCACTGGCTGCTTCTCTA
Psmb5	CCACAGCAGGTGCTTATATTGC	GCTCATAGATCGACACTGCC
Psmb6	GAAAACCGGGAAGTCTCCAC	CTCGATTGGCGATGTAGGAC
Psmd1	GTGATAAAACACTTTCGAGGCCA	TGAATGCAGTCGTGAATGACTT
Psmc3	TTTTCATAGACGAATTGGATGC	CATGGTCCTCTGCACCTCTC
Atf3	GAGGATTTTGCTAACCGACACC	TTGACGGTAACTGACTCCAGC
Ddit3	CTGGAAGCCTGGTATGAGGAT	CAGGGTCAAGAGTAGTGAAGG T
Adipoq	GGAGAGAAAGGAGATGCAGGT	CTTTCCTGCCAGGGGTTC
Ucp1	AGGCTTCCAGTACCATTAGGT	CTGAGTGAGGCAAAGCTGATTT
Fabp4	GGATGGAAAGTCGACCACAA	TGGAAGTCACGCCTTTCATA
Scd1	TTCTTGCGATACACTCTGGTGC	CGGGATTGAATGTTCTTGTCGT
Glut4	GACGGACACTCCATCTGTTG	GCCACGATGGAGACATAGC
Ppargc1α	TCTGAGTCTGTATGGAGTGACAT	CCAAGTCGTTCACATCTAG-TTCA
Pparα	AGAGCCCCATCTGTCCTCTC	ACTGGTAGTCTGCAAAACCAAA
Pparg	TCGCTGATGCACTGCCTATG	GAGAGGTCCACAGAGCTGATT
Cebpb	ATCGACTTCAGCCCCTACCT	TAGTCGTCGGCGAAGAGG

Mlxipl	ATCCAGCCAGACCTGACG	CGGTAATTGGTGAA-GAAATCTGA
Ywhaz	GAAAAGTTCTTGATCCCCAATGC	TGTGACTGGTCCACAATTCCTT

2.11 Protein digestion and purification for MS

Protein digestion and DiGly peptide enrichment was performed as described previously (158, 159). Cells were lysed in sodium deoxycholate (SDC) buffer (1 % w/v SDC in 100 mM Tris-HCl, pH 8.5) followed by boiling at 95°C for 5 minutes while shaking at 1000 rpm. Samples were centrifuged at 10000 *g* for 15 minutes and supernatant was isolated for analysis. Protein concentrations of lysates were determined after 15 minutes of sonication via a Bioruptor (Diagenode, cycles of 30 s) using the Pierce BCA Protein Assay. CAA and TCEP (final concentrations: 40 mM and 10 mM, respectively) were added to 5 mg protein. Samples were incubated for 10 min at 45°C in the dark while shaking at 1000 rpm. Trypsin (1:50 w/w) and LysC (1:50 w/w, Wako) were added to samples for overnight digestion at 37°C while shaking at 1000 rpm. For total proteome analysis, 15 µg of sample aliquots were desalted in self-made 3 layered SDB-RPS StageTips (Empore). Briefly, samples were diluted with 2 % TFA in isopropanol (1:1) to a final volume of 200 µl. Next, samples were loaded onto StageTips and consecutively washed with 200 µl of 2 % TFA in isopropanol (1:1) and 200 µl 0.2 % TFA/2 % ACN. Peptides were eluted with freshly prepared 60 µl of 1.25 % v/v ammonium hydroxide (NH_4OH) in 80 % v/v CAN, and dried using a SpeedVac centrifuge (Eppendorf) for 45 minutes. Dried peptides were thoroughly suspended in 6 µL buffer A (2 % v/v ACN/0.1 % v/v TFA) and protein concentration determined via a NanoDrop spectrophotometer (Implen). For Di-Gly enrichment, samples were diluted with 1 % v/v TFA in isopropanol (1:5) and subsequent peptide cleanup was performed using SDB-RPS cartridges (Strata™-X-C, 200 mg/6 ml, Phenomenex Inc.). Cartridges were equilibrated with 8 bed volumes (BV) of 30 % v/v MeOH/1 % v/v TFA and washed with 8 BV of 0.2 % v/v TFA. Samples were loaded by gravity flow and sequential washing steps with 8 BV 1 % TFA in isopropanol and once with 8 BV 0.2 % TFA/2 % ACN. Peptides were eluted twice with 4 BV of 1.25 % NH_4OH in 80 % CAN and diluted with ddH2O to a final of 35 % v/v ACN. Samples were dried at 45°C via a SpeedVac Centrifuge (Eppendorf) overnight.

2.12 DiGly peptide enrichment

We used the PTMScan® Ubiquitin Remnant Motif (Cell Signaling) for DiGly peptide enrichment. In short, peptides were resuspended in 500 µL immunoaffinity purification (IAP) buffer and sonicated (Bioruptor) for 15 min. Concentration of proteins was determined by BCA Protein Assay. The antibody-coupled beads were cross-linked as previously described (159). One vial of antibody coupled beads was washed for one minute with cold cross-linking buffer at 2000 *g*. Subsequently the beads were incubated in 1 mL cross-linking buffer for 30 minutes at room temperature under mild agitation. The reaction was stopped by washing with 1 mL cold quenching buffer (200 mM ethanolamine, pH 8.0) twice followed by 2 h incubation in quenching buffer whilst gentle agitation at room temperature. Cross-linked beads were washed three times with 1 mL of cold IAP buffer and then directly used for peptide enrichment. 3 mg of peptide is used with 1/8 of a vial of cross-linked antibody beads for DiGly enrichment. Peptides were added to the cross-linked beads and the volume was adjusted to 1 mL with IAP buffer with 2 h incubation at 4°C under gentle agitation. The beads are washed twice with cold IAP buffer and twice ddH_2O. The enriched peptides were eluted by adding 200 µL 0.2 % TFA onto the beads whilst shaking for 5 min at 1400 rpm followed by centrifugation for 1 min at 100 *g*. The supernatant was transferred to SDB-RPS StageTips and the peptides washed, eluted, and dried as previously described for total proteome samples.

2.13 LC-MS/MS proteome and ubiquitome measurements.

Liquid chromatography of total proteome and ubiquitome samples was performed on an EASYnLCTM 1200 (Thermo). Constant flow rate was maintained at 10 µL/min at 60°C using a dual buffer system consisting of buffer A (0.1 % v/v formic acid) and buffer B (80 % v/v acetonitrile, 0.1 % v/v formic acid). The column was in-house made with 50 cm long and had 75 µm inner diameter and was packed with C18 ReproSil (Dr. Maisch GmbH, 1.9 µm). For ubiquitome, the elution gradient started with 5 % buffer B, increasing to 25 % over 73 min, 50 % after 105 min and remaining steady at 95 % after 110 min. The gradient for total proteome started at 5 % buffer B and increased to 20 % after 30 min, further increased at a rate of 1 % per minute to 29 %, following up to 45 % after 45 min and to 95 % after 50 min. The MS/MS measurement was completed on a Exploris 480 with injection of 500 ng peptide (Thermo). For the ubiquitome, fragmented ions were analyzed in Data Independent Acquisition (DIA) mode with 66 isolation windows of variable sizes. The scan range was 300 – 1650 *m/z* with a scan time of 120 min, an Orbitrap resolution of 120,000 by maximum injection time of 54 ms. MS2 scans were performed with a higher-energy collisional dissociation (HCD) of 30 % at a resolution of 15,000 and

a maximum injection time of 22 ms. The MS measurement of the proteome was performed equivalently, but including High-Field Asymmetric Waveform Ion Mobility (FAIMS) with a correction voltage of -50 V and a total scan time of 60 min. The injection time for the full scan was 45 s and the MS2 injection time of 22 s.

2.14 Proteome and Ubiquitome data acquisition and analysis

DIA raw files were processed using Spectronaut (13.12.200217.43655) in directDIA mode. The FASTA files used for the search were: Uniprot Homo sapiens (29.03.2022) with 20609 entries, Uniprot Homo sapiens isoforms (29.03.2022) with 77157 entries and MaxQuant Contaminants for filtering: 245 entries. Analysis was performed by Perseus (version 1.6.2.3). For the ubiquitome samples the output was converted with the plugin "Peptide Collapse" (version 1.4.2). Values were log2-transformed, and the missing values were replaced by imputation from normal distribution with a width of 0.3 and downshift 1.8 separately for each sample. Ubiquitome was normalized to total proteome. Comparison between conditions of proteome and ubiquitome was performed via Student's T-test in R 4.2.2 (*P* value cutoff 0.5).

2.15 Extracellular flux analysis (Seahorse)

Analysis of mitochondrial respiration with Seahorse Cell Mito Stress Test (Agilent) was performed with manufacturer's protocol with some adjustments. 50,000 cells were counted and equally seeded in 24-well Seahorse plates and left on room temperature under cell culture hood for 2 hours with or without transfection (if required). Cell plates were at 37°C incubator for 48 hours. Culture medium was then replaced with Seahorse medium (XF DMEM pH 7.4, 10 mM glucose, 1 mM Pyruvate, 2 mM L-glutamine) and incubated for 60 min at 37°C incubator without CO_2. 10x compounds were distributed into the ports of the sensor cartridge with a multichannel pipette (as listed in the table 4) followed by 3 minutes of mixing, incubation and measurement with Seahorse XF24-analyzer (Agilent).

Table 4: Mitochondrial Stress Test

port	Compounds	Stock con. [µM]	10x in Port [µM]	µL for 10x	µL assay medium	Final conc. [µM]	µL injected
A	NE	10000	10	3	2997	1	56

B	Oligomycin A	6320	10	4.7	2995	1	62
C	FCCP	25000	40	4.8	2995.2	4	69
D	Antimycin A + Rotenon	5000	5	3.0	2997	0.5	75

2.16 Oil Red O staining

Oil Red O (ORO) staining was used to measure lipid content in brown WT-1 adipocytes. Cells were seeded in 24-well plates followed by washing twice with cold DPBS (Gibco). Cells were fixed in 1 mL zinc formalin solution at room temperature (Merck) for 60 min, and then again washed with DPBS. Meanwhile, Oil Red O solution was pre-filtered through a 70 µm, 30 µm, and 0.2 µm filter). Samples were washed with 60% isopropanol, completely dried and stained with ORO mix (60% v/v Oil-Red-O solution (Sigma), 40% v/v H2O) for 60 min. Cells were washed several times with distilled water, dried over-night, and they were ready for taking pictures for visualizing lipid content. To quantify lipid content, the remaining bound ORO staining was eluted with 100% isopropanol, followed by measuring absorption at 500 nm in a Tecan plate reader.

2.17 Statistics

All data were analyzed with Microsoft Excel, GraphPad Prism, and R (4.2.2). Data were visualized in GraphPad Prism and shown as mean ± standard deviation (SD) with plotting individual data distribution of technical replicates. Except for the proteomics, every experiment was replicated twice. 1-way ANOVA with Dunnett's Post-hoc Test was used when comparing three or more groups and one variable, and 2-way ANOVA followed by Dunnett's, Sidak's, or Tukey's Test was used for comparing two groups with two variables. *P*-values lower than 0.05 were considered significant and are as such indicated in the graphs with an asterisk between groups.

3. Results

3.1 The role of Ddi2 in Nfe2l1 turnover and brown fat proteostasis

3.1.1 Cold-induced Ddi2 is highly expressed in brown adipose tissue (BAT)

Activation of BAT naturally occurs in response to cold exposure, which results in production of heat to maintain the normal body temperature through NST. As Nfe2l1 is highly expressed in BAT and is induced by cold (160), I first checked the existance of Ddi2 in various AT depots. Ddi2 was enriched in BAT compared to two other type of white adipose tissues (WAT): inguinal (ingWAT) and epididymal (EpiWAT) samples from C57BL/6J mice (Fig. 13a). To determine the role of cold regulation, I measured Ddi2 mRNA levels in BAT from wild-type (WT) mice housed in thermoneutrality (30°C), cold (4°C) for 24 hours, or cold (4°C) for 7 days. Cold adaptation either for 24 hours or 7 days was associated with higher mRNA expression of *Ddi2* gene (Fig. 13b).

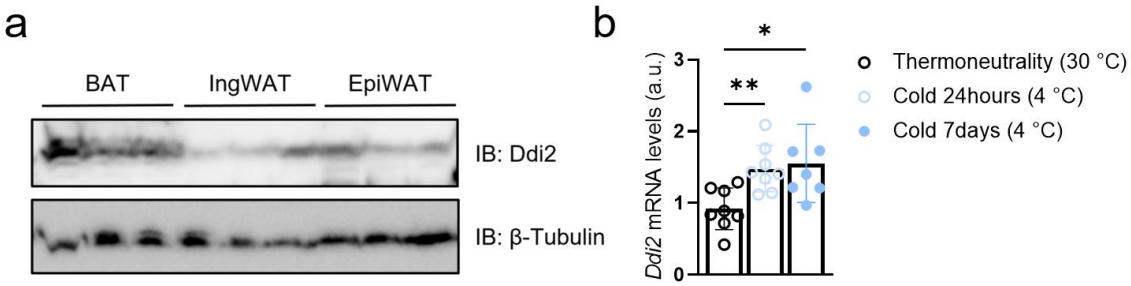

Figure 13: Ddi2 expression is abundant in brown adipocytes and induced by cold exposure. a) Western blot of Ddi2 in brown adipose tissue (BAT), inguinal white adipose tissue (IngWAT), and epididymal white adipose tissue (EpiWAT) from C57BL/6J mice (n=3). b) Gene expression levels of *Ddi2* in BAT from wild-type mice housed in thermoneutrality (30°C), cold (4°C) for 24 hours, or cold (4°C) for 7 days (n = 8 biological replicates) normalized to *Tbp* levels. Data is presented as mean ± SD, *p < 0.05, **p<0.01.

To assess if Ddi2 level is changed during differentiation of preadipocytes to mature adipocytes, I used immortalized mouse brown preadipocytes (WT-1). Cells after 1, 3, and 5 days of differentiation displayed higher protein of Ddi2 and Ucp1 compared to undifferentiated (undif/day0) cells (Fig. 14). In summary, these data shows that cold adaptation in *in vivo* tissue samples and differentiation of brown adipocytes *in vitro* led to markedly higher Ddi2 level.

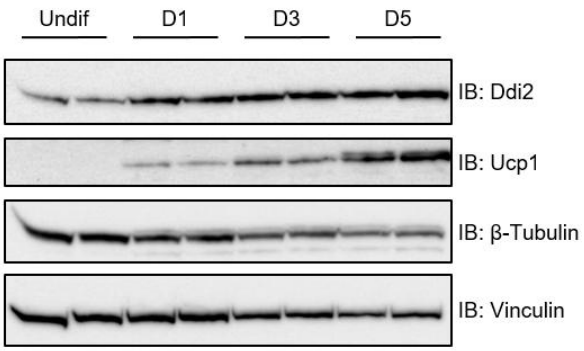

Figure 14: Ddi2 protein and gene level increases during differentiation of brown adipocytes in vitro. Western blot analysis of Ddi2 and Ucp1 in WT-1 undifferentiated (day0) and differentiated (day1, day3, and day5) cells.

3.1.2 Loss of Ddi2 is affected by inhibiting proteasome but does not exacerbate proteasome inhibitor toxicity

To establish a functional link between proteasome activity and Ddi2, I aimed to investigate whether impairments in proteasome function and the absence of Ddi2 influence each other. Already previous studies have shown in cultured cells (*in vitro*) and mice (*in vivo*) (64, 118, 160, 161) that proteasome inhibition leads to higher levels of Nfe2l1 protein but not mRNA levels. Therefore, I isolated and cultured stromal-vascular fraction (SVF) from interscapular BAT (iBAT) of C57BL/6J wild-type mice. Using *Ddi2* siRNA as an indicator for lower protein level in immunoblot, I treated these primary brown adipocytes (priBATs) with proteasome inhibitor epoxomicin in which Ddi2 protein band showed a decrease upon epoxomicin treatment (Fig. 15a). However, this effect was not aligned with gene expression of *Ddi2* in WT-1 cells (Fig. 15b). Loss of Ddi2 exacerbated the susceptibility of cells to epoxomicin-induced cell death (Fig. 15c). These data suggests that proteasome inhibition does not induce gene expression of *Ddi2*. Moreover, Ddi2 presence does not seems to be required to combat cell death mechanism.

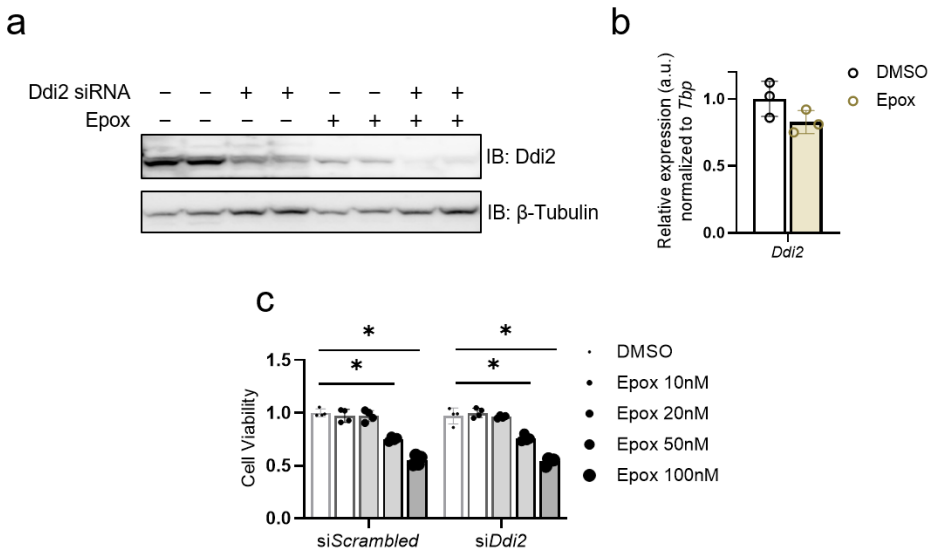

Figure 15: Ddi2 protein is less upon treatments with proteasome inhibitor but does not increase its toxicity. a) Western blot analysis of Ddi2 in primary brown adipocytes (priBATs) transfected with *Ddi2* siRNA followed by 100nM epoxomicin treatment for 6h. b) Gene expression levels of *Ddi2* in Undifferentiated WT-1 cells treated with 100nM epoxomicin for 6h (*n* = 3 technical replicates) normalized to *Tbp*. c) Cell viability assessed by Aqua Bluer in undifferentiated WT-1 treated with indicated concentration of epoxomicin for 20h. Data is presented as mean ± SD. Two-way analysis of variance (ANOVA) followed by Tukey's multiple comparisons test was performed. *p < 0.05.

3.1.3 Ddi2 mediates PI-induced proteolytic processing and nuclear translocation of Nfe2l1

As previously described (97, 98), post-translational modifications of Nfe2l1 involves de-glycosylation of N-glycan residues by Ngly1 and cleavage of full length Nfe2l1 (120 kDa) by Ddi2 to release the cleaved form (95kDa) of the protein. Cleaved form of Nfe2l1 then translocate to nucleus to increase expression of proteasome subunit genes, which is required for compensation of proteasome dysfunction. To initiate this cascade of Nfe2l1 activation, I used either Epoxomicin (Epox) or Bortezomib (BTZ) proteasome inhibitors in my cell experiments. Firstly, I showed the buildup of cleaved form of Nfe2l1 upon treatment with epoxomicin in a time dependent manner in WT-1 cells (Fig. 16a). To prove the importance of Ddi2 in cleavage of Nfe2l1, I transfected Synthetic Single Guide RNA (sygRNA) which transiently silences Ddi2 and leads to lower protein level in immunoblot. This genetic manipulation of Ddi2 led to less accumulated active form of Nfe2l1 in cells in protein level but no changes in mRNA expression (Fig. 16a, b). Following Nfe2l1 cleavage, the next step involves the translocation of Nfe2l1 to the nucleus. To achieve this aim, I employed a nuclear fractionation protocol to partition cellular components into cytoplasmic and nuclear fractions followed by immunoblots of each fraction. Upon PI treatment, cleaved form of Nfe2l1 accumulated on nuclear fraction (Fig. 16c).

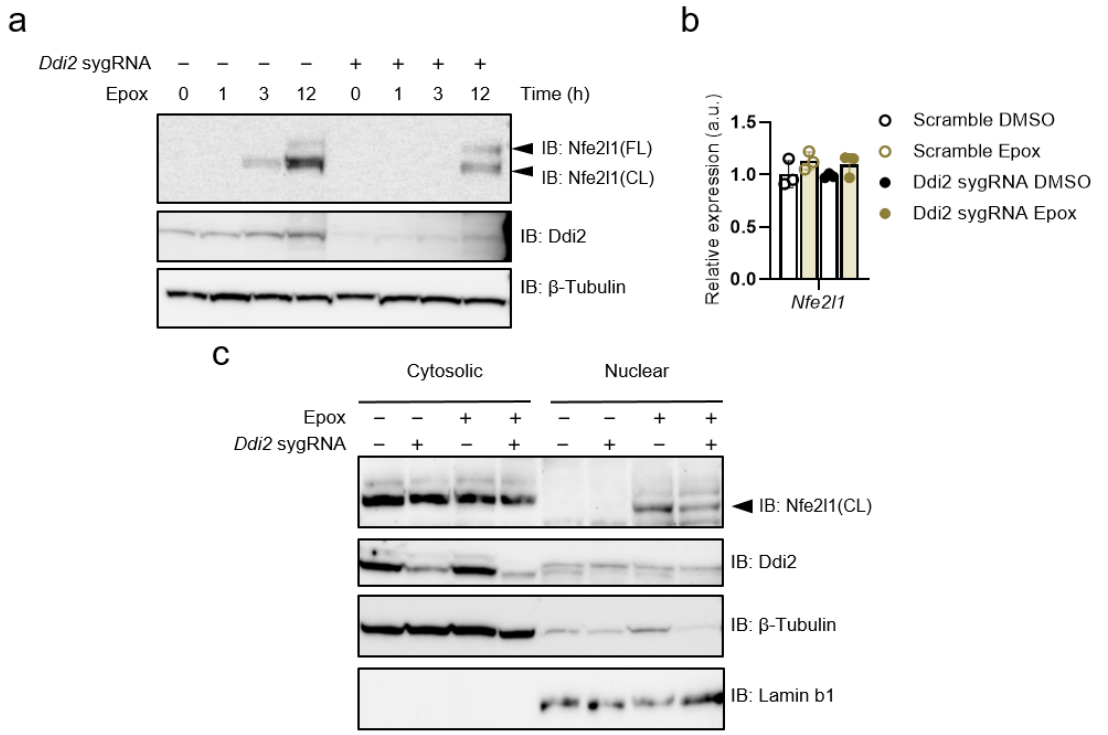

Figure 16: Ddi2 proteolytic activity is required for accumulation and nuclear translocation of Nfe2l1. a) Western blot of Nfel21 and Ddi2 with *Ddi2* sygRNA transfected WT-1 cells followed by 100nM epoxomicin treatment. (FL: full-length form ca. 120 kDa; CL: cleaved ca. 95 kDa). b) Gene expression in *Ddi2*-silenced WT-1 cells after 6h treatment with 100nM epoxomicin. c) immunoblot of cytoplasmic and nuclear fractions of *Ddi2* siRNA transfected WT-1 cells followed by 100nM epoxomicin treatment for 3h.

To provide more evidence for the crucial role of Ddi2 in Nfe2l1 cleavage, I used EA.hy926 human cell line, in which DDI2 was deleted by CRISPR/Cas9 Knockout (KO) technology (64). Three different plasmid constructs: Empty plasmid vector, wild type DDI2 (DDI2 WT), and protease dead form of DDI2 (DDI2 D252) were separately transfected to EA.hy926 *DDI2* KO cells. Re-expression of wild-type DDI2 could restore BTZ-induced cleaved NFE2L1 (95kDa). However, similar effect was not observed when the construct carrying proteolytically inactive DDI2 (DDI2-D252) was transfected to KO cells (Fig. 17).

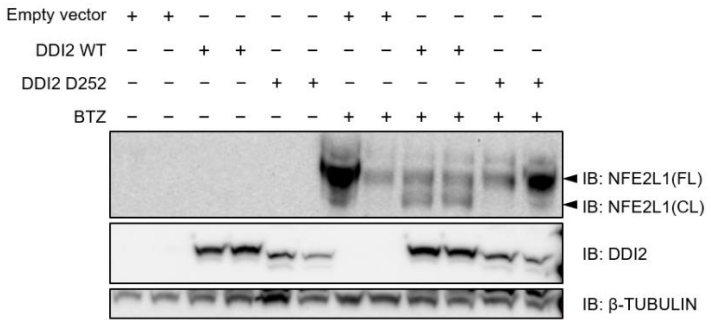

Figure 17: Proteolytic-inactive Ddi2 cannot rescue Nfe2l1 activation. Western blot of NFE2L1 in *DDI2* KO cells transfected with empty vector, wild type and D252 protease-dead DDI2 carrying plasmids followed by h treatment with 100 nM bortezomib (BTZ). Figure adapted from (162).

In addition to genetic manipulation of Ddi2, I employed Nelfinavir (NFV) as a well-established chemical inhibitor of Ddi2 (Schematic Fig. 18a). Due to the structural similarity between the RVP domain of Ddi2 and HIV, NFV as an FDA-approved anti-HIV drug, directly inhibits Ddi2 protease activity (163). Immunoblot analysis data showed that epoxomicin treatment led to higher protein levels of Nfe2l1 but NFV treatment repressed DDI2-mediated Nfe2l1 cleavage (Fig. 18b).

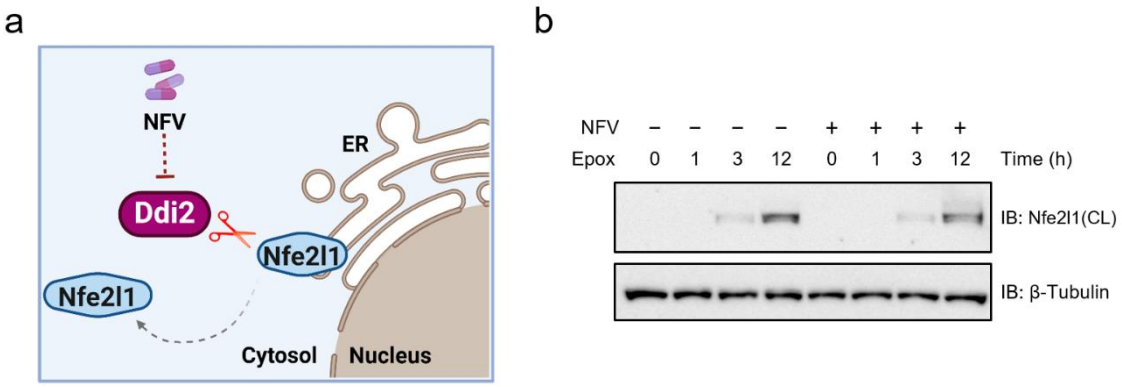

Figure 18: Chemical inhibition of Ddi2 by NFV leads inhibits Nfe2l1 cleavage. a) NFV-mediated inhibition of Ddi2. Created with Biorender.com. b) Western blot of EA.hy926 cells treated with 5µM NFV for 12h and 100nM epoxomicin.

Taken together, these experiments demonstrates that proteolytic activity of Ddi2 plays a crucial role in posttranslational modifications of transcription factor Nfe2l1. Genetic or chemical inhibition of Ddi2 activity markedly inhibits accumulation and nuclear translocation of cleaved form of Nfe2l1 in cells.

3.1.4 Ddi2 is required for proteolytic cleavage of Nfe2l1

Transcription factor Nfe2l1 is the key regulator to restore proteasomal activity by stimulating expression of proteasome subunits (64). Here I investigated the potential outcome

of Ddi2 loss of function on ubiquitin proteasome system dysfunction, proteasome biogenesis, and activity. As also described before in cell and animal models (160) treatment of cells with epoxomicin led to higher expression of proteasome subunit gene (*Psm*) and stress markers such as Activating Transcription Factor 3 (*Atf3)* and DNA-damage inducible transcript 3 (*Ddit3*, also known as Chop) (Fig. 19a). Surprisingly, unlike *Nfe2l1* KD, *Ddi2* KD did not blunt the ability of cells to compensate proteasome inhibition through increasing expression of *Psm* genes ((Supplementary Fig. 1a & Fig. 19a). However, chemical inhibition of Ddi2 via NFV treatment displayed opposite effect in which mRNA expression of *Psmb2*, *Psmb4*, and *Psmd1* did not increase upon PI treatment (Fig. 19b).

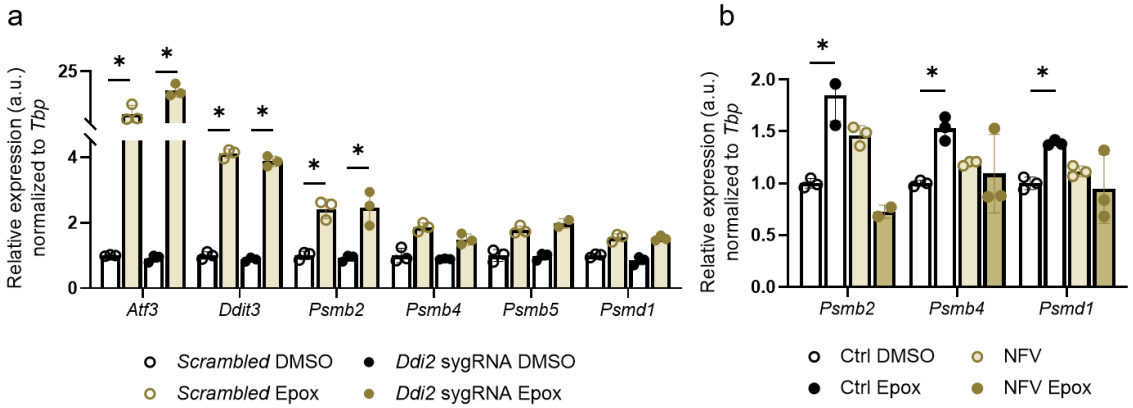

Figure 19: Silencing, but not chemical inhibition of Ddi2, does not affect biosynthesis of proteasome subunit genes via Nfe2l1 activation immortalized adipocytes. a) Expression of Stress marker and proteasome subunit genes after transient silencing of Ddi2 with sygRNA, followed by 100nM epoxomicin for 6h in differentiated WT-1 cells. b) Expression of proteasome subunit genes after NFV (10µM) treatment for 18h and 100nM epoxomicin for 3h in differentiated WT-1 cells. Data is presented as mean ± SD. Two-way analysis of variance (ANOVA) followed by Dunnett's multiple comparisons test was performed. *p < 0.05.

Due to the unexpected result in *Psm* gene expression in immortalized brown adipocytes, I used differentiated 3T3L1 cell line to investigate if the same applies in immortalized white preadipocytes. Firstly, Immunoblots showed that *Ddi2* KD decreases cleaved form of Nfe2l1 protein with no changes in mRNA expression (Fig. 20a). Also similar to WT-1 cells as immortalized brown adipocytes, KD of *Ddi2* in 3T3L1 cells successfully compensated expression of multiple proteasome subunits after PI treatment (Fig. 20b, c).

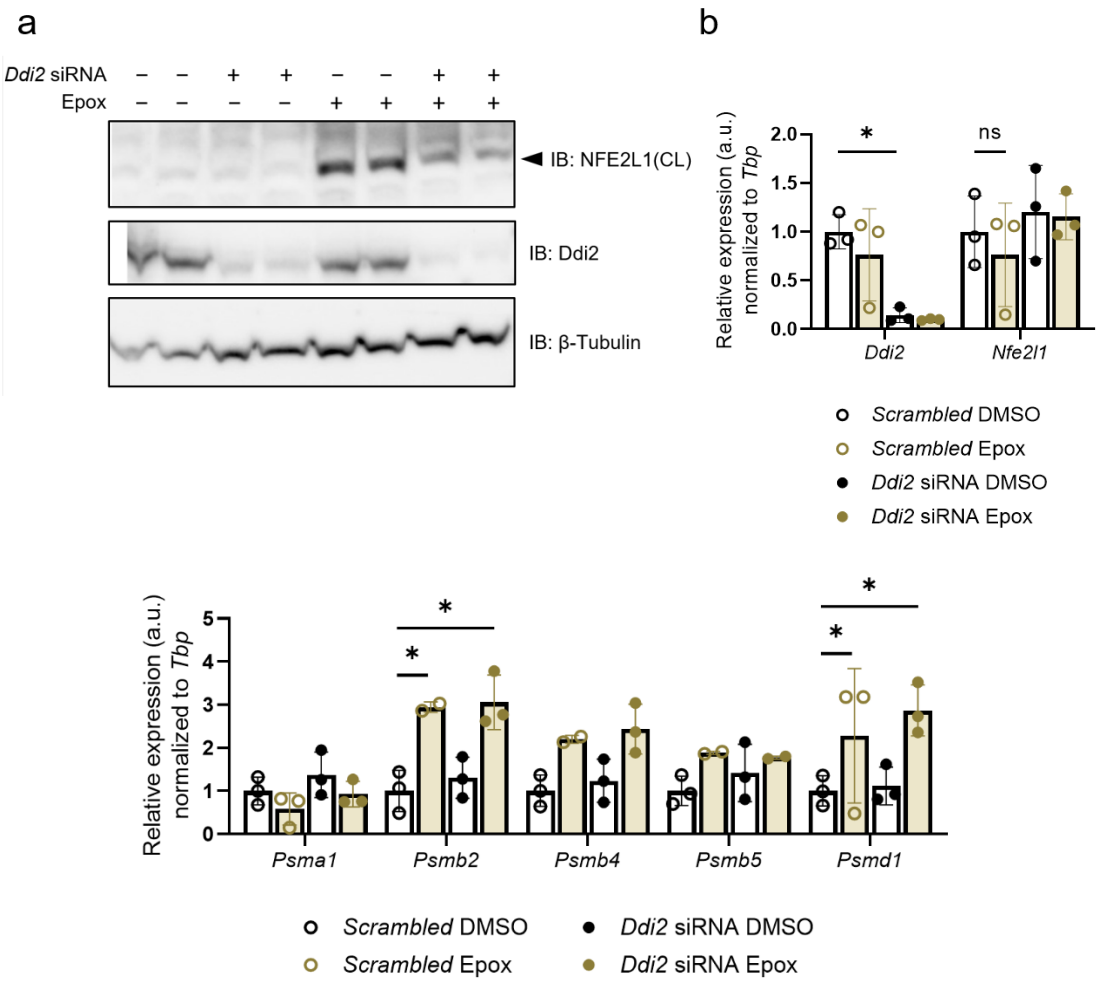

Figure 20: DDI2 is required for proteolytic cleavage but not transcriptional activity of Nfe2l1 in immortalized white adipocytes. a) western blot of Nfe2l1 and Ddi2 in 3T3L1 cells transfected with *Ddi2* siRNA and 100nM epoxomicin treatment for 6h. b-c) Gene expression of 3T3L1 cells transfected with *Ddi2* siRNA and 100nM epoxomicin treatment for 6h. Data is presented as mean ± SD. Two-way analysis of variance (ANOVA) followed by Tukey's multiple comparisons test was performed. *p < 0.05.

In order to evaluate the significance of Ddi2 in a physiological setting, we generated a mouse model in which Ddi2 was disrupted in Ucp1-expressing adipocytes (*Ddi2*$^{\Delta BAT}$) (Schematic Fig. 21a). In this model, Ddi2 mRNA expression level of isolated brown adipose tissue of *Ddi2* KO mice was markedly lower compared to wild type controls (Fig. 21b). Similar to in vitro experiments, mRNA expression level of proteasome subunits exhibited no significant changes between *Ddi2* KO and wild type animals (Fig.21c). Taken together, no changes in proteasome biogenesis through bounce back response mediated by activity of transcription factor Nfe2l1 in, both transient loss of Ddi2 in immortalized cell lines and in vivo tissue from KO mice. These observations raise a question of whether there is a functional relationship between Ddi2-mediated cleavage of Nfe2l1 and proper transcriptional activation of cleaved form (versus uncleaved Nfe2l1), which requires further investigations.

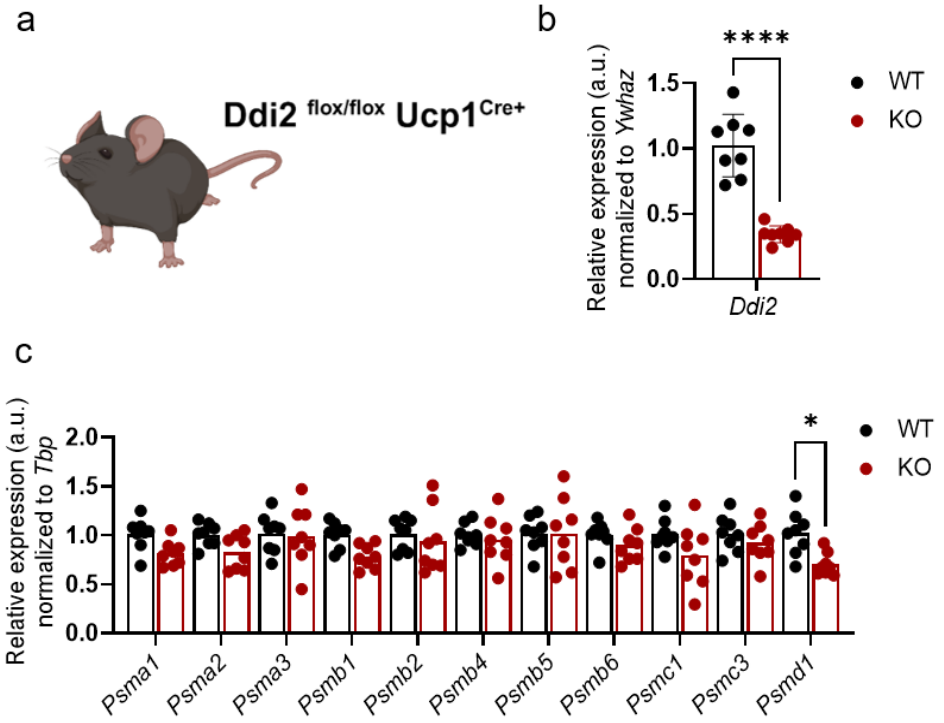

Figure 21: Loss of Ddi2 in vivo does not disrupt UPS bounce back response. a) Schematic model of BAT-specific *Ddi2* KO mice. Created with Biorender.com. b) Gene expression *Ddi2* in brown adipose tissue comparing wild type and *Ddi2* KO male mice (n=8). Data normalized to *Ywhaz* housekeeping gene. c) mRNA expression of proteasome subunit genes in brown adipose tissue of wild type and *Ddi2* KO male mice (n=8). Data normalized to *Tbp* housekeeping gene. Data is presented as mean ± SD. b) *t*-test. ****$p < 0.0001$. c) Two-way analysis of variance (ANOVA) followed by Sidak's multiple comparisons test was performed. *$p < 0.05$. Thanks to Dr. Gökhan S. Hotamışlıgil, Karen Inouye, and Jilian Riveros from Sabri Ülker Center Harvard T.H. Chan School of Public Health for performing mouse experiments and providing tissue samples.

3.1.5 Loss of Ddi2 disrupts UPS function

Moving forward with the project I wanted to investigate the activity of proteasome upon loss of Ddi2. I used commercial kits measuring degradation of fluorometric peptides by different subunits of proteasome complex. The simplest outcome of insufficient activity of proteasome is accumulation of ubiquitination proteins in cells. Immunoblots of cells undergoing loss of Ddi2 function showed a higher amount of accumulated proteins following PI treatment compare to scrambled controls (Fig. 22a). Similar to genetic manipulation, chemical inhibition of Ddi2 exacerbated effect of epoxomicin treatment in time dependent manner (Fig. 21b). To measure the activity of different subunits of proteins, I used an in-gel measurement analysis, native PAGE, which NFV-mediated inhibition of DDI2 led to lower activity of 30S proteasome subunit (Chymotrypsin-like subunit), followed by less expression of 26S subunit using α1-7 subunits antibody in immunoblot analysis (Fig. 21c).

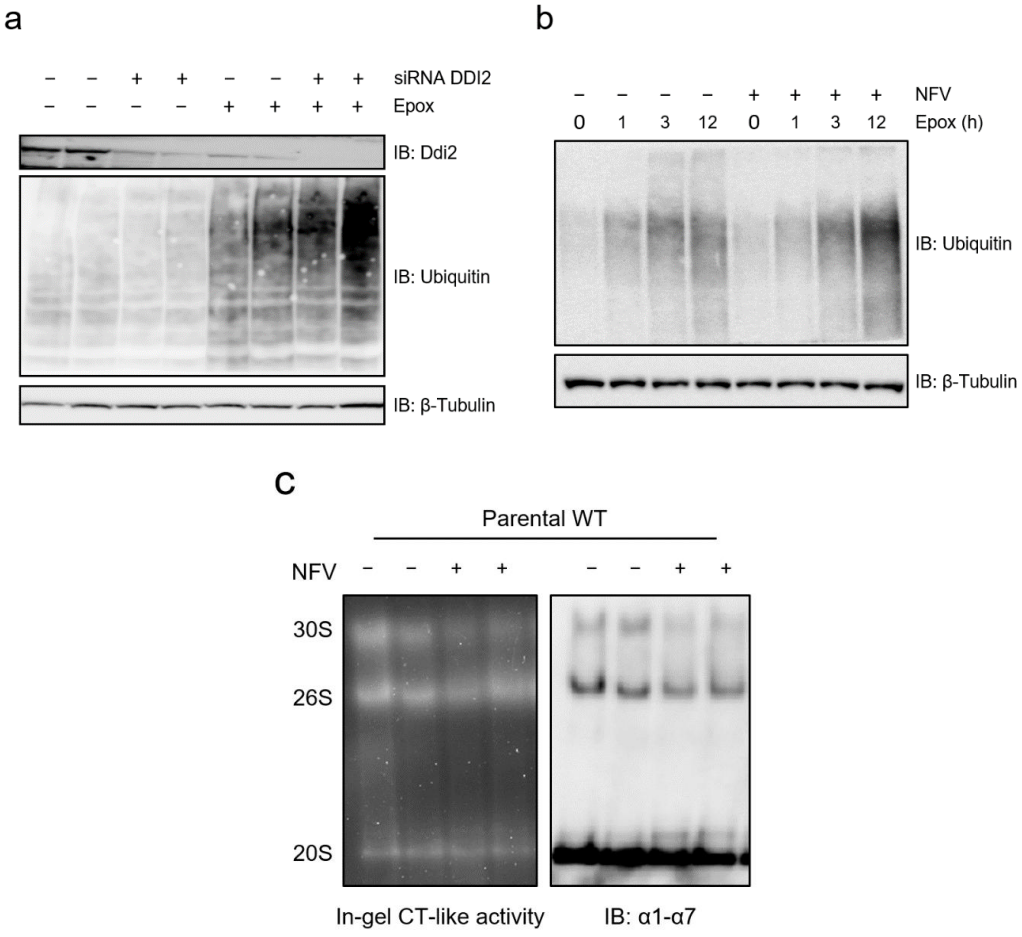

Figure 22: Insufficient protease activity of Ddi2 leads to accumulation of highly ubiquitinated proteins with high molecular weight and proteasome dysfunction. a) Immunoblot of Ddi2 and ubiquitin in differentiated WT-1 cells after transfection with *Ddi2* siRNA and 100nM epox treatment for 6h. b) Immunoblot of ubiquitin in EA.hy926 cells treated with 5 μM NFV for 12h and 100nM epoxomicin for indicated timepoints. c) Native PAGE of EA.hy926 cells treated with 10μM NFV for 20h and immunoblot of the α1-7 (20S) subunits. Figure adapted from (162).

To better understand the calibration of UPS and untangle Nfe2l1-dependant or -independent role of Ddi2 in these processes I performed a mass spectrometry-based analysis of the proteome and ubiquitinated proteins using the so-called Di-Gly method of immunoprecipitating ubiquitin remnant motifs that are produced by trypsin digestion (Schematic Fig 23. a). Here I used wild type and *Ddi2* KO EA.hy926 cells to make sure DDI2-dependentent activation of Nfe2l1 in completely blunted by knockout technology. GO analysis shows that the most impacted pathway is proteasome-mediated ubiquitin-dependent protein catabolic process (Fig. 23b). Volcano blot visualization showed an increase in ubiquitin levels upon ablation of DDI2 (Fig. 23c) which further proves the observed accumulation of ubiquitinated proteins in immunoblots of Ddi2 inhibited cells (Fig. 22a, b). Also, principal component analysis (PCA) displayed two markedly distant clusters comparing *DDI2* KO and parental wild type cells (Fig. 23d). In summary, these data demonstrate that loss of DDI2 can cause dysregulated proteostasis status, which leads to a global increase in ubiquitinated proteins within the cells in an opposite trend as of proteasome inhibitors.

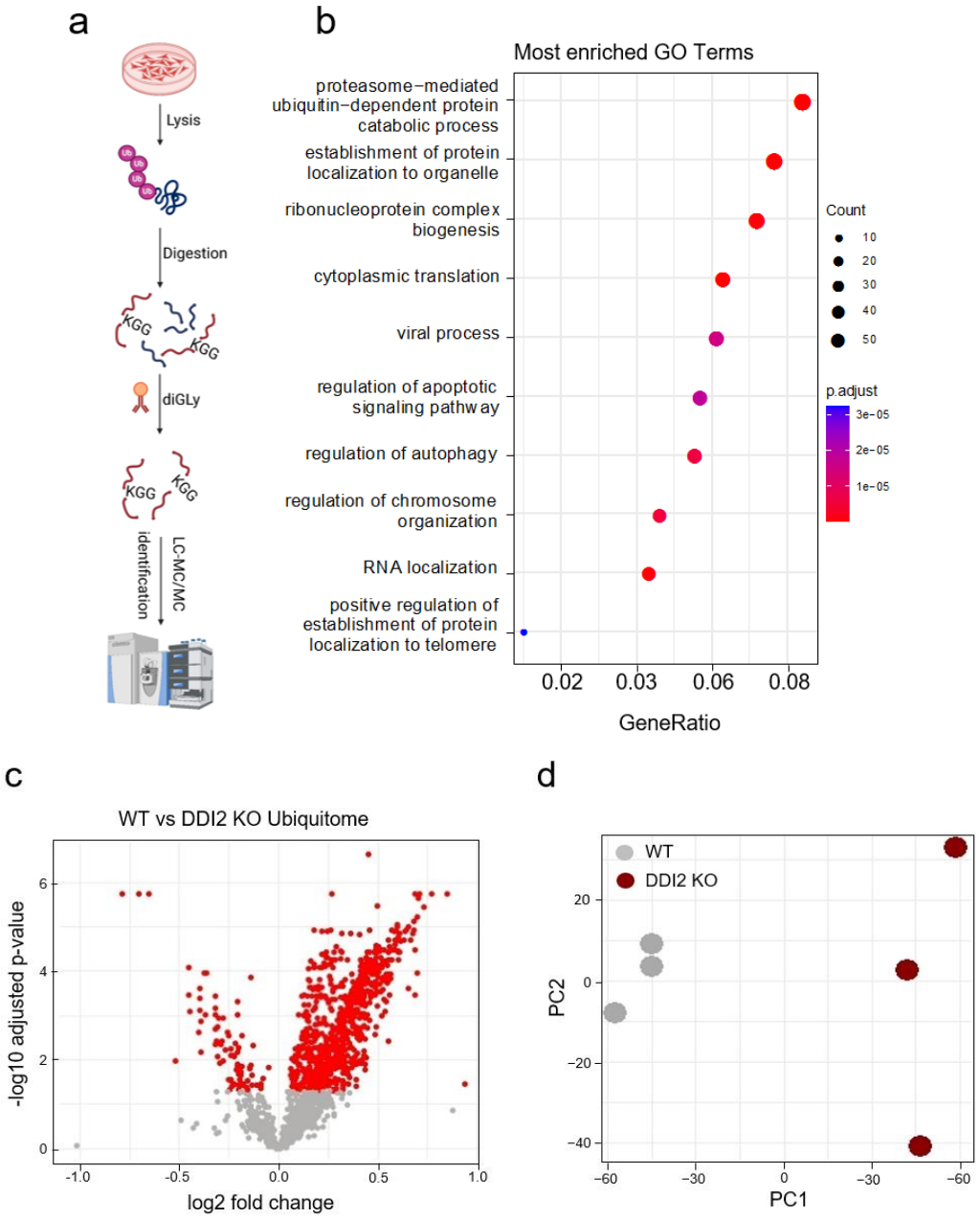

Figure 23: Remodeling of the ubiquitome in *DDI2* knockout cell models. a) Schematic Workflow for ubiquitomics analysis. Created with Biorender.com. b) Top 10 enriched gene ontology (GO) terms in the ubiquitome of EaHy926 *DDI2* KO compared to parental wild type cells. c) Volcano Plot of the ubiquitome in EaHy926 *DDI2* KO cells compared to parental wild type cells. P_{adj} < 0.05 indicated in red. d) Principal component analysis (PCA) of the ubiquitome of EaHy926 parental wild type cells vs. *DDI2* KO cells (n = 4 replicates). Figure adapted from (162).

3.1.6 Disruption in PTM of Nfe2l1 affects mitochondria function

Brown adipose tissue, as an active metabolic tissue, contains high content of mitochondria and brown adipocyte-specific deletion of Nfe2l1 in mice displays diminished mitochondrial function under thermogenic conditions (160). Therefore, it is crucial to test the effect of Ddi2-mediated activation of Nfe2l1 in mitochondrial function in context of non-shivering thermogenesis. To this end, I used the Seahorse Analyzer to measure NE-stimulated oxygen consumption followed by mitostress test. While knocking down *Ddi2* in WT-1 cells showed no significant changes compared to control cells (Fig. 24a, b), NFV-mediated inhibition of Ddi2 abolished NE-stimulated activation of brown adipocytes and led to lowe ATP production, carbonyl cyanide-4-(trifluoromethoxy)phenylhydrazone (FCCP)-induced (maximal capacity), and spare respiratory capacity compared to DMSO-treated cells (Fig. 24c, d). Due to discrepancy of this results, I checked whether different player of Nfe2l1 activation, which is deglycosylation by Ngly1, shows any effect on mitochodrial resiparation (Fig. 24e, f). These results indicates that post-translational modifications of Nfe2l1 by *Ngly1* KD and chemical inhibiton of Ddi2, but not *Ddi2* knockdown, plays a role in mitochondrial respiration and non shivering thermogenesis.

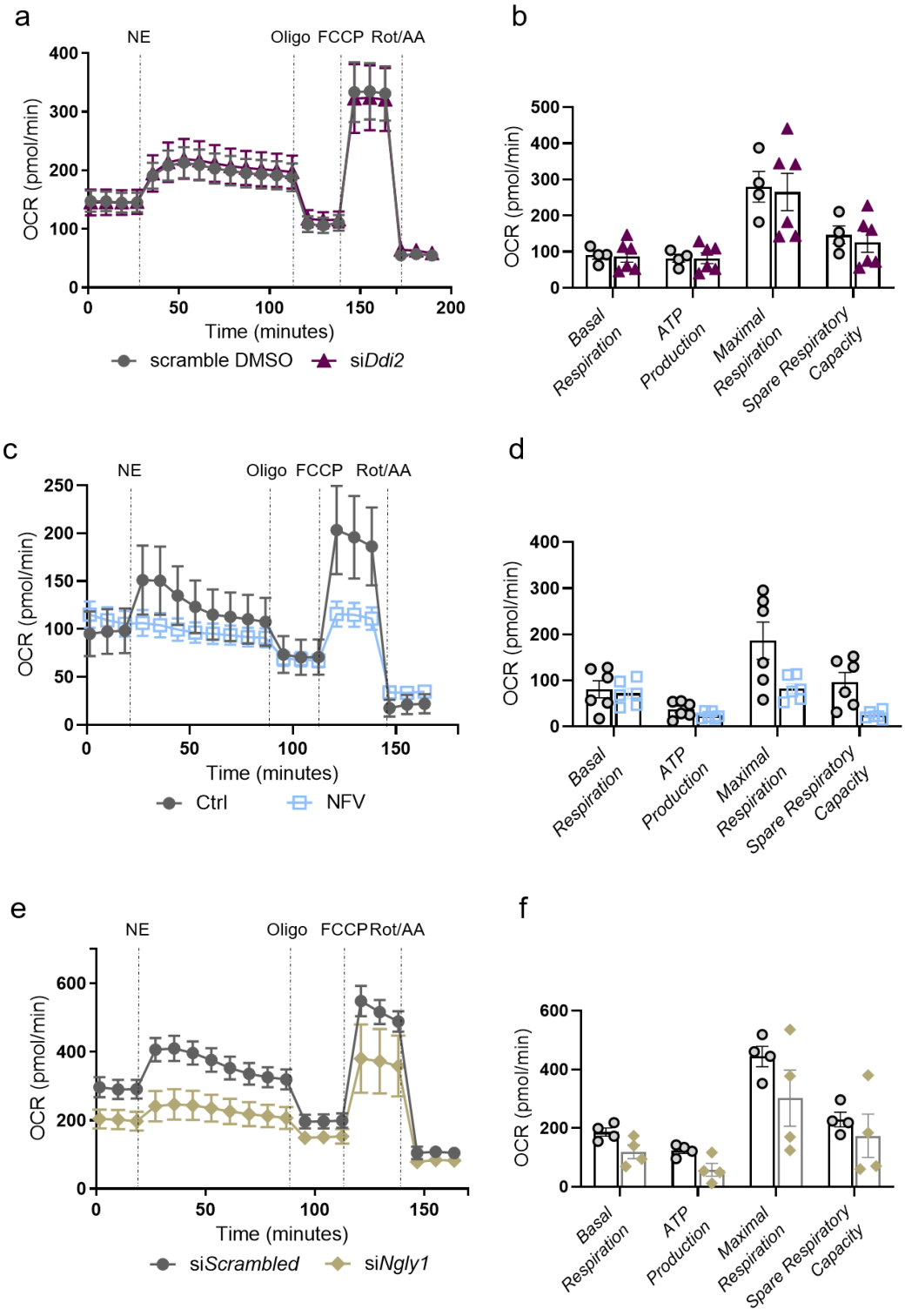

Figure 24: Disruption in Nfe2l1 activation pathways reduces OCR and mitochondrial respiration of brown adipocytes. a, b) OCR and calculated metabolic parameters in differentiated WT-1 cells upon transfection with *Scrambled* (n=4 replicates) and *Ddi2* siRNA (n=6 replicates). c,d) OCR and calculated parameters of OCR in differentiated WT-1 cells NFV (10µM) treatment for 3h (n=6 replicates). e-f) Oxygen consumption rate (OCR) and calculated parameters of OCR in differentiated WT-1 cells upon transfection *Ngly1* siRNA (n=4 replicates).

3.1.7 Loss of Ddi2 does not affect differentiation of brown adipocytes

Considering an increase in existing adipocyte function is required for highly metabolic demanding conditions, I checked if loss of Ddi2 interferes with adipocytes adipogenesis or differentiation. Here I used both *Ddi2*-silenced differentiated immortalized WT-1 cells and BAT tissue from *Ddi2* KO animal models. Silencing *Ddi2* in mature brown adipocytes did not cause any significant alteration in mRNA expression level of classical differentiation markers, Fatty acid binding protein 4 (*Fabp4*), Peroxisome Proliferator Activated Receptor Gamma (*Pparγ*), and Adiponectin (*Adipoq*), peroxisome proliferator receptor-γ, co-activator 1-α (*Pgc1α*, encoded by *Ppargc1a*) Glucose transporter type 4 (*Glut4*), and uncoupling protein-1 (*Ucp1*) (Fig. 25a). Similarly, except an increase in *Pparγ* in KO animals, no significant changes in *Ddi2* KO compared to wild type control mice was detected (Fig. 25b). To check the lipogenesis status of cells, Oil-red-O staining of mature brown adipocytes showed no changes in lipid content after *Ddi2* KD compared to control cells (Fig. 25c, d).

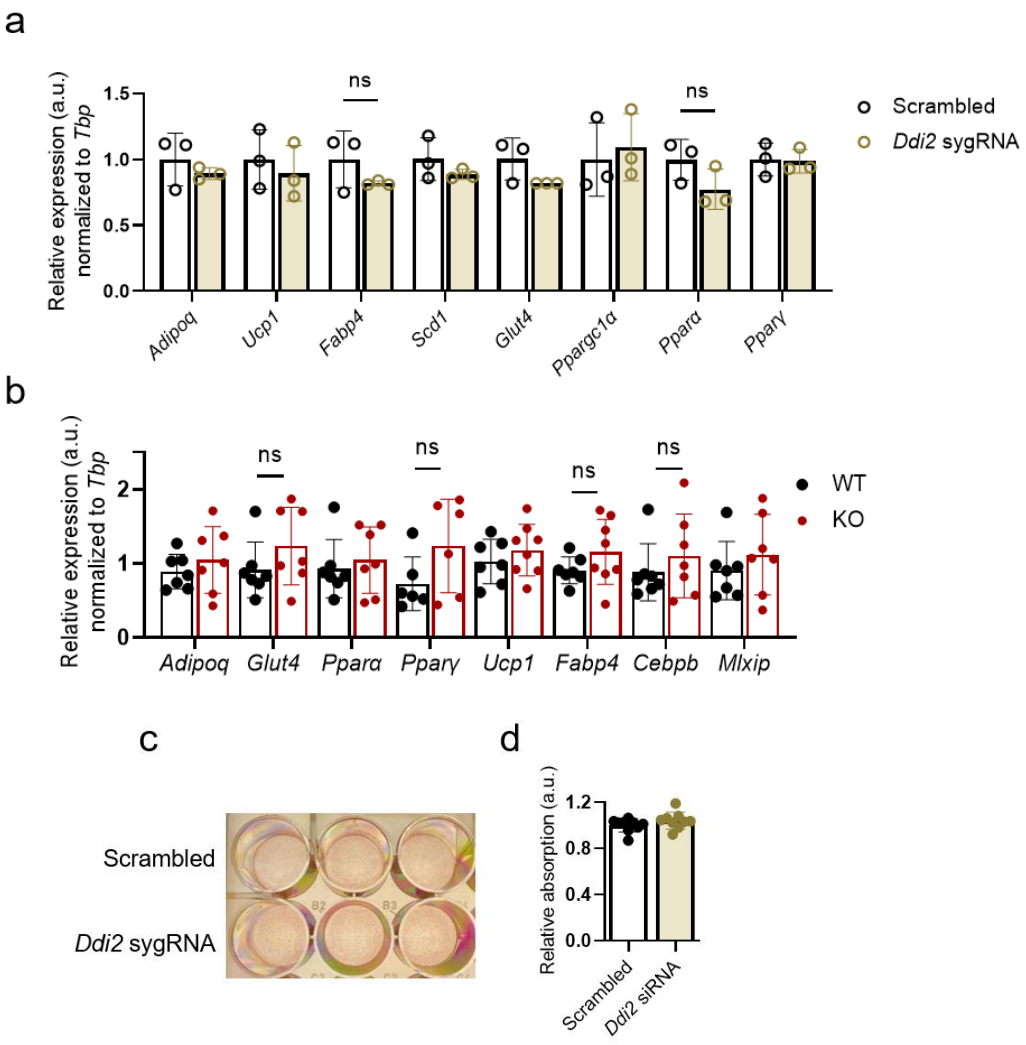

Figure 25: Loss of Ddi2 did not affect differentiation of brown adipocytes in vitro and in vivo. a) Gene expression of adipogenesis markers in differentiated WT-1 cells. b) mRNA expression level of adipogenesis markers in *Ddi2* KO and wild type mice (n=8 replicates). c) Oil-Red-O staining of differentiated WT-1 cells after transfection of Scrambled and *Ddi2* sygRNA (n=3 per group). d) Quantification of Oil-Red-O staining of differentiated WT-1 cells silenced with *Ddi2* siRNA (n=9 per group). Data is presented as mean ± SD. Two-way analysis of variance (ANOVA) followed by Tukey's multiple comparisons test was performed. *$p < 0.05$. Thanks to Dr. Gökhan S. Hotamışlıgil, Karen Inouye, and Jilian Riveros from Sabri Ülker Center Harvard T.H. Chan School of Public Health for performing mouse experiments and providing tissue samples.

3.1.8 Loss of Ddi2 do not cause any changes in BAT and energy metabolism function *in vivo*

It is vital to evaluate if *Ddi2*$^{\Delta BAT}$ disrupts metabolic activity of brown adipose. Therefore, I measured metabolic parameters of *Ddi2* KO and wild type control mice via indirect calorimetry. As first observation, these animals did not display any difference in food or water intake and body weight (Fig. 26a-c). Stimulation of whole-body oxygen consumption in vivo was performed by injection of a major physiologic activator of BAT, CL316,243. No difference was observed between *Ddi2* KO and control mice (Fig. 26d).

In line with this observation, respiratory exchange ratio (RER), as an indicator of fuel usage, of these two groups showed similar trend over the course of measurement (Fig. 26e). These data support the conclusion that Ddi2 dysfunction in brown adipose tissue does not alter energy metabolism of mice and has no significant BAT-specific phenotype.

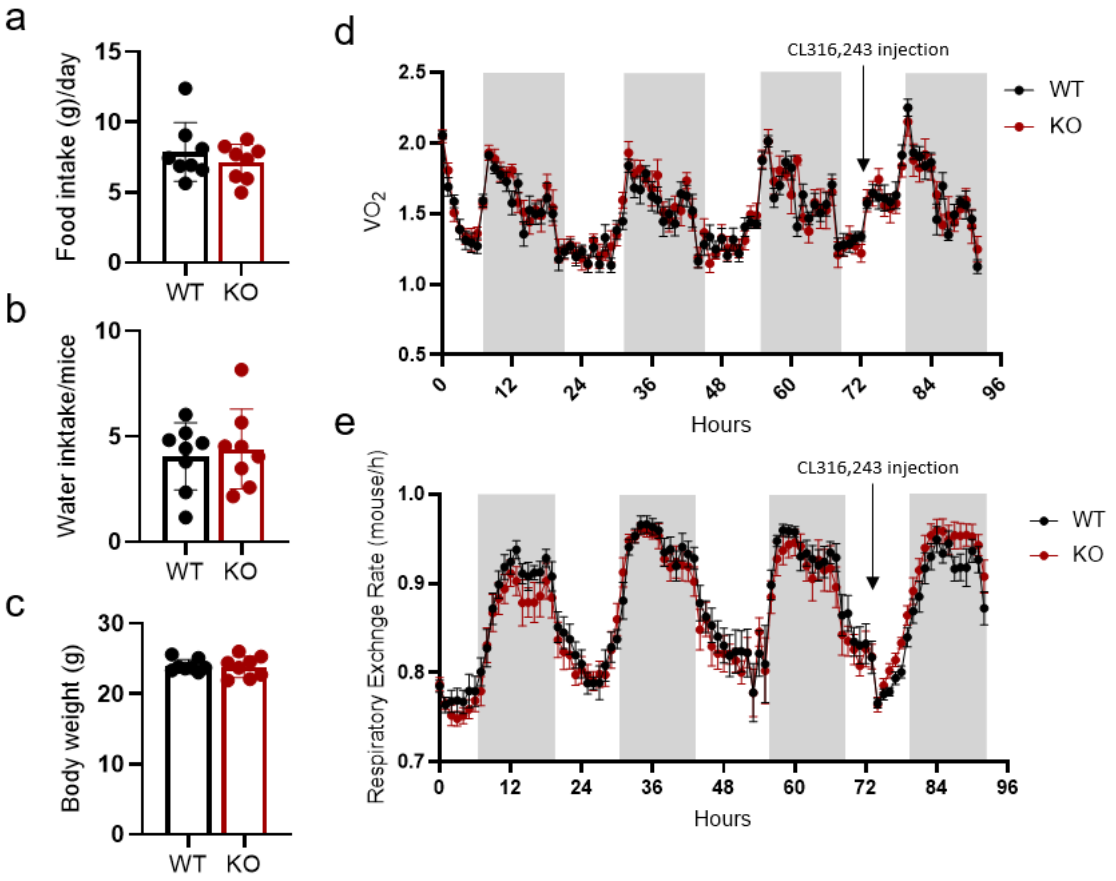

Figure 26: BAT-specific *Ddi2* knockout did not impact energy metabolism. Indirect calorimetry of WT controls and *Ddi2* KO mice (n=8 mice per group). a) Food intake. b) Water consumption. c) Weight gain. d) Time course of CL316,243 (CL)-stimulated oxygen consumption e) Time course of CL316,243 (CL)-stimulated respiratory exchange ratio (RER). Thanks to Dr. Gökhan S. Hotamışlıgil, Karen Inouye, and Jilian Riveros from Sabri Ülker Center Harvard T.H. Chan School of Public Health for performing mouse experiments and providing tissue samples.

3.2 Activating the NFE2L1-ubiquitin-proteasome system by DDI2 protects from ferroptosis

3.2.1 Proteasomal activity is diminished upon induction of ferroptosis cell death

It is largely unknown how induction of ferroptosis affects the ubiquitin proteasome system. It is crucial to differentiate between two different mechanisms: First, if proteasome dysfunction is a consequence of ferroptosis induction. Or second, UPS-dependent regulation of ferroptosis inducers such as GPX4 is playing the main role in this model (164). In order to study regulation of proteasome system I needed stable loss of Ddi2 via knockout technology in cells, but not partial silencing of *DDI2* by siRNA. Therefore, I performed experiments in EA.hy926 human cells in which *DDI2* was deleted by CRISPR/Cas9 technology. In the first observation, treatment of parental wild type cell lines with ferroptosis inducer RSL3 and proteasome inhibitor bortezomib (BTZ) led to accumulation of ubiquitinated proteins with high molecular weight. To prove that these observations are not simply off-target effect of RSL3, I used Ferrostatin-1 (Fer-1) as a well-known inhibitor of ferroptosis in cell models which displayed less ubiquitination (Fig. 27a). Based on this result, I further asked if this increase in ubiquitination level is the result of diminished proteasomal function. Indeed, induction of ferroptosis led to less activity in multiple proteasome subunits measured by commercial kit for degradation of fluorometric peptides and in gel activity of proteasome subunits by native PAGE analysis (Fig. 27b, c). The question arise was the possibility of off-target effect of RSL3 on proteasomal activity. Therefore, I measured fluorometric peptides degradation directly in cell lysates of parental WT cells at concentrations used in our cell assays. Unlike BTZ, RSL3 showed no direct inhibitory effect (Fig. 27d). These results exclude the possibility that the RSL3-induced decrease in proteasome activity and increase in ubiquitin levels in blots are cconsequences of off-target pharmacological inhibition of the proteasome by direct chemical binding of RSL3.

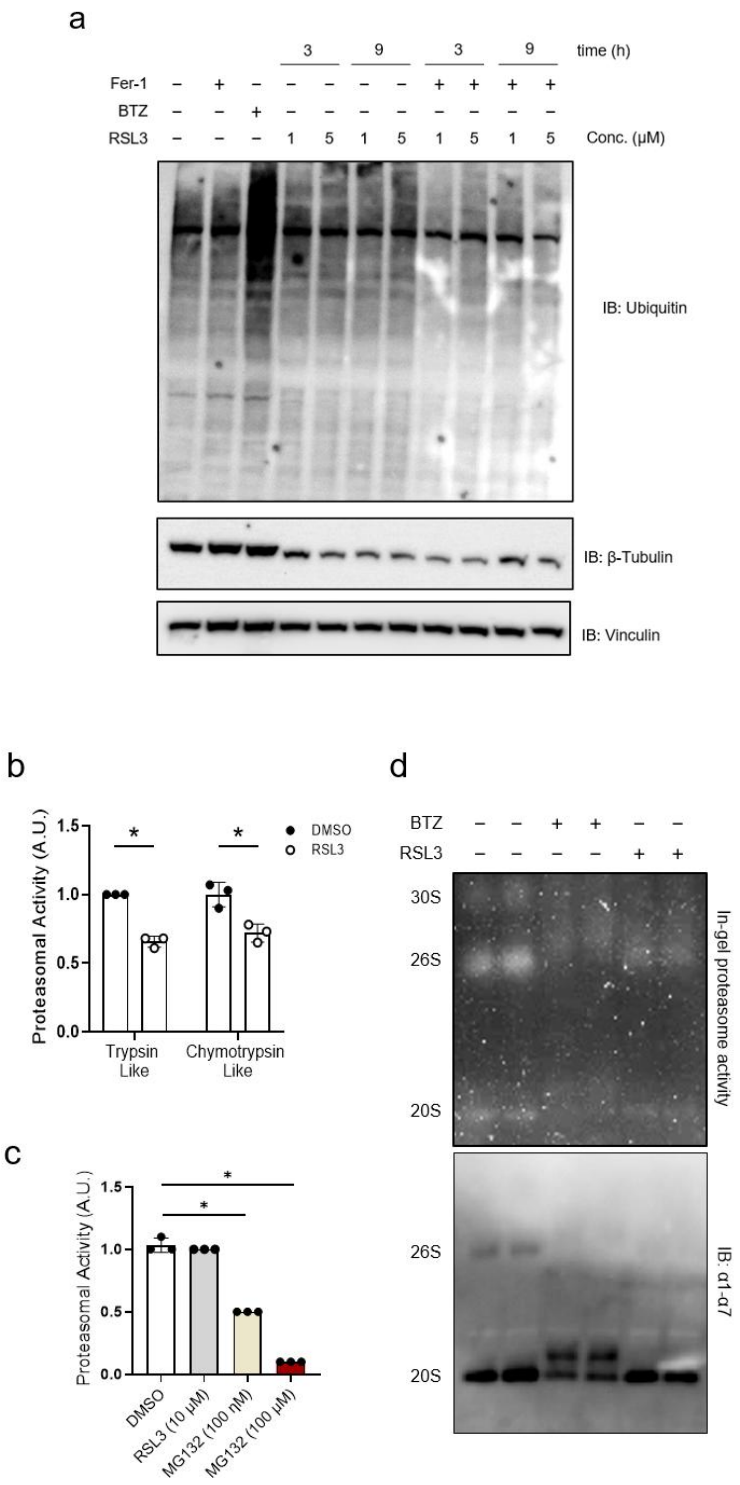

Figure 27: Remodeling of the ubiquitome in ferroptosis is distinct from proteasome inhibition. a) Immunoblot of ubiquitin from EA.hy926 cells treated with 5 μM RSL3 and 100 nM bortezomib (BTZ) for 9 h and 3 h, respectively. b) Proteasomal activity in EA.hy926 cells treated with 5 μM RSL3 for 3 h. c) Proteasomal activity assay in EA.hy926 cells with the extracts being incubated with indicated concentrations and time points of RSL3 and proteasome inhibitor MG132. d) Native page of EA.hy926 cells treated with 5 μM RSL3 and 100 nM BTZ for 6 h with in-gel activity and immunoblot of the α1-7 (20S) subunits. b-d) Figure adapted from (162). Data is presented as mean ± SD. b) One-way analysis of variance (ANOVA) followed by Dunnette's multiple comparisons test was performed. *$p < 0.05$. c) Two-way analysis of variance (ANOVA) followed by Sidak's multiple comparisons test was performed. *$p < 0.05$.

To better understand the calibration of UPS during ferroptosis, and study the nature of accumulated ubiquitinated proteins, I performed proteomics and ubiquitomics on RSL3-treated cells (23). Volcano blots showed an increase in ubiquitin levels upon RSL3 treatment (Fig. 28a). To determine how chemical inhibition of proteasome by BTZ and RSL3 affects the ubiquitome, I performed principal component analysis (PCA) which displayed three significantly apart clusters (Fig. 28b). This is an indication that ubiquitome remodeling induced by RSL3 is distinct from proteasome inhibition, e.g. by BTZ. Next, to better understand which pathways are hampered in the execution of ferroptosis, I analyzed the cellular pathways implicated in the remodeling of the ubiquitome. I found that gene ontology (GO) terms linked to UPS, cell death, cell cycle were among the differentially regulated pathways (Fig. 28c). KEGG pathway analysis of ferroptosis supported that RSL3 treatment leads to higher target-specific ubiquitination of ferroptosis markers (Fig. 28d). In conclusion, this set of data highlights the remodeling of the ubiquitome and elucidates an alteration in cell death signaling pathways by the UPS upon RSL3-induced ferroptosis.

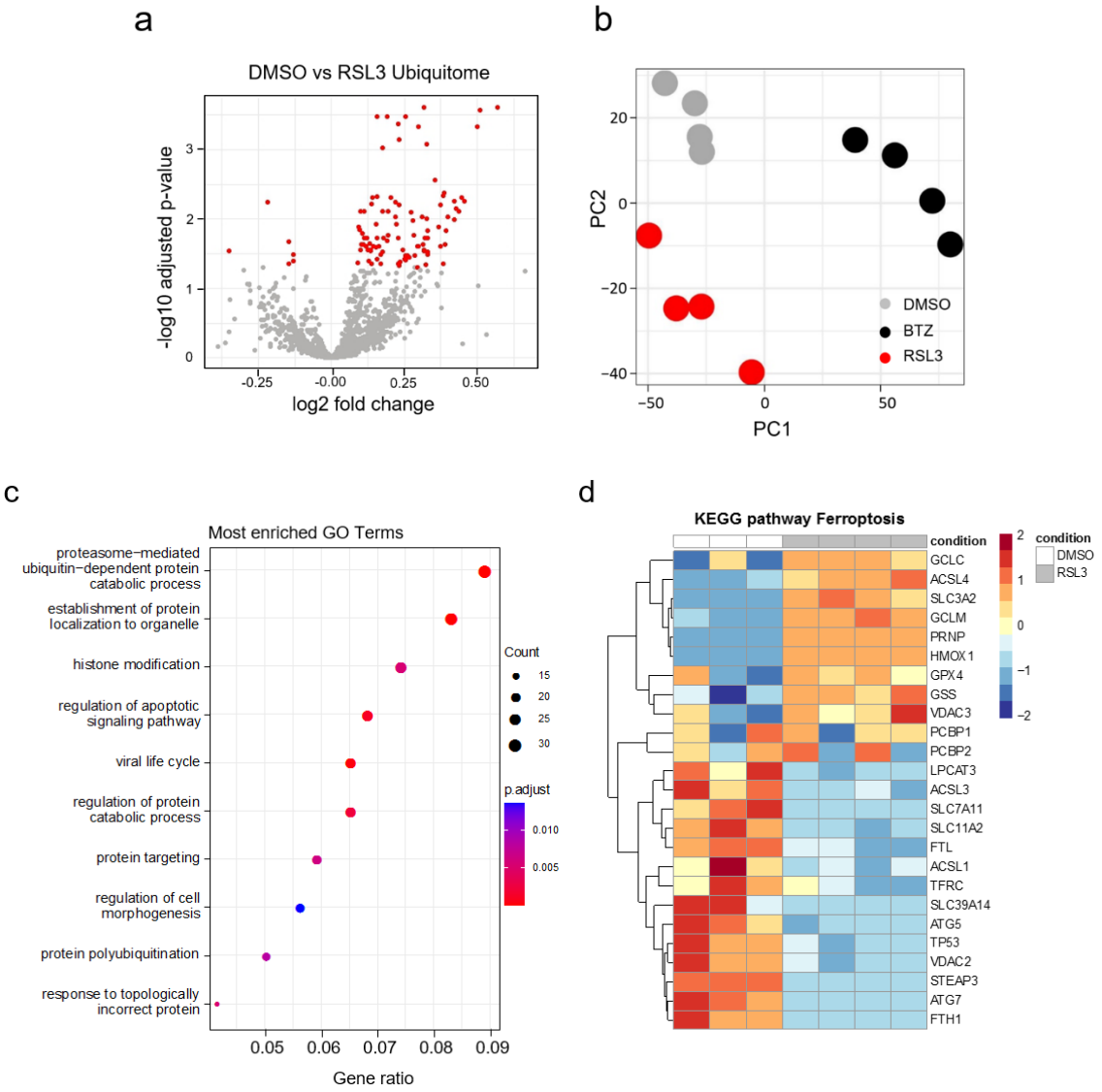

Figure 28: RSL3-induced calibration the UPS in ferroptosis. a-d) Analysis of the ubiquitome of parental wild type EA.hy926 cells treated with 5 µM ferroptosis inducer RSL3, 100nM proteasome inhibitor bortezomib (BTZ) and DMSO for 9h time course. (n = 4 replicates per group) a) volcano plot of the ubiquitome of EA.hy926 cells treated with RSL3 $P_{adj} < 0.05$ indicated in red. b) Principal component analysis (PCA) of the ubiquitome of cells treated with BTZ and RSL3. c) Top 10 enriched gene ontology (GO) terms in the ubiquitome cells treeated with RSL3. d) KEGG pathway analysis of ferroptosis from total proteome. Figure adapted from (162).

3.2.2 Activation of the NFE2L1-proteasome system by DDI2 upon ferroptosis induction

Transcription factor NFE2L1, as crucial regulator of proteasome function, protects cells in response to ferroptosis (154). I asked if the impact on UPS in my result is through activation of NFE2L1 and NFE2L1-dependant signaling in the cell. Indeed, RSL3 treatment led to higher protein levels of the cleaved fragment of NFE2L1 (ca. 95 kDa) and less full-length form of protein in a time- and dose-dependent manner (Fig. 29a). Nuclear fractionation of parental WT cells treated with increasing concentration of RSL3 showed higher levels of NFE2L1 in nuclear fraction of cells (Fig. 29b). Co-treatment with Fer-1

successfully restored RSL3-induced induction of NFE2L1 (Fig. 29c). Taken together, induction of ferroptosis with RSL3 induces activation and nuclear translocation of transcription factor NFE2L1 in a ferroptosis-specific manner as this effect can be reversed by ferroptosis inhibitor Fer-1.

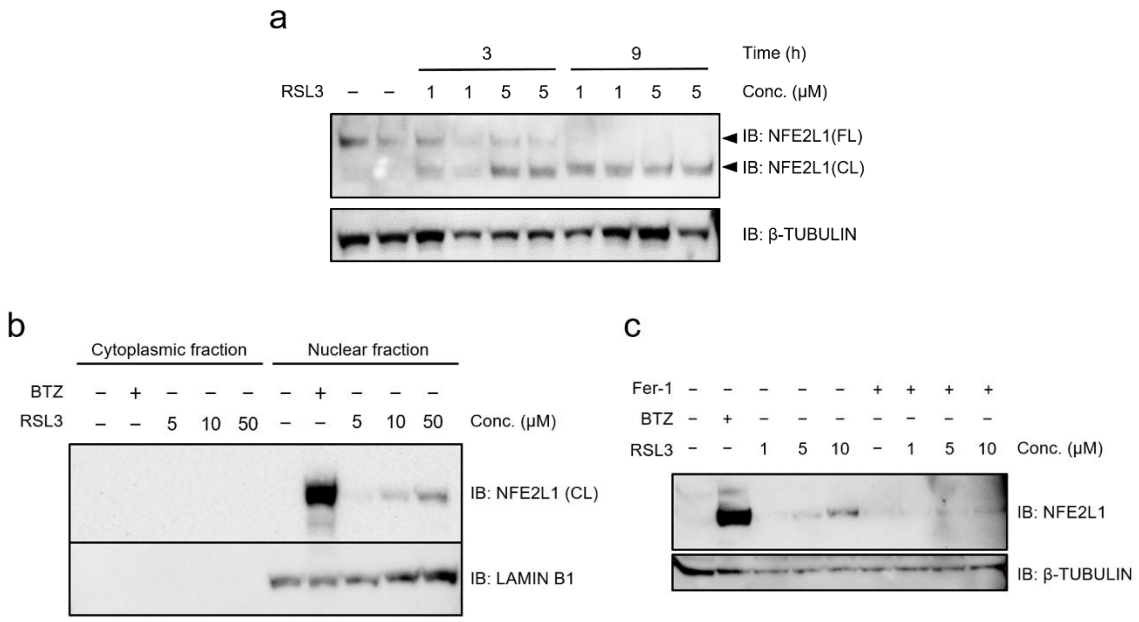

Figure 29: RSL3-induction of ferroptosis increased cleaved form of NFE2L1 and its translocation to the nucleus. a) Western blot of 120kDa (uncleaved full length) and 95 kDa (cleaved) NFE2L1 in parental WT EA.hy926 cells treated with RSL3 in time and concentrations indicated. b) Immunoblot of NFE2L1 in nuclear and cytoplasmic fractions isolated from EA.hy926 cells treated with 100nM BTZ and indicated concentrations of RSL3 for 3h. c) Western blot of NFE2L1 in EA.hy926 cells treated with 100nM BTZ for 3h, 10μM ferroptosis inhibitor Fer-1 and indicated concentrations of RSL3 for 9h. Figure adapted from (162).

3.2.3 Ddi2 is required for proteolytic processing of NFE2L1 during ferroptosis

Pervious experiments successfully showed the critical role of DDI2 in proteolytic activation of NFE2L1 in adipocytes (Fig. 16a & Fig. 17). However, I questioned if modulation of UPS in context of ferroptosis is also dependent on activity of DDI2 or not. Both BTZ and RSL3 led to activation of NFE2L1 in the parental WT cells. However, In the *DDI2* KO cells, no changes in NFE2L1 protein levels were observed (Fig. 30a). NFE2L1 activation also was diminished upon silencing *DDI2* with siRNA in Parental WT cells (Fig. 30b). Next, in order to prove that the activation of NFE2L1 is solely related to induction of ferroptosis, and not some off-target effect of RSL3 as a chemical, we reproduced the same results using FIN56 (Fig. 30c).

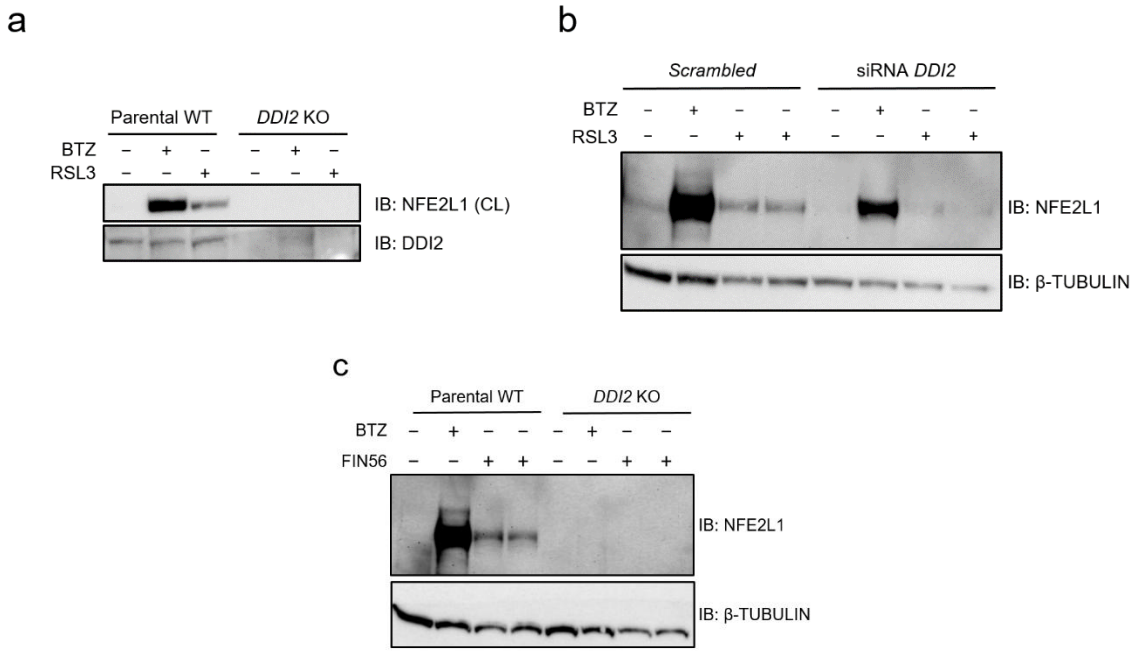

Figure 30: Ddi2 is required for proteolytic processing of NFE2L1 during ferroptosis. a) Immunoblot of NFE2L1 in Parental WT and *DDI2* KO cells treated with 5μM RSL3 and 100nM BTZ for 9 and 3h, respectively. b) Immunoblot of NFE2L1 EA.hy926 Parental wild type with si*Scrambled* and si*Ddi2* followed by 9h treatment with 5μM RSL3 or 3h treatment with 100nM BTZ. c) Immunoblot of NFE2L1 EA.hy926 wild type and *DDI2* KO cells treatment with FIN56 10μM for 9h or 100nM BTZ for 3h. Figure adapted from (162).

Chemical inhibition of DDI2 using Nelfinavir (NFV) upon BTZ and RSL3 treatment led to lower active NFE2L1 protein levels (Fig. 31a). In addition, no changes in gene expression of NFE2L1 was detected in response to chemical inhibition of DDI2 by NFV, indicating the role of DDI2 in specifically posttranslational modifications of NFE2L1 (Fig. 31b). Next, I measured nuclear translocation of NFE2L1 and its transactivation by binding of NFE2L1-UAS to a luciferase promoter in engineered HEK cells (165). When cells are

treated by NFV, nuclear translocation of NFE2L1 is enabled by DDI2 (Fig. 31d, e). Altogether, these results show that DDI2 facilitates the proteolytic activation and nuclear translocation of NFE2L1 upon induction of ferroptosis.

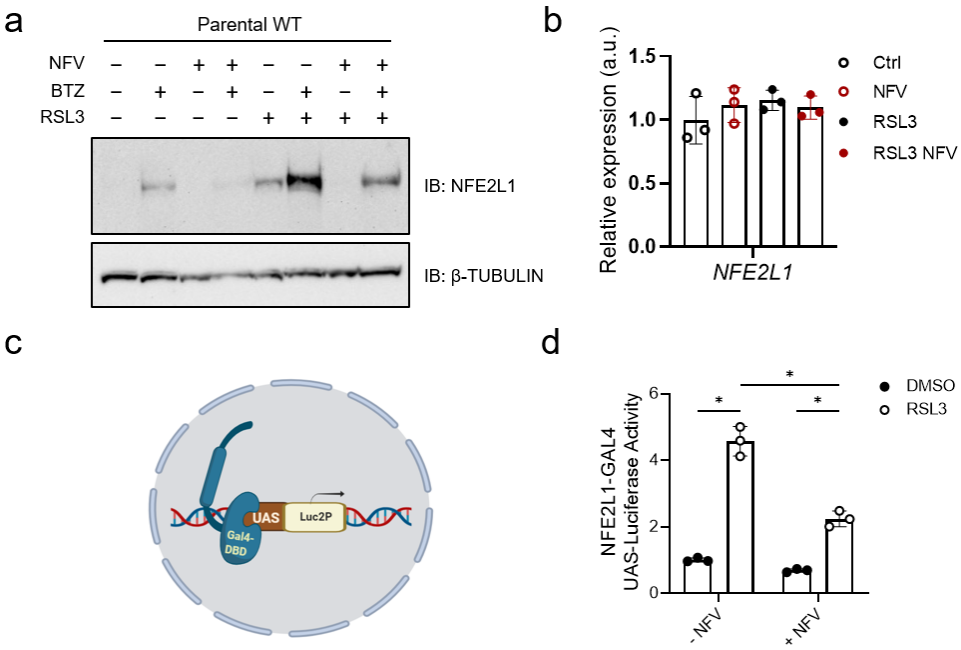

Figure 31: Protease activity of DDI2 during ferroptosis in inhibited by Nelfinavir (NFV). a) Immunoblot of NFE2L1 in parental WT cells after treatment with 50µM of NFV for 4h, 5µM RSL3 for 9h, and 100nM BTZ for 3h. b) *NFE2L1* mRNA levels of parental WT cells treated with 10µM of NFV and 5µM RSL3 for 9h. c) schematic illustration of NFE2L1-UAS luciferase reporter system. Created with Biorender.com. d) NFE2L1 luciferase nuclear translocation reporter assay in HEK293a cells after 24h treatment with 5µM of NFV and 20h treatment with 5µM RSL3. Figure adapted from (162). Data is presented as mean ± SD. Two-way analysis of variance (ANOVA) followed by Sidak's multiple comparisons test was performed. *$p < 0.05$.

3.2.4 Protease DDI2 is required for securing proteasome activity during ferroptosis

To study the impact of DDI2-NFE2L1 pathway for maintaining proper proteostasis in response to ferroptosis inducers I analyzed ubiquitination levels of parental WT and *DDI2* KO cells after BTZ and RSL3 treatment. In both cases, *DDI2* KO cells showed an accumulation of slow migrating ubiquitinated proteins in immunoblots, highlighting the necessity of DDI2 in adaptation of proteostasis during ferroptosis (Fig. 32a). Next, I checked if activity of proteasome is affected by DDI2 inhibition in context of ferroptosis. Measuring degradation of fluorometric peptides showed lowered activity in the trypsin-like subunit of proteasome in cells treated with NFV (Fig. 32b). These results show that DDI2 is needed for sustaining proteasomal function during ferroptosis.

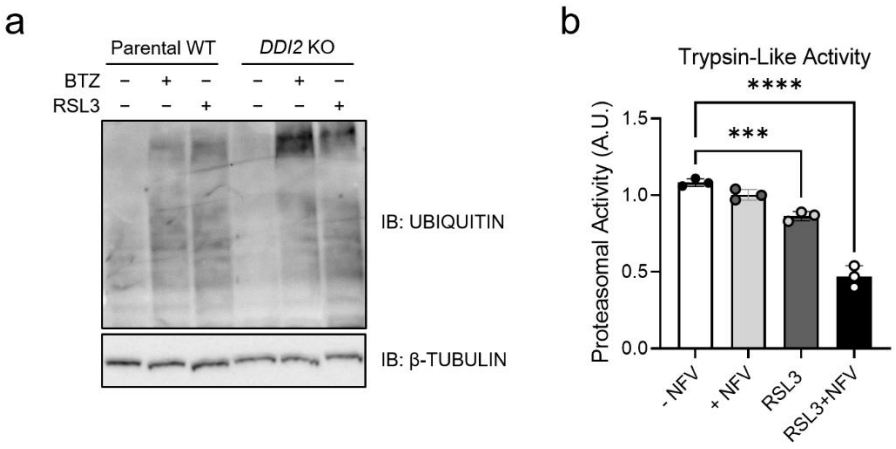

Figure 32: Loss of DDI2 leads to lower proteasomal activity during ferroptosis. a) Immunoblot of ubiquitin in EA.hy926 parental WT and *Ddi2* KO cells treated with 5μM RSL3 and 100nM BTZ for 9 and 3h, respectively. b) Proteasomal activity of EA.hy926 cells treated with 5μM NFV for 9h and of 5μM RSL3 for 3h. Figure adapted from (162). Data is presented as mean ± SD. One-way analysis of variance (ANOVA) followed by Dunnette's multiple comparisons test was performed. ***$p < 0.001$, ****$p < 0.0001$.

3.2.5 DDI2-mediated PTM of NFE2L1 protects from ferroptotic cell death

Cell death is the main outcome of ferroptosis induction. Therefore, it is crucial to check the viability of DDI2 deficiency in cells that are either chemically or genetically susceptible to ferroptosis. *DDI2* KO cells displayed less survival to RSL3-induced ferroptosis compared to the parental WT cells (Fig. 33a). Moreover, to check if targeting proteolytic activity of DDI2 sensitizes cells to ferroptosis, I treated cells with NFV, which increased the cytotoxicity of RSL3, followed by Fer-1 treatment to reverse this effect (Fig. 33b). More-

over, silencing both *NFE2L1* and *DDI2* using siRNA decreased viability of primary fibroblasts from a patient with Sedaghatian-type Spondylometaphyseal Dysplasia (SSMD), carrying mutant GPX4 compared to parental healthy controls (Fig. 33c).

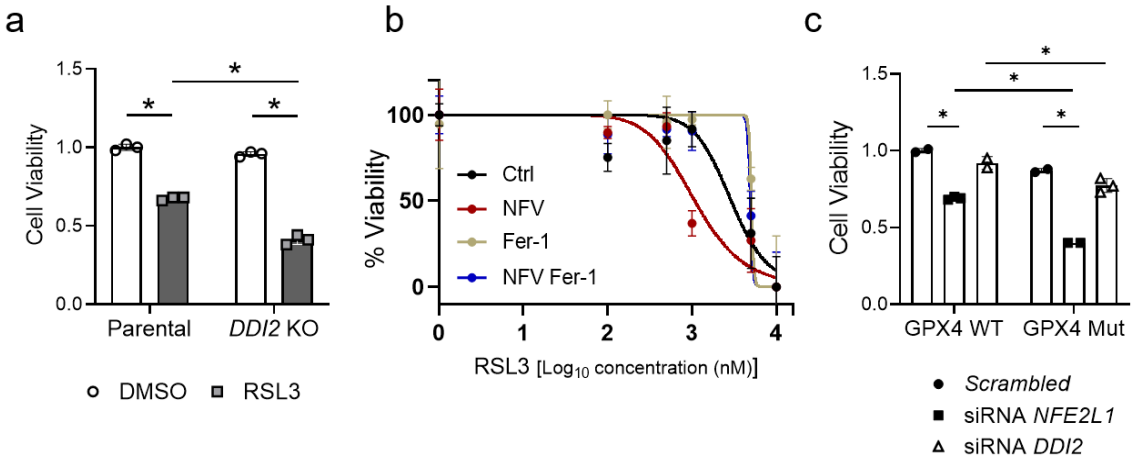

Figure 33: Loss of DDI2 sensitizes cells to chemical and genetic ferroptosis. a) Cell viability of *DDI2* KO versus parental WT EA.hy926 cells after 20h of treatment with 5µM RSL3. b) Cell viability in EA.hy926 cells treated with 5µM NFV and 10µM Fer-1 for 20h. c) Cell viability of SSMD cells (*GPX4* mut) and healthy controls (*GPX4* WT) after siRNA-mediated silencing of *NFE2L1* and *DDI2*. Figure adapted from (162). Data is presented as mean ± SD. Two-way analysis of variance (ANOVA) followed by Tukey's multiple comparisons test was performed. *p < 0.05.

Proteolytic processing of NFE2L1 is not the only posttranslational modification required for its activation. NGLY1 plays a critical role in the deglycosylation of NFE2L1 and modulates susceptibility of cells to ferroptosis. In line with this background, WRR139, as the chemical inhibitor of NGLY1 activity, diminished NFE2L1 activation in immunoblot (Fig. 34a). To investigate the effect of DDI2 absence under ferroptotic conditions I used two constructs to cells: wild type NFE2L1 (NFE2L1 WT) and NFE2L1-8ND mutant, which contains mutations in the glycosylation sites and is considered constitutively active (153). Viability assay of cells transfected by NFE2L1-8ND construct, followed by RSL3 treatment, showed no difference compare to wild type of NFE2L1 (Fig. 34b), which further validates that uncleaved deglycosylated NFE2L1 is not protector against ferroptosis. Unlike *DDI2* KO cells, BTZ- and RSL3-induction showed higher level of cleaved form of NFE2L1 in parental cells. This effect was not overcome by transfection of the 8ND mutant form of NFE2L1 to *DDI2* KO cells (Fig. 34c). In summary, these experiments highlight the crucial role of DDI2 in NFE2L1 posttranslational modification processes and subsequent protection from ferroptosis.

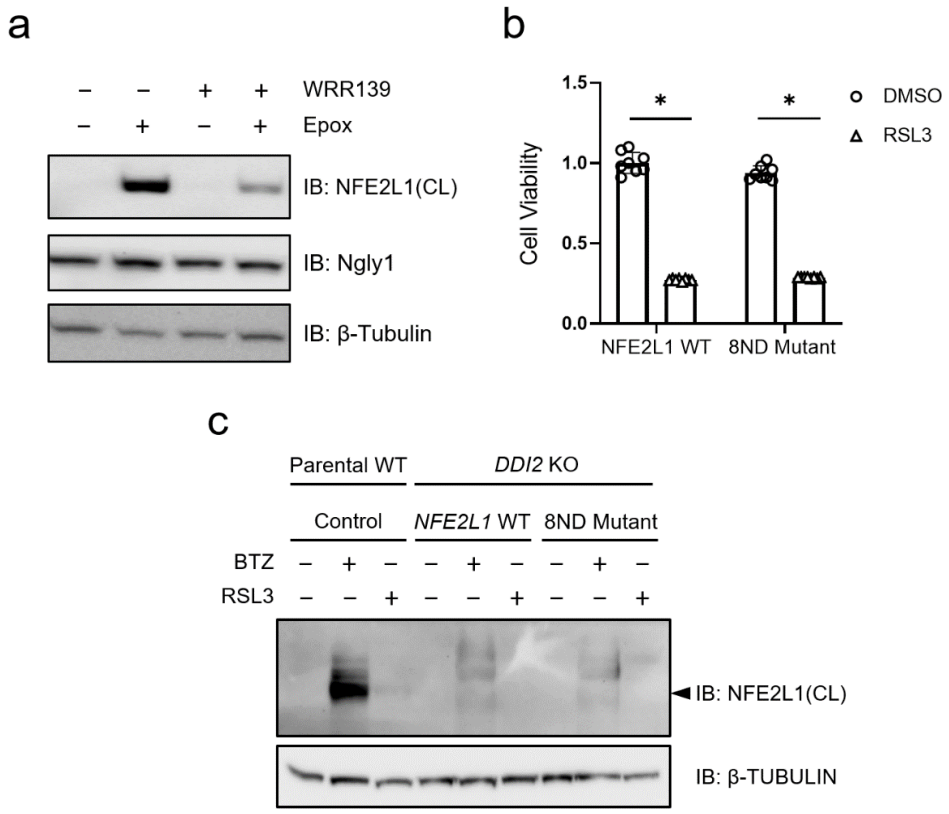

Figure 34: Proteolytic cleavage by DDI2 is required prior to deglycosylation of NFE2L1 by NGLY1. a) Immunoblot of NFE2L1 and NGLY1 in parental WT EA.hy926 cells treated with 10 µM NGLY1 inhibitor WRR139 and 100nM proteasome inhibitor epoxomicin for 12 and 3h, respectively. b) Cell viability of *DDI2* KO cells transfected with wild type NFE2L1 and NFE2L1-8ND mutant plasmids followed by 9h treatment with 5µM RSL3. d) Immunoblot of 95 kDa cleaved form of NFE2L1 in parental WT and *DDI2* KO EA.hy926 cells transfected with WT NFE2L1 and NFE2L1-8ND mutant plasmids followed by 9h treatment with 5µM RSL3 and 100nM BTZ. b, c) Figure adapted from (162). Data is presented as mean ± SD. Two-way analysis of variance (ANOVA) followed by Tukey's multiple comparisons test was performed. *$p < 0.05$.

3.2.6 Higher sensitivity to ferroptosis in immortalized brown adipocytes

EA.hy926 cells showed very resistance to ferroptosis induction in all my experiments. Therefore, in the next step I induced ferroptosis by RSL3 in immortalized brown preadipocytes WT-1 (undifferentiated). Unlike EA.hy926 cells, which requires micro molar concentrations of RSL3 for death induction, 68.13nM of RSL3 induced 50% cell death in WT-1 undifferentiated adipocytes (Fig. 35a). This effect successfully was reversed by ferroptosis inhibitor Fer-1 treatment (Fig. 35b). As shown before, induction of NFE2L1 happens in course of ferroptosis. Hence, I repeated the same experiments in a more sensitive WT-1 preadipocyte cell line which 50nM and 100nM concentrations of RSL3 significantly induced cleaved form of NFE2L1 in immunoblot analysis (Fig. 35c). Furthermore, increasing concentrations of RSL3 did lead to accumulation of ubiquitinated proteins in the immunoblots (Fig. 35c). To further prove the induction of NFE2L11 is the result of ferroptosis, and not an off-target effect of RSL3, I treated the cells with Fer-1, which diminished NFE2L1 cleaved band (Fig. 35d).

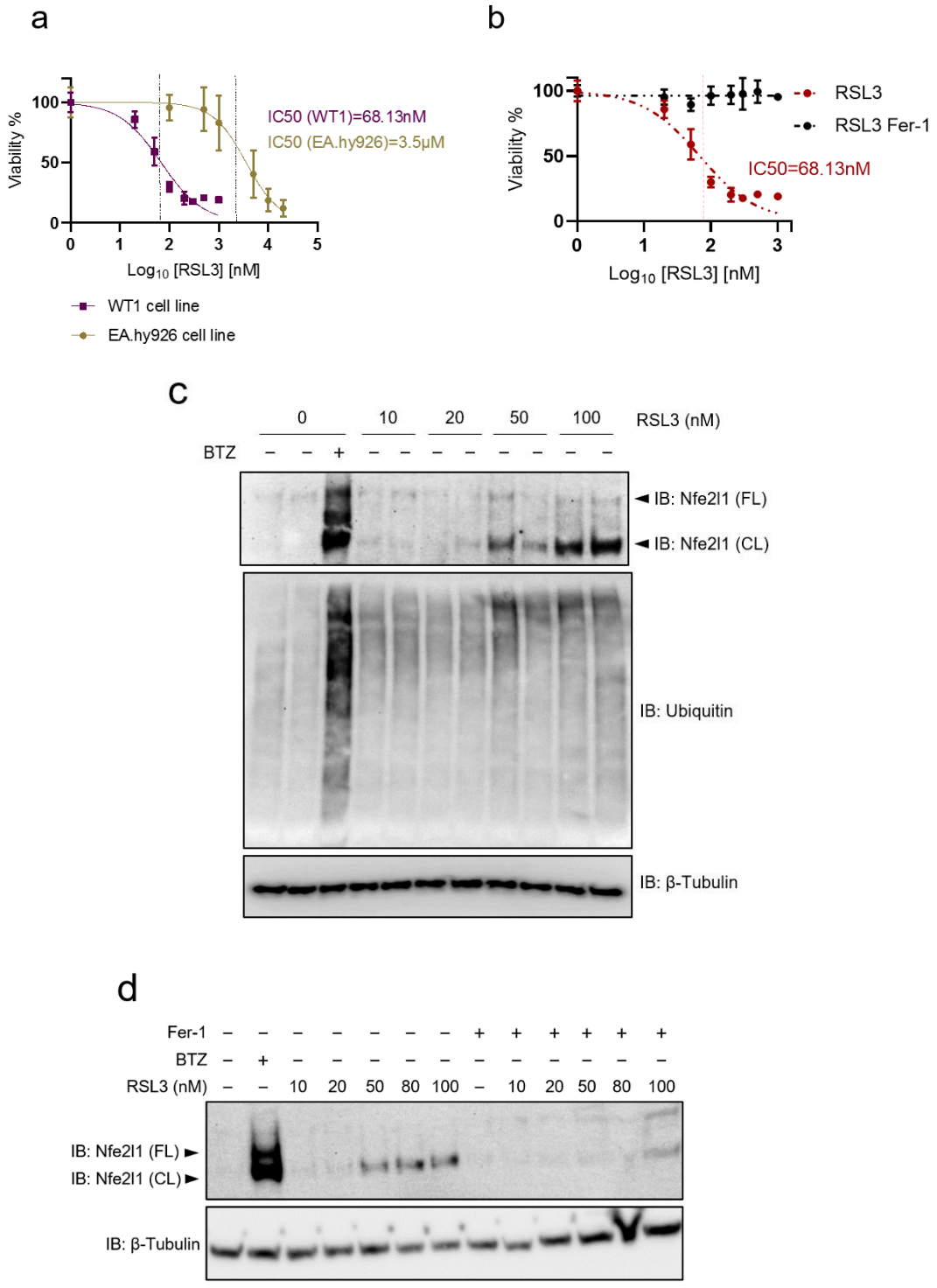

Figure 35: Preadipocytes are highly sensitive to RSL3-induced ferroptosis. a) LC50 of RSL3 in WT-1 and EA.hy926 cells treated with increasing concentrations of RSL3 for 20h. b) RSL3 dose-response curve in the presence or absence of 10 µM Ferrostatin-1 (Fer-1) for 20h in undifferentiated WT-1 preadipocytes. c) Impact of RSL3 treatment for 6 h on NFE2L1 and ubiquitin levels in undifferentiated WT-1 preadipocytes. d) Effects of co-incubation with 10 µM Fer-1 in undifferentiated WT-1 preadipocytes.

Similar to previous results in EA.hy926 cells, inhibition of DDI2 either genetically by siRNA or chemically by NFV led to lower NFE2L1 protein level in immunoblots of RSL3-treated WT-1 preadipocytes (Fig. 36a, b). Cell viability assay also showed more susceptibility to cell death in DDI2-inhibited cells (Fig. 36c). In summary these data proves that different cell lines display higher or lower sensitivity to ferroptosis and DDI2/NFE2L1 pathway is a protector against this form of cell death.

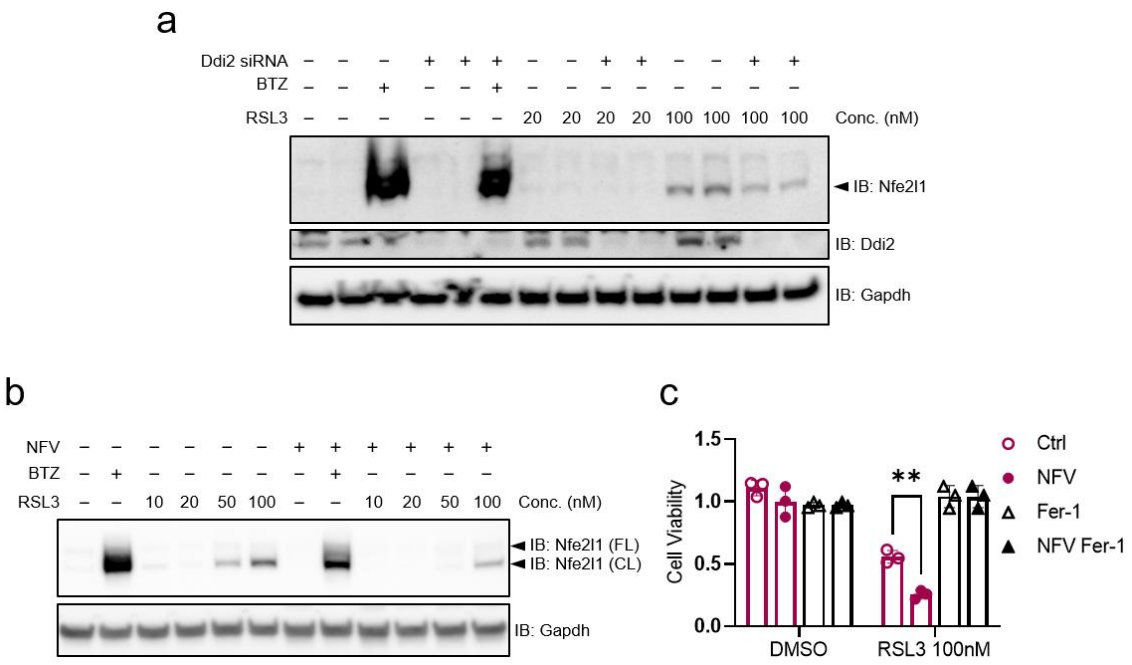

Figure 36: NFV-mediated inhibition of DDI2 in ferroptosis leads to less NFE2L1 cleavage at nanomolar concentrations. a, b) Treatment with 50 nM Bortezomib for 3 h. a) effects of co-treatment of *scrambled* and *DDI2*-siRNA transfected cells with 10 µM Fer-1 and RSL3. b) Effect of NFV on RSL3-dependent NFE2L1 protein for 6h. c) RSL3-dependent cell viability with co-treatments of either 10 µM NFV or 10 µM Fer-1 for 20 h. Data is presented as mean ± SD. Two-way analysis of variance (ANOVA) followed by Tukey's multiple comparisons test was performed. **$p < 0.01$.

4. Discussion

4.1 Ddi2-mediated cleavage of Nfe2l1

BAT is considered a high metabolically active tissue which by using intracellular and circulating nutrients can positively improve overall metabolic health. Endoplasmic reticulum is the key organelle for maintaining homeostasis balance by enhancing protein folding via unfolded protein response (UPR) or clearing damaged proteins via ubiquitin proteasome system (UPS) (55). In the first step of my thesis, I investigated the role of the Ddi2/Nfe2l1 pathway in UPS from two perspectives: 1) Nfe2l1-dependant proteasome biosynthesis, or 2) alterations in proteasome activity.

To begin with, I examined whether the loss of Ddi2 hinders the increase in proteasome biosynthesis through Nfe2l1 activation and bounce-back response. In order to produce the cleaved active form, full-length form of Nfe2l1 tethered in the ER-membrane undergoes multiple PTM steps in the cytosol. Ddi2 and Ngly1 are among many players in Nfe2l1 PTM processes, which in the end lead to the translocation of the deglycosylated cleaved form of Nfe2l1 to the nucleus to increase *Psm* genes expression and proteasome synthesis (97, 98). Supported by literature, Ddi2 deficiency shifts the balance in favor of the uncleaved form of Nfe2l1 compared to the cleaved form with no alterations in *Nfe2l1* mRNA level. This observation suggests that Ddi2 acts solely through post-translational modification of pre-existing Nfe2l1, rather than through changes at the pre-translation or gene expression levels. Having established that Nfe2l1 undergoes cleavage by Ddi2, the subsequent step involves the translocation of Nfe2l1 to the nucleus. In addition, I aimed to investigate whether Ddi2 itself translocates to the nucleus and potentially acts as a shuttle for Nfe2l1 translocation or not. Despite conducting nuclear fractionation experiments that confirmed increased translocation of Nfe2l1 into the nucleus, the hypothesis regarding Ddi2 could not be validated, as it appears that Ddi2 is primarily present in the cytosol. Ddi2 contains a C-terminus retroviral aspartyl protease (RVP) domain, similar to what can be found in human immunodeficiency virus (HIV-1) protease. Based on several previous studies, the inhibition of Ddi2 proteolytic activity by nelfinavir (NFV), as the FDA approved drug against HIV, can potentiate cytotoxicity of proteasome inhibitors (166). NFV-mediated inhibition of Ddi2 displayed lower level of cleaved Nfe2l1 protein with no effect on mRNA expression level.

Using siRNA-mediated gene knockdown technology and chemical inhibition of Ddi2 by NFV were primarily suitable approaches for the aims of my project. However, due to challenges in generating stable knockout adipocyte-specific cell models, I utilized human EA.hy926 cells in certain experiments to examine the complete loss of DDI2. In these

cells *DDI2* was completely knocked out via using CRISPR/Cas9 technology (64). Taking advantage of structural characteristics in Ddi2, containing RVP and UBL domains, Koizumi et al. re-expressed two different mutant form of DDI22 in HEK293A cells followed by proteasome inhibitor bortezomib treatment (98). Replacing aspartic acid 252 in the active site of DDI2 by asparagine to produce protease-dead DDI2 (D252N) did not rescue Nfe2l1 cleavage process in *DDI2* KD cells. They also showed that DDI2 mutant, which lacks UBL domain, could partially restore the *DDI2* KD effect, which suggests a potential role of UBL domain the cleavage activity. Similarly, Re-expression of the wild type Ddi2, but not the protease-dead (D252N) construct, successfully restored the cleavage of Nfe2l1 in blots in my study. Up to this point, these results have not been particularly surprising yet crucial to prove the proper cleavage activity of Ddi2. However, what is of greater importance is investigating if Nfe2l1 bounce back response and proteasome biosynthesis is dependent on Ddi2 presence and activity.

4.2 Genetic deficiency of Ddi2 does not affect transcriptional activity of Nfe2l1

Mimicking proteotoxic stress by treating cells with PI increases the gene expression of proteasome subunits in the context of BAT function (160). Previous studies reported similar results regarding necessity of Ddi2 for activation of Nfe2l1 to compensate for proteasome dysfunction (98, 119). Multiple myeloma cells require effective DDI2/NFE2L1 pathway mechanisms for their survival against PI-induced proteotoxic stressor (119). Interestingly, the link between Ddi2 and proteasome homeostasis is not limited to only PI, but also heavy metal mediated toxicity such as Cadmium (167). Therefore, it was expected that cells in which *Ddi2* is silenced would struggle to match the increase in *Psm* gene expression. However, I detected no significant difference in the of *Psm* gene expression comparing *Ddi2*-silenced and control cells in my experiments. While the mRNA expression of various *Psm* genes were initially increased in response to proteasome inhibitors, KD of *Ddi2* did not reverse this increase. I considered two potential explanations contributed to this observation: the efficiency of siRNA transfection protocol or PI treatment. To check siRNA effectiveness, when transfecting *Nfe2l1* siRNA, cells are not able to increase expression of PSM genes after PI treatment. Indeed, co-treatment with epoxomicin led to lower expression of multiple proteasome subunits such as *Psma2*, *Psmb4*, *Psmc3*, *Psmd1* in *Nfe2l1*-silenced cells (Supplementary Fig. 1a). The other possible explanation could be insufficient inhibition of proteasome by commercially available PIs. The significant increase in ER and oxidative stress markers *Atf3* and *Ddit3* (also known as *CHOP*) in epoxomicin treated cells confirmed effectiveness of PI treatment. To ensure these results are not cell specific, the same experiments were repeated in 3T3L1

cell line as immortalized white adipocytes. In absence of *Ddi2*, 3T3L1 cells also adequately compensate for proteasome inhibition at the level of *Psm* gene expression.

In vivo mouse model, wherein *Ddi2* is genetically ablated in all *Ucp1*-expressing cells, represented a more robust tool to evaluate the significance of my *in vitro* findings. Both wild-type and BAT-specific *Ddi2* KO animals exhibited successful biosynthesis of new proteasomes in BAT tissues. Due to limited access to animals and the apparent lack of phenotype in *Ddi2* KO mice, I did not pursue further experiments such as cold exposure or feeding animals with special diets.

So far, both *in vitro* and *in vivo* experiments displayed no difference in Nfe2l1-mediated proteasome biosynthesis in genetically manipulation of *Ddi2*. However, next result regarding chemical inhibition of Ddi2 by NFV was intriguing. Unlike genetic manipulation, when treating cells with NFV and PI, cells were unable to increase *Psm* gene expression. Therefore, this unanswered question remains that why there is discrepancy between genetic and chemical inhibition of Ddi2 concerning *Psm* gene expression and proteasome biosynthesis.

4.3 Ddi2/Nfe2l1 pathway regulates UPS

In the previous chapter, I focused on the Nfe2l1-dependant effect of *Ddi2* manipulation on *Psm* gene expression and biosynthesis of the proteasome. Considering that proteasome synthesis was able to keep pace with the high demand imposed by the accumulation of ubiquitinated proteins in the absence of DDI2, here I used multiple techniques to investigate any alteration in function or assembly of proteasome. Insufficient activity of Ddi2 leads to accumulation of highly ubiquitinated proteins in my immunoblots and other reported studies (168). Accumulation of ubiquitinated proteins is one of main outcomes of proteasome malfunction. This issue can arise from the inhibition of various subunits within the complex structure of the proteasome. Ddi2 inhibition led to lower activity of 30S proteasome subunit (Chymotrypsin-like subunit). As previously shown, *DDI2* KO and protease-dead D252 knock-in cells have significantly lower proteasomal activity compared to control WT and WT *DDI2* knock-in cells (98). The initial observation regarding ubiquitin blots and given that ubiquitination is a fundamental regulatory PTM in cell biology, highlighted the necessity of exploring ubiquitination pattern in cell lacking Ddi2. Ddi2, an understudied yet highly promising protein, must play various roles in processing of cellular proteins. The proteolytic activity of Ddi2 is not limited to Nfe2l1 PTM, as Nfe2l3 is a known target of Ddi2 (99). The scaffolding protein angiomotin (AMOT) is another reported protein that undergoes cleavage by Ddi2 (115). Moreover, *in vitro* data has been

shown that purified DDI2 can directly cleaves highly ubiquitylated proteins (168). In addition, due to special structure of the protein, Ddi2 possess the ability to bind to Ub conjugates and proteasome through its Ub-like domain. Therefore, Ddi2 can play a role as a shuttling factor in ERAD machinery and delivers proteins to the proteasome for degradation (169). Ablation of *Ddi2* significantly induced remodeling of ubiquitination. This resulted in a global increase in ubiquitination of proteins within the cells supported by gene ontology (GO) analysis, where the proteasome-mediated ubiquitin-dependent protein catalytic process emerged as the top significantly impacted pathway. However, since the end goal of ubiquitination extends beyond just protein degradation via UPS, further exploration in data remains. It is interesting to delve deeper into the ubiquitome data to recognize various ubiquitin linkages and identifying altered pathways and proteins.

4.4 Ddi2 deficiency does not affect β-Adrenergic signaling or thermogenesis of adipose tissue

After establishing foundational significance of Ddi2 in processing and cleavage of Nfe2l1, the pivotal next step involved the exploration of DDI2/NFE2L1 pathway in diverse functions of BAT (160). Ddi2 protein levels were by far higher when comparing BAT versus WAT samples. Differentiated mature preadipocytes displayed higher Ddi2 protein band in immunoblot analysis compared to undifferentiated cells. Although the experimental flow primarily focused on Nfe2l1-related role of Ddi2 through proteasome inhibition, exploring the direct impact of proteasome inhibitor (PI) on Ddi2 was also intriguing. While some blots displayed less protein level, PI treatment did not seem to be a potential direct activator or suppressor of Ddi2 at least on transcriptional level. While it has been reported that *DDI2* KO significantly sensitizes MM cells to carfilzomib (119), deficiency in Ddi2 alone does not exacerbate proteasome inhibitor toxicity in brown adipocytes, as evidenced by cell survival analysis. Advancing to the next step, not only UPS, but also mitochondrial activity plays a central role in BAT function and thermogenesis. Lower mitochondrial respiration witnessed in isolated mitochondria from BAT of mice treated with PI highlights the importance of proteasome inhibition on bioenergetics and oxidative capacity of mitochondria (160). Real-time measurement of mitochondrial respiration is the key indicator of various aspects of mitochondrial activity in cell and isolated tissue models. In this stage of project, cells silenced with *Ddi2* siRNA were subjected to injection of series of compounds that modulates the mitochondrial function. Changes in oxygen consumption rate (OCR) then were measured through mitochondrial stress test. In order to activate BAT thermogenesis and stimulate mitochondrial activation, I added one more injection prior to the conventional mitostress test protocol. Nor-epinephrine (NE) stimulates β3-adneregic receptors and triggers the signaling pathway that activates Ucp1,

which then increase mitochondrial respiration and heat production. Lack of *Ddi2* did not affect activation of brown adipocytes via NE. It is known that the deletion of *Nfe2l1* markedly diminish mitochondrial function *in vivo (160).* To make sure that this lack of response in *Ddi2* KD cells is dependent of Nfe2l1 or not, I tested whether Ngly1, as the other protein involved in ERAD and ER stress, can lead to the similar result. In fact, Nfe2l1-independent *Ngly1* deficiency impairs mitochondrial function including reduced mitochondrial content, reduced mitochondrial membrane potential and increased mitochondrial matrix oxidant burden in *C. elegance* and human fibroblasts (170). Here, *Ngly1* KD in cells disrupted NE-stimulated activation of BAT and mitochondrial function as well. Once again, to make sure whether lack of Ddi2 is generally compensable for cells, I treated cell with NFV. Aligned with previous results, chemical inhibition of Ddi2 showed opposite results compared to *Ddi2* siRNA. NFV-treated displayed lower NE-stimulated activation of BAT, lower oxygen consumption rate and disrupted mitochondrial function compared to DMSO-treated controls.

Following this, it is pivotal to check adipocyte function from NE-stimulated adipogenesis or differentiation state of existing adipocytes perspective. *Nfe2l1* KO mice have reduced subcutaneous WAT mass, adipocytes hypertrophy, and exhibit decrease in expression of lipolytic genes (171-173). However, *Ddi2* KD cells or KO animals did not exhibit any difference in classical differentiation marker genes at basal level. Previous study showed *Nfe2l1* KD does not affect lipid contents in ORO staining plates of immortalized brown adipocytes (174). Oil-red-O staining and quantification of cells lacking Ddi2 also displayed no significant changes in lipid content of these two groups. In conclusion, these sets of data containing both *in vitro* and *in vivo* examinations of adipocytes function nicely proved that although Ddi2 is required for cleavage and nuclear translocation of Nfe2l1, it is complicated to prove the relevance to BAT function. It is unlikely that a direct connection exists between a protease aspect of Ddi2 activity and the thermogenic activity of BAT. Therefore, I propose that the proteolytic activity of Ddi2 is one of many potential functions of this understudied protein in cells.

In obesity and related metabolic complications, the energy intake consistently exceeds energy expenditure. Therefore, increasing energy expenditure *in vivo* through activation of BAT is a potential approach to treat metabolic diseases such as obesity and diabetes. Indirect calorimetry provides an estimation of whole-body energy expenditure by measuring various metabolic parameters and probing the relationship between fuel consumption and energy production. *Ddi2*$^{\Delta BAT}$ disruption in mice had no effect in food or water consumption of KO animals compared to the wild type littermates. These two groups also showed no significant changes in body weight. To unequivocally determine that

browning and NST of BAT, multiple metabolic factors such as O_2 consumption and respiratory exchange rate after injection of β3-adrenoceptor agonist, CL316,243, were measured. However, contrary to my presumptions, *Ddi2* KO showed no difference compared to wild type mice.

The absence of BAT specific phenotype similar to that of *Nfe2l1* KO, led me to conclude that while Ddi2 cleaves Nfe2l1, this proteolytic function does not appear to be essential for activating Nfe2l1. Therefore, I propose that either the unprocessed form of Nfe2l1 retains sufficient activity on its own, or the lack of Ddi2/Nfe2l1 pathway have developed compensatory mechanisms for absence of active Nfe2l1. The first hypothesize seems less likely, given the effect of NFV-mediated inhibition of Ddi2 in proteasome biogenesis and function and mitochondrial activity. This suggests that silencing *Ddi2* with siRNA might not be precise enough. Interestingly I found that due to overlap in genetic codes, *Ddi2* siRNA targets a sodium/glucose cotransporter called Rsc1a1 (Regulator of solute carrier 1). While brown adipocytes transfected with *Ddi2* siRNA showed significant decrease in mRNA expression of *Rsc1a1*, the gene expression of *Rsc1a1* remains unchanged in *Ddi2* KO mice (Supplementary Fig. 1b, c). Considering the potential effects of this transporter in glucose homeostasis and inducing obesity (175), siRNA-silencing technique is not a reliable for studying disrupted Ddi2/Nfe2l1 pathway. Moreover, since *Ngly1* KD also negatively affects brown adipocyte function, I am skeptical that unprocessed Nfe2l1 alone is sufficient to maintain normal cellular function.

To elaborate the second hypothesis regarding identifying compensatory factors, I specifically examined the gene expression of other members of Nfe family. No changes were observed in well-reported *Nfe2l2* along with its downstream targets *Hmox1* or *Nqo1* as well as the understudied Nfe2l3 (Supplementary Fig. 1d). Therefore, mice lacking Ddi2/Nfe2l1 pathway might have developed other compensatory mechanisms to fulfill the roles that typically are performed by Nfe2l1. Further studies is required to elucidate these mechanisms fully.

4.5 Ddi2/Nfe2l1 pathway and ubiquitin remodeling in Ferroptosis

We established the role of Ddi2 in Nfe2l1 cleavage and subsequent activation in regulation of ubiquitin proteasome system in the context of adipose tissue physiology. Important to mention that the role of this transcription factor was vastly studied in various forms of cell death (17). As reported recently (154), Nfe2l1 is a novel protector of cells against a non-oxidative iron dependent form of cell death, ferroptosis. The execution of ferroptosis and molecular approaches to manipulate its outcomes is an emerging field of research with important implications for metabolism, cancer, and neurodegenerative diseases. Post-translational modification of Nfe2l1 by Ngly1 in context of ferroptosis is also established (153). Therefore, it is crucial to investigate if Ddi2 can also play a role in these defense mechanisms or not. Hence, I investigated if loss of Ddi2 functionality shows similar phenotype through Nfe2l1-proteasome pathway, and if not, what are the compensatory mechanisms to cover this gap. RSL3 and Fin56 were two chemical inducers of ferroptosis cell death in my experiments. Alongside, I used proteasome inhibitor bortezomib as an established positive control for detecting Nfe2l1 95kDa cleaved form and accumulation of ubiquitinated proteins in the blots.

Reduced proteasome function is a hallmark of ferroptosis, and there is overlap between BTZ and RSL3-induced hyperubiquitylation (154). Here, I unequivocally demonstrated the RSL3-induced recalibration of UPS leads to accumulation of hyperubiquitylated proteins, reflecting a maladaptive regulation of the UPS. Upon induction of ferroptosis, cells are required to increase proteostatic defense mechanisms, possibly caused by lipid ROS-induced perturbations before the eventual death of the cell. Usually, proteasome defuses and recycles damaged or obsolete proteins by ubiquitin-dependent and independent degradation. Perhaps, one key finding of our study is that RSL3-induced ferroptosis compromises proteasome activity. However, the nature of this insult was distinct from chemical proteasome inhibition by itself, arguing for more than impact on the ubiquitome. In other words, the recalibration of UPS and ubiquitome during ferroptosis is not only caused by proteasome inhibition. Interestingly, among the ubiquitylated proteins that increased upon RSL3 treatment we found many UPS components, including those constituting proteasomes itself. Future work will have to investigate the relevance of these modifications and delineate the posttranslational regulation of proteasome activity during ferroptosis.

In the global ubiquitome analysis, I found several known players that either suppress or promote ferroptosis. Previous studies investigating deubiquitylating enzymes have found a role for ubiquitylation and degradation of GPX4, Nedd4 or VDAC2/3 (176, 177) but the relevance for these mechanisms is still unclear. I also found GPX4 and enzymes of glutathione production to be hyperubiquitylated upon RSL3 treatment, suggesting that there

is a specific impact on reduced proteasome function on key pathways of ferroptosis. As Nfe2l1 is the regulator of proteasome function in ferroptosis (154), in next step Ddi2-mediated cleavage of Nfe2l1 was established upon the use of ferroptosis inducers in my experiments. Viability of cells in both genetic and chemical inhibition of DDI2 was lower compared to control cells. Therefore, DDI2 is required to proteolytically activate NFE2L1 and protect from RSL3-induced and genetically driven ferroptotic cell death. On a more general note, my results show that lack or dysfunction of DDI2 lead to a global increase in ubiquitylation. While hyperubiquitylation increases proteotoxic stress levels, it is possible that the turnover of certain key regulators is disturbed and contributes to the observed ferroptosis sensitivity of *DDI2* KO cells. However, as my means of inducing ferroptosis are largely GPX4-dependent, GPX4 is likely not required for the execution of this response. We have previously shown that also other distinct means of inducing ferroptosis such as erastin or FIN56 exhibit changes in proteasomal activity (154).

Back to Nfe2l1-UPS system, I then tried to check if the increase in susceptibility of cells to ferroptosis is due to disrupted bounce back activity of Nfe2l1. The role of DDI2 in the complex series of events leading to NFE2L1 activation should be viewed as required and permissive for the bounce-back response. However, proteolytic processing is not the only posttranslational modification required for the activation of NFE2L1, as NGLY1 plays a critical role deglycosylation of NFE2L1 and modulates susceptibility of cells to ferroptosis (153). In my hands, overexpression of deglycosylated NFE2L1 did not rescue the sensitivity of *DDI2* KO cells, which underlines the importance of the DDI2-mediated proteolytic cleavage step for the activation of NFE2L1 during ferroptosis. My data using NFV for inhibiting DDI2 indicates that this could be a potential add-on treatment for targeting ferroptosis in cancer therapy, similar to what has been rationalized for proteasome inhibitors. Interfering with proteasome function and preventing NFE2L1 activation at the same time might further sensitize cancer cells to ferroptosis. Finally, NFE2L1 is also ubiquitylated by the E3 ubiquitin ligase Hrd1 at the ER for ER-associated protein degradation (64), by β-TrCP in the nucleus for removal of NFE2L1 (95), or by UBE4A for cleavage by DDI2 (178), but the details of these regulatory steps for ferroptosis remain unexplored. It will be important to further dissect the posttranslational regulation of NFE2L1 during ferroptosis, as this might reveal more angles to therapeutically exploit the calibration of the UPS for manipulating ferroptosis outcomes.

In conclusion, I have shown that Ddi2 plays a vital role in proteolytic cleavage of transcription factor Nfe2l1 *in vitro.* Loss of Ddi2 genetically leads to lower activity of proteasome and calibration of UPS but did not affect the function of adipocytes. Moreover, in vivo data from *Ddi2*$^{\Delta BAT}$ did not display any disruption in BAT activation or thermogenesis function. However, chemical induction of Ddi2 showed negative impact in various

aspects of immortalized brown adipocytes function such as proteasome inhibition and mitochondrial dysfunction, necessitating further investigation to identify compensatory mechanisms in Ddi2 deficient mice. This research also introduces Ddi2 as a major player in UPS adaptation in context of ferroptosis and can increase cell survival of cells sensitive to this form of cell death.

References

1. Nuttall FQ. Body Mass Index: Obesity, BMI, and Health: A Critical Review. Nutr Today. 2015;50(3):117-28.

2. Chait A, den Hartigh LJ. Adipose Tissue Distribution, Inflammation and Its Metabolic Consequences, Including Diabetes and Cardiovascular Disease. Front Cardiovasc Med. 2020;7:22.

3. Kesztyus D, Lampl J, Kesztyus T. The Weight Problem: Overview of the Most Common Concepts for Body Mass and Fat Distribution and Critical Consideration of Their Usefulness for Risk Assessment and Practice. Int J Environ Res Public Health. 2021;18(21).

4. Volpe M, Gallo G. Obesity and cardiovascular disease: An executive document on pathophysiological and clinical links promoted by the Italian Society of Cardiovascular Prevention (SIPREC). Front Cardiovasc Med. 2023;10:1136340.

5. Ding Y, Deng Q, Yang M, Niu H, Wang Z, Xia S. Clinical Classification of Obesity and Implications for Metabolic Dysfunction-Associated Fatty Liver Disease and Treatment. Diabetes Metab Syndr Obes. 2023;16:3303-29.

6. Katsiki N, Ntaios G, Vemmos K. Stroke, obesity and gender: a review of the literature. Maturitas. 2011;69(3):239-43.

7. Jiang SZ, Lu W, Zong XF, Ruan HY, Liu Y. Obesity and hypertension. Exp Ther Med. 2016;12(4):2395-9.

8. Jehan S, Zizi F, Pandi-Perumal SR, Wall S, Auguste E, Myers AK, et al. Obstructive Sleep Apnea and Obesity: Implications for Public Health. Sleep Med Disord. 2017;1(4).

9. Flores-Cordero JA, Perez-Perez A, Jimenez-Cortegana C, Alba G, Flores-Barragan A, Sanchez-Margalet V. Obesity as a Risk Factor for Dementia and Alzheimer's Disease: The Role of Leptin. Int J Mol Sci. 2022;23(9).

10. Pati S, Irfan W, Jameel A, Ahmed S, Shahid RK. Obesity and Cancer: A Current Overview of Epidemiology, Pathogenesis, Outcomes, and Management. Cancers (Basel). 2023;15(2).

11. Khan S, Chan YT, Revelo XS, Winer DA. The Immune Landscape of Visceral Adipose Tissue During Obesity and Aging. Front Endocrinol (Lausanne). 2020;11:267.

12. Luo L, Liu M. Adipose tissue in control of metabolism. J Endocrinol. 2016;231(3):R77-R99.

13. de Mello AH, Costa AB, Engel JDG, Rezin GT. Mitochondrial dysfunction in obesity. Life Sci. 2018;192:26-32.

14. Flores-Dorantes MT, Diaz-Lopez YE, Gutierrez-Aguilar R. Environment and Gene Association With Obesity and Their Impact on Neurodegenerative and Neurodevelopmental Diseases. Front Neurosci. 2020;14:863.

15. Xu H, Barnes GT, Yang Q, Tan G, Yang D, Chou CJ, et al. Chronic inflammation in fat plays a crucial role in the development of obesity-related insulin resistance. J Clin Invest. 2003;112(12):1821-30.

16. Sakers A, De Siqueira MK, Seale P, Villanueva CJ. Adipose-tissue plasticity in health and disease. Cell. 2022;185(3):419-46.

17. Liu X, Xu C, Xiao W, Yan N. Unravelling the role of NFE2L1 in stress responses and related diseases. Redox Biol. 2023;65:102819.

18. Chusyd DE, Wang D, Huffman DM, Nagy TR. Relationships between Rodent White Adipose Fat Pads and Human White Adipose Fat Depots. Front Nutr. 2016;3:10.

19. Pan R, Zhu X, Maretich P, Chen Y. Metabolic Improvement via Enhancing Thermogenic Fat-Mediated Non-shivering Thermogenesis: From Rodents to Humans. Front Endocrinol (Lausanne). 2020;11:633.

20. Cohade C, Osman M, Pannu HK, Wahl RL. Uptake in supraclavicular area fat ("USA-Fat"): description on 18F-FDG PET/CT. J Nucl Med. 2003;44(2):170-6.

21. Haman F, Blondin DP. Shivering thermogenesis in humans: Origin, contribution and metabolic requirement. Temperature (Austin). 2017;4(3):217-26.

22. Rezende EL, Bacigalupe LD. Thermoregulation in endotherms: physiological principles and ecological consequences. J Comp Physiol B. 2015;185(7):709-27.

23. Lowell BB, Spiegelman BM. Towards a molecular understanding of adaptive thermogenesis. Nature. 2000;404(6778):652-60.

24. Feldmann HM, Golozoubova V, Cannon B, Nedergaard J. UCP1 ablation induces obesity and abolishes diet-induced thermogenesis in mice exempt from thermal stress by living at thermoneutrality. Cell Metab. 2009;9(2):203-9.

25. Stanford KI, Middelbeek RJ, Townsend KL, An D, Nygaard EB, Hitchcox KM, et al. Brown adipose tissue regulates glucose homeostasis and insulin sensitivity. J Clin Invest. 2013;123(1):215-23.

26. Berbee JF, Boon MR, Khedoe PP, Bartelt A, Schlein C, Worthmann A, et al. Brown fat activation reduces hypercholesterolaemia and protects from atherosclerosis development. Nat Commun. 2015;6:6356.

27. Matthias A, Ohlson KB, Fredriksson JM, Jacobsson A, Nedergaard J, Cannon B. Thermogenic responses in brown fat cells are fully UCP1-dependent. UCP2 or UCP3 do not substitute for UCP1 in adrenergically or fatty scid-induced thermogenesis. J Biol Chem. 2000;275(33):25073-81.

28. Berry DC, Jiang Y, Graff JM. Emerging Roles of Adipose Progenitor Cells in Tissue Development, Homeostasis, Expansion and Thermogenesis. Trends Endocrinol Metab. 2016;27(8):574-85.

29. Wu J, Bostrom P, Sparks LM, Ye L, Choi JH, Giang AH, et al. Beige adipocytes are a distinct type of thermogenic fat cell in mouse and human. Cell. 2012;150(2):366-76.

30. Ahima RS, Lazar MA. Adipokines and the peripheral and neural control of energy balance. Mol Endocrinol. 2008;22(5):1023-31.

31. Rodgers A, Sferruzzi-Perri AN. Developmental programming of offspring adipose tissue biology and obesity risk. Int J Obes (Lond). 2021;45(6):1170-92.

32. Geloen A, Collet AJ, Guay G, Bukowiecki LJ. In vivo differentiation of brown adipocytes in adult mice: an electron microscopic study. Am J Anat. 1990;188(4):366-72.

33. Cedikova M, Kripnerova M, Dvorakova J, Pitule P, Grundmanova M, Babuska V, et al. Mitochondria in White, Brown, and Beige Adipocytes. Stem Cells Int. 2016;2016:6067349.

34. Carpentier AC, Blondin DP, Haman F, Richard D. Brown Adipose Tissue-A Translational Perspective. Endocr Rev. 2023;44(2):143-92.

35. Straat ME, Hoekx CA, van Velden FHP, Pereira Arias-Bouda LM, Dumont L, Blondin DP, et al. Stimulation of the beta-2-adrenergic receptor with salbutamol activates human brown adipose tissue. Cell Rep Med. 2023;4(2):100942.

36. Jockers R, Issad T, Zilberfarb V, de Coppet P, Marullo S, Strosberg AD. Desensitization of the beta-adrenergic response in human brown adipocytes. Endocrinology. 1998;139(6):2676-84.

37. Shi F, Collins S. Second messenger signaling mechanisms of the brown adipocyte thermogenic program: an integrative perspective. Horm Mol Biol Clin Investig. 2017;31(2).

38. Tripathy D, Mohanty P, Dhindsa S, Syed T, Ghanim H, Aljada A, et al. Elevation of free fatty acids induces inflammation and impairs vascular reactivity in healthy subjects. Diabetes. 2003;52(12):2882-7.

39. Unger RH, Zhou YT. Lipotoxicity of beta-cells in obesity and in other causes of fatty acid spillover. Diabetes. 2001;50 Suppl 1:S118-21.

40. Samuel VT, Shulman GI. The pathogenesis of insulin resistance: integrating signaling pathways and substrate flux. J Clin Invest. 2016;126(1):12-22.

41. Ariyasu D, Yoshida H, Hasegawa Y. Endoplasmic Reticulum (ER) Stress and Endocrine Disorders. Int J Mol Sci. 2017;18(2).

42. Yang L, Zhao D, Ren J, Yang J. Endoplasmic reticulum stress and protein quality control in diabetic cardiomyopathy. Biochim Biophys Acta. 2015;1852(2):209-18.

43. Nicholls DG, Locke RM. Thermogenic mechanisms in brown fat. Physiol Rev. 1984;64(1):1-64.

44. Fedorenko A, Lishko PV, Kirichok Y. Mechanism of fatty-acid-dependent UCP1 uncoupling in brown fat mitochondria. Cell. 2012;151(2):400-13.

45. Chang JS. Recent insights into the molecular mechanisms of simultaneous fatty acid oxidation and synthesis in brown adipocytes. Front Endocrinol (Lausanne). 2023;14:1106544.

46. Jonckheere AI, Smeitink JA, Rodenburg RJ. Mitochondrial ATP synthase: architecture, function and pathology. J Inherit Metab Dis. 2012;35(2):211-25.

47. Wong HS, Dighe PA, Mezera V, Monternier PA, Brand MD. Production of superoxide and hydrogen peroxide from specific mitochondrial sites under different bioenergetic conditions. J Biol Chem. 2017;292(41):16804-9.

48. Dlaskova A, Clarke KJ, Porter RK. The role of UCP 1 in production of reactive oxygen species by mitochondria isolated from brown adipose tissue. Biochim Biophys Acta. 2010;1797(8):1470-6.

49. Nguyen KD, Qiu Y, Cui X, Goh YP, Mwangi J, David T, et al. Alternatively activated macrophages produce catecholamines to sustain adaptive thermogenesis. Nature. 2011;480(7375):104-8.

50. Sentis SC, Oelkrug R, Mittag J. Thyroid hormones in the regulation of brown adipose tissue thermogenesis. Endocr Connect. 2021;10(2):R106-R15.

51. Choe SS, Huh JY, Hwang IJ, Kim JI, Kim JB. Adipose Tissue Remodeling: Its Role in Energy Metabolism and Metabolic Disorders. Front Endocrinol (Lausanne). 2016;7:30.

52. Basseri S, Austin RC. Endoplasmic reticulum stress and lipid metabolism: mechanisms and therapeutic potential. Biochem Res Int. 2012;2012:841362.

53. Ajoolabady A, Aslkhodapasandhokmabad H, Libby P, Tuomilehto J, Lip GYH, Penninger JM, et al. Ferritinophagy and ferroptosis in the management of metabolic diseases. Trends Endocrinol Metab. 2021;32(7):444-62.

54. Rao RV, Bredesen DE. Misfolded proteins, endoplasmic reticulum stress and neurodegeneration. Curr Opin Cell Biol. 2004;16(6):653-62.

55. Lemmer IL, Willemsen N, Hilal N, Bartelt A. A guide to understanding endoplasmic reticulum stress in metabolic disorders. Mol Metab. 2021;47:101169.

56. Sage AT, Holtby-Ottenhof S, Shi Y, Damjanovic S, Sharma AM, Werstuck GH. Metabolic syndrome and acute hyperglycemia are associated with endoplasmic

reticulum stress in human mononuclear cells. Obesity (Silver Spring). 2012;20(4):748-55.

57. Zhang J, Guo J, Yang N, Huang Y, Hu T, Rao C. Endoplasmic reticulum stress-mediated cell death in liver injury. Cell Death Dis. 2022;13(12):1051.

58. Kobayashi M, Nezu Y, Tagawa R, Higami Y. Mitochondrial Unfolded Protein Responses in White Adipose Tissue: Lipoatrophy, Whole-Body Metabolism and Lifespan. Int J Mol Sci. 2021;22(6).

59. Schooneman MG, Vaz FM, Houten SM, Soeters MR. Acylcarnitines: reflecting or inflicting insulin resistance? Diabetes. 2013;62(1):1-8.

60. Andreux PA, Houtkooper RH, Auwerx J. Pharmacological approaches to restore mitochondrial function. Nat Rev Drug Discov. 2013;12(6):465-83.

61. Travers KJ, Patil CK, Wodicka L, Lockhart DJ, Weissman JS, Walter P. Functional and genomic analyses reveal an essential coordination between the unfolded protein response and ER-associated degradation. Cell. 2000;101(3):249-58.

62. Hu S, Feng J, Wang M, Wufuer R, Liu K, Zhang Z, et al. Nrf1 is an indispensable redox-determining factor for mitochondrial homeostasis by integrating multi-hierarchical regulatory networks. Redox Biol. 2022;57:102470.

63. Functional and genomic analyses reveal an essential coordination between the unfolded protein response and ER-associated degradation.

64. Steffen J, Seeger M, Koch A, Kruger E. Proteasomal degradation is transcriptionally controlled by TCF11 via an ERAD-dependent feedback loop. Mol Cell. 2010;40(1):147-58.

65. Nrf1 is an indispensable redox-determining factor for mitochondrial homeostasis by integrating multi-hierarchical regulatory networks.

66. Ray PD, Huang BW, Tsuji Y. Reactive oxygen species (ROS) homeostasis and redox regulation in cellular signaling. Cell Signal. 2012;24(5):981-90.

67. Park SY, Kim SH, Yoon HK, Yim CH, Lim SK. The Role of Nuclear Factor-E2-Related Factor 1 in the Oxidative Stress Response in MC3T3-E1 Osteoblastic Cells. Endocrinol Metab (Seoul). 2016;31(2):336-42.

68. Birben E, Sahiner UM, Sackesen C, Erzurum S, Kalayci O. Oxidative stress and antioxidant defense. World Allergy Organ J. 2012;5(1):9-19.

69. Checa J, Aran JM. Reactive Oxygen Species: Drivers of Physiological and Pathological Processes. J Inflamm Res. 2020;13:1057-73.

70. Abou-Rjeileh U, Contreras GA. Redox Regulation of Lipid Mobilization in Adipose Tissues. Antioxidants (Basel). 2021;10(7).

71. Korac B, Kalezic A, Pekovic-Vaughan V, Korac A, Jankovic A. Redox changes in obesity, metabolic syndrome, and diabetes. Redox Biol. 2021;42:101887.

72. Chouchani ET, Kazak L, Spiegelman BM. Mitochondrial reactive oxygen species and adipose tissue thermogenesis: Bridging physiology and mechanisms. J Biol Chem. 2017;292(41):16810-6.

73. Nguyen T, Nioi P, Pickett CB. The Nrf2-antioxidant response element signaling pathway and its activation by oxidative stress. J Biol Chem. 2009;284(20):13291-5.

74. Xu J, Kulkarni SR, Donepudi AC, More VR, Slitt AL. Enhanced Nrf2 activity worsens insulin resistance, impairs lipid accumulation in adipose tissue, and increases hepatic steatosis in leptin-deficient mice. Diabetes. 2012;61(12):3208-18.

75. Biswas M, Chan JY. Role of Nrf1 in antioxidant response element-mediated gene expression and beyond. Toxicol Appl Pharmacol. 2010;244(1):16-20.

76. Kwong M, Kan YW, Chan JY. The CNC basic leucine zipper factor, Nrf1, is essential for cell survival in response to oxidative stress-inducing agents. Role for Nrf1 in gamma-gcs(l) and gss expression in mouse fibroblasts. J Biol Chem. 1999;274(52):37491-8.

77. Lee TD, Yang H, Whang J, Lu SC. Cloning and characterization of the human glutathione synthetase 5'-flanking region. Biochem J. 2005;390(Pt 2):521-8.

78. Myhrstad MC, Husberg C, Murphy P, Nordstrom O, Blomhoff R, Moskaug JO, et al. TCF11/Nrf1 overexpression increases the intracellular glutathione level and can transactivate the gamma-glutamylcysteine synthetase (GCS) heavy subunit promoter. Biochim Biophys Acta. 2001;1517(2):212-9.

79. Ohtsuji M, Katsuoka F, Kobayashi A, Aburatani H, Hayes JD, Yamamoto M. Nrf1 and Nrf2 play distinct roles in activation of antioxidant response element-dependent genes. J Biol Chem. 2008;283(48):33554-62.

80. Motohashi H, O'Connor T, Katsuoka F, Engel JD, Yamamoto M. Integration and diversity of the regulatory network composed of Maf and CNC families of transcription factors. Gene. 2002;294(1-2):1-12.

81. Nguyen T, Sherratt PJ, Pickett CB. Regulatory mechanisms controlling gene expression mediated by the antioxidant response element. Annu Rev Pharmacol Toxicol. 2003;43:233-60.

82. Andrews NC, Erdjument-Bromage H, Davidson MB, Tempst P, Orkin SH. Erythroid transcription factor NF-E2 is a haematopoietic-specific basic-leucine zipper protein. Nature. 1993;362(6422):722-8.

83. Chan JY, Han XL, Kan YW. Isolation of cDNA encoding the human NF-E2 protein. Proc Natl Acad Sci U S A. 1993;90(23):11366-70.

84. Chan JY, Han XL, Kan YW. Cloning of Nrf1, an NF-E2-related transcription factor, by genetic selection in yeast. Proc Natl Acad Sci U S A. 1993;90(23):11371-5.

85. Oyake T, Itoh K, Motohashi H, Hayashi N, Hoshino H, Nishizawa M, et al. Bach proteins belong to a novel family of BTB-basic leucine zipper transcription factors that interact with MafK and regulate transcription through the NF-E2 site. Mol Cell Biol. 1996;16(11):6083-95.

86. Kensler TW, Wakabayashi N, Biswal S. Cell survival responses to environmental stresses via the Keap1-Nrf2-ARE pathway. Annu Rev Pharmacol Toxicol. 2007;47:89-116.

87. Kobayashi M, Yamamoto M. Molecular mechanisms activating the Nrf2-Keap1 pathway of antioxidant gene regulation. Antioxid Redox Signal. 2005;7(3-4):385-94.

88. Venugopal R, Jaiswal AK. Nrf1 and Nrf2 positively and c-Fos and Fra1 negatively regulate the human antioxidant response element-mediated expression of NAD(P)H:quinone oxidoreductase1 gene. Proc Natl Acad Sci U S A. 1996;93(25):14960-5.

89. Reichard JF, Motz GT, Puga A. Heme oxygenase-1 induction by NRF2 requires inactivation of the transcriptional repressor BACH1. Nucleic Acids Res. 2007;35(21):7074-86.

90. Kuda O, Brezinova M, Silhavy J, Landa V, Zidek V, Dodia C, et al. Nrf2-Mediated Antioxidant Defense and Peroxiredoxin 6 Are Linked to Biosynthesis of Palmitic Acid Ester of 9-Hydroxystearic Acid. Diabetes. 2018;67(6):1190-9.

91. Chan JY, Kwong M, Lu R, Chang J, Wang B, Yen TS, et al. Targeted disruption of the ubiquitous CNC-bZIP transcription factor, Nrf-1, results in anemia and embryonic lethality in mice. EMBO J. 1998;17(6):1779-87.

92. Leung L, Kwong M, Hou S, Lee C, Chan JY. Deficiency of the Nrf1 and Nrf2 transcription factors results in early embryonic lethality and severe oxidative stress. J Biol Chem. 2003;278(48):48021-9.

93. Sekine H, Motohashi H. Roles of CNC Transcription Factors NRF1 and NRF2 in Cancer. Cancers (Basel). 2021;13(3).

94. Wang W, Chan JY. Nrf1 is targeted to the endoplasmic reticulum membrane by an N-terminal transmembrane domain. Inhibition of nuclear translocation and transacting function. J Biol Chem. 2006;281(28):19676-87.

95. Tsuchiya Y, Morita T, Kim M, Iemura S, Natsume T, Yamamoto M, et al. Dual regulation of the transcriptional activity of Nrf1 by beta-TrCP- and Hrd1-dependent degradation mechanisms. Mol Cell Biol. 2011;31(22):4500-12.

96. Bartelt A, Widenmaier SB. Proteostasis in thermogenesis and obesity. Biol Chem. 2020;401(9):1019-30.

97. Tomlin FM, Gerling-Driessen UIM, Liu YC, Flynn RA, Vangala JR, Lentz CS, et al. Inhibition of NGLY1 Inactivates the Transcription Factor Nrf1 and Potentiates Proteasome Inhibitor Cytotoxicity. ACS Cent Sci. 2017;3(11):1143-55.

98. Koizumi S, Irie T, Hirayama S, Sakurai Y, Yashiroda H, Naguro I, et al. The aspartyl protease DDI2 activates Nrf1 to compensate for proteasome dysfunction. Elife. 2016;5.

99. Chowdhury A, Katoh H, Hatanaka A, Iwanari H, Nakamura N, Hamakubo T, et al. Multiple regulatory mechanisms of the biological function of NRF3 (NFE2L3) control cancer cell proliferation. Sci Rep. 2017;7(1):12494.

100. Moi P, Chan K, Asunis I, Cao A, Kan YW. Isolation of NF-E2-related factor 2 (Nrf2), a NF-E2-like basic leucine zipper transcriptional activator that binds to the tandem NF-E2/AP1 repeat of the beta-globin locus control region. Proc Natl Acad Sci U S A. 1994;91(21):9926-30.

101. Derjuga A, Gourley TS, Holm TM, Heng HH, Shivdasani RA, Ahmed R, et al. Complexity of CNC transcription factors as revealed by gene targeting of the Nrf3 locus. Mol Cell Biol. 2004;24(8):3286-94.

102. Chevillard G, Nouhi Z, Anna D, Paquet M, Blank V. Nrf3-deficient mice are not protected against acute lung and adipose tissue damages induced by butylated hydroxytoluene. FEBS Lett. 2010;584(5):923-8.

103. Kobayashi A, Waku T. New addiction to the NRF2-related factor NRF3 in cancer cells: Ubiquitin-independent proteolysis through the 20S proteasome. Cancer Sci. 2020;111(1):6-14.

104. Aono S, Hatanaka A, Hatanaka A, Gao Y, Hippo Y, Taketo MM, et al. beta-Catenin/TCF4 Complex-Mediated Induction of the NRF3 (NFE2L3) Gene in Cancer Cells. Int J Mol Sci. 2019;20(13).

105. Kobayashi A. Roles of NRF3 in the Hallmarks of Cancer: Proteasomal Inactivation of Tumor Suppressors. Cancers (Basel). 2020;12(9).

106. Waku T, Nakamura N, Koji M, Watanabe H, Katoh H, Tatsumi C, et al. NRF3-POMP-20S Proteasome Assembly Axis Promotes Cancer Development via Ubiquitin-Independent Proteolysis of p53 and Retinoblastoma Protein. Mol Cell Biol. 2020;40(10).

107. Waku T, Katayama H, Hiraoka M, Hatanaka A, Nakamura N, Tanaka Y, et al. NFE2L1 and NFE2L3 Complementarily Maintain Basal Proteasome Activity in Cancer Cells through CPEB3-Mediated Translational Repression. Mol Cell Biol. 2020;40(14).

108. Hirsch C, Blom D, Ploegh HL. A role for N-glycanase in the cytosolic turnover of glycoproteins. EMBO J. 2003;22(5):1036-46.

109. Suzuki T, Seko A, Kitajima K, Inoue Y, Inoue S. Identification of peptide:N-glycanase activity in mammalian-derived cultured cells. Biochem Biophys Res Commun. 1993;194(3):1124-30.

110. Suzuki T, Park H, Hollingsworth NM, Sternglanz R, Lennarz WJ. PNG1, a yeast gene encoding a highly conserved peptide:N-glycanase. J Cell Biol. 2000;149(5):1039-52.

111. Wang T, Yu H, Hughes NW, Liu B, Kendirli A, Klein K, et al. Gene Essentiality Profiling Reveals Gene Networks and Synthetic Lethal Interactions with Oncogenic Ras. Cell. 2017;168(5):890-903 e15.

112. Zhang Y, Ren Y, Li S, Hayes JD. Transcription factor Nrf1 is topologically repartitioned across membranes to enable target gene transactivation through its acidic glucose-responsive domains. PLoS One. 2014;9(4):e93458.

113. Pandey A, Adams JM, Han SY, Jafar-Nejad H. NGLY1 Deficiency, a Congenital Disorder of Deglycosylation: From Disease Gene Function to Pathophysiology. Cells. 2022;11(7).

114. Lehrbach NJ, Ruvkun G. Proteasome dysfunction triggers activation of SKN-1A/Nrf1 by the aspartic protease DDI-1. Elife. 2016;5.

115. Wang Y, Zhu Y, Wang Y, Chang Y, Geng F, Ma M, et al. Proteolytic activation of angiomotin by DDI2 promotes angiogenesis. EMBO J. 2023;42(15):e112900.

116. Kottemann MC, Conti BA, Lach FP, Smogorzewska A. Removal of RTF2 from Stalled Replisomes Promotes Maintenance of Genome Integrity. Mol Cell. 2018;69(1):24-35 e5.

117. Siva M, Svoboda M, Veverka V, Trempe JF, Hofmann K, Kozisek M, et al. Human DNA-Damage-Inducible 2 Protein Is Structurally and Functionally Distinct from Its Yeast Ortholog. Sci Rep. 2016;6:30443.

118. Radhakrishnan SK, Lee CS, Young P, Beskow A, Chan JY, Deshaies RJ. Transcription factor Nrf1 mediates the proteasome recovery pathway after proteasome inhibition in mammalian cells. Mol Cell. 2010;38(1):17-28.

119. Chen T, Ho M, Briere J, Moscvin M, Czarnecki PG, Anderson KC, et al. Multiple myeloma cells depend on the DDI2/NRF1-mediated proteasome stress response for survival. Blood Adv. 2022;6(2):429-40.

120. Lei L, Zhao X, Liu S, Cao Q, Yan B, Yang J. MicroRNA-3607 inhibits the tumorigenesis of colorectal cancer by targeting DDI2 and regulating the DNA damage repair pathway. Apoptosis. 2019;24(7-8):662-72.

121. Nath SR, Yu Z, Gipson TA, Marsh GB, Yoshidome E, Robins DM, et al. Androgen receptor polyglutamine expansion drives age-dependent quality control defects and muscle dysfunction. J Clin Invest. 2018;128(8):3630-41.

122. Park J, Cho J, Song EJ. Ubiquitin-proteasome system (UPS) as a target for anticancer treatment. Arch Pharm Res. 2020;43(11):1144-61.

123. Pohl C, Dikic I. Cellular quality control by the ubiquitin-proteasome system and autophagy. Science. 2019;366(6467):818-22.

124. McKeon JE, Sha D, Li L, Chin LS. Parkin-mediated K63-polyubiquitination targets ubiquitin C-terminal hydrolase L1 for degradation by the autophagy-lysosome system. Cell Mol Life Sci. 2015;72(9):1811-24.

125. Dantuma NP, Lindsten K. Stressing the ubiquitin-proteasome system. Cardiovasc Res. 2010;85(2):263-71.

126. Lee D, Ryu KY. Effect of cellular ubiquitin levels on the regulation of oxidative stress response and proteasome function via Nrf1. Biochem Biophys Res Commun. 2017;485(2):234-40.

127. Marinovic AC, Zheng B, Mitch WE, Price SR. Ubiquitin (UbC) expression in muscle cells is increased by glucocorticoids through a mechanism involving Sp1 and MEK1. J Biol Chem. 2002;277(19):16673-81.

128. Bianchi M, Crinelli R, Arbore V, Magnani M. Induction of ubiquitin C (UBC) gene transcription is mediated by HSF1: role of proteotoxic and oxidative stress. FEBS Open Bio. 2018;8(9):1471-85.

129. Kocberber Z, Willemsen N, Bartelt A. The role of proteasome activators PA28alphabeta and PA200 in brown adipocyte differentiation and function. Front Endocrinol (Lausanne). 2023;14:1176733.

130. Peth A, Uchiki T, Goldberg AL. ATP-dependent steps in the binding of ubiquitin conjugates to the 26S proteasome that commit to degradation. Mol Cell. 2010;40(4):671-81.

131. Kisselev AF, Akopian TN, Castillo V, Goldberg AL. Proteasome active sites allosterically regulate each other, suggesting a cyclical bite-chew mechanism for protein breakdown. Mol Cell. 1999;4(3):395-402.

132. Davies F, Rifkin R, Costello C, Morgan G, Usmani S, Abonour R, et al. Real-world comparative effectiveness of triplets containing bortezomib (B), carfilzomib (C), daratumumab (D), or ixazomib (I) in relapsed/refractory multiple myeloma (RRMM) in the US. Ann Hematol. 2021;100(9):2325-37.

133. Meng L, Mohan R, Kwok BH, Elofsson M, Sin N, Crews CM. Epoxomicin, a potent and selective proteasome inhibitor, exhibits in vivo antiinflammatory activity. Proc Natl Acad Sci U S A. 1999;96(18):10403-8.

134. Hu J, Van Valckenborgh E, Xu D, Menu E, De Raeve H, De Bruyne E, et al. Synergistic induction of apoptosis in multiple myeloma cells by bortezomib and hypoxia-activated prodrug TH-302, in vivo and in vitro. Mol Cancer Ther. 2013;12(9):1763-73.

135. Kuhn DJ, Chen Q, Voorhees PM, Strader JS, Shenk KD, Sun CM, et al. Potent activity of carfilzomib, a novel, irreversible inhibitor of the ubiquitin-proteasome pathway, against preclinical models of multiple myeloma. Blood. 2007;110(9):3281-90.

136. Collins GA, Goldberg AL. The Logic of the 26S Proteasome. Cell. 2017;169(5):792-806.

137. Galluzzi L, Vitale I, Aaronson SA, Abrams JM, Adam D, Agostinis P, et al. Molecular mechanisms of cell death: recommendations of the Nomenclature Committee on Cell Death 2018. Cell Death Differ. 2018;25(3):486-541.

138. Dixon SJ, Patel DN, Welsch M, Skouta R, Lee ED, Hayano M, et al. Pharmacological inhibition of cystine-glutamate exchange induces endoplasmic reticulum stress and ferroptosis. Elife. 2014;3:e02523.

139. Dixon SJ, Lemberg KM, Lamprecht MR, Skouta R, Zaitsev EM, Gleason CE, et al. Ferroptosis: an iron-dependent form of nonapoptotic cell death. Cell. 2012;149(5):1060-72.

140. Gao M, Monian P, Pan Q, Zhang W, Xiang J, Jiang X. Ferroptosis is an autophagic cell death process. Cell Res. 2016;26(9):1021-32.

141. Hadian K, Stockwell BR. A roadmap to creating ferroptosis-based medicines. Nat Chem Biol. 2021;17(11):1113-6.

142. Scarpellini C, Klejborowska G, Lanthier C, Hassannia B, Vanden Berghe T, Augustyns K. Beyond ferrostatin-1: a comprehensive review of ferroptosis inhibitors. Trends Pharmacol Sci. 2023;44(12):902-16.

143. Liu J, Liu M, Zhang H, Wei X, Wang J, Xian M, et al. Exploring cysteine regulation in cancer cell survival with a highly specific "Lock and Key" fluorescent probe for cysteine. Chem Sci. 2019;10(43):10065-71.

144. Conrad M, Moreno SG, Sinowatz F, Ursini F, Kolle S, Roveri A, et al. The nuclear form of phospholipid hydroperoxide glutathione peroxidase is a protein thiol peroxidase contributing to sperm chromatin stability. Mol Cell Biol. 2005;25(17):7637-44.

145. Sun Y, Zheng Y, Wang C, Liu Y. Glutathione depletion induces ferroptosis, autophagy, and premature cell senescence in retinal pigment epithelial cells. Cell Death Dis. 2018;9(7):753.

146. Nie Q, Hu Y, Yu X, Li X, Fang X. Induction and application of ferroptosis in cancer therapy. Cancer Cell Int. 2022;22(1):12.

147. Dixon SJ. Ferroptosis: an iron-dependent form of nonapoptotic cell death. 2012.

148. Yang WS. Regulation of ferroptotic cancer cell death by GPX4. cell. 2014

149. Dixon SJ. Pharmacological inhibition of cystine-glutamate exchange induces endoplasmic reticulum stress and ferroptosis. Elife. 2014.

150. Yagoda N, von Rechenberg M, Zaganjor E, Bauer AJ, Yang WS, Fridman DJ, et al. RAS-RAF-MEK-dependent oxidative cell death involving voltage-dependent anion channels. Nature. 2007;447(7146):864-8.

151. Zhang C, Liu X, Jin S, Chen Y, Guo R. Ferroptosis in cancer therapy: a novel approach to reversing drug resistance. Mol Cancer. 2022;21(1):47.

152. Seiler A. Glutathione peroxidase 4 senses and translates oxidative stress into 12/15-lipoxygenase dependent- and AIF-mediated cell death. Cell Metab. 2008.

153. Forcina GC, Pope L, Murray M, Dong W, Abu-Remaileh M, Bertozzi CR, et al. Ferroptosis regulation by the NGLY1/NFE2L1 pathway. Proc Natl Acad Sci U S A. 2022;119(11):e2118646119.

154. Kotschi S, Jung A, Willemsen N, Ofoghi A, Proneth B, Conrad M, et al. NFE2L1-mediated proteasome function protects from ferroptosis. Mol Metab. 2022;57:101436.

155. Nowak K. Inhibition of calpain-1 stabilizes TCF11/Nrf1 but does not affect its activation in response to proteasome inhibition. Biosci Rep. 2018.

156. Yazgili AS. In-gel proteasome assay to determine the activity, amount, and composition of proteasome complexes from mammalian cells or tissues. STAR Protoc. 2021.

157. Widenmaier SB. NRF1 Is an ER Membrane Sensor that Is Central to Cholesterol Homeostasis. Cell. 2017.

158. Hansen FM. Data-independent acquisition method for ubiquitinome analysis reveals regulation of circadian biology. Nat Commun. 2021.

159. Udeshi ND. Large-scale identification of ubiquitination sites by mass spectrometry. Nat Protoc. 2013.

160. Bartelt A, Widenmaier SB, Schlein C, Johann K, Goncalves RLS, Eguchi K, et al. Brown adipose tissue thermogenic adaptation requires Nrf1-mediated proteasomal activity. Nat Med. 2018;24(3):292-303.

161. Sha Z, Goldberg AL. Proteasome-mediated processing of Nrf1 is essential for coordinate induction of all proteasome subunits and p97. Curr Biol. 2014;24(14):1573-83.

162. Ofoghi A, Kotschi S, Lemmer IL, Haas DT, Willemsen N, Bayer B, et al. Activating the NFE2L1-ubiquitin-proteasome system by DDI2 protects from ferroptosis. bioRxiv. 2023:2023.07.04.547652.

163. Driessen C, Muller R, Novak U, Cantoni N, Betticher D, Mach N, et al. Promising activity of nelfinavir-bortezomib-dexamethasone in proteasome inhibitor-refractory multiple myeloma. Blood. 2018;132(19):2097-100.

164. Kotschi S. NFE2L1-mediated proteasome function protects from ferroptosis. Mol Metab. 2022.

165. Widenmaier SB, Snyder NA, Nguyen TB, Arduini A, Lee GY, Arruda AP, et al. NRF1 Is an ER Membrane Sensor that Is Central to Cholesterol Homeostasis. Cell. 2017;171(5):1094-109 e15.

166. Gu Y, Wang X, Wang Y, Wang Y, Li J, Yu FX. Nelfinavir inhibits human DDI2 and potentiates cytotoxicity of proteasome inhibitors. Cell Signal. 2020;75:109775.

167. Ribeiro ST, de Gassart A, Bettigole S, Zaffalon L, Chavarria C, Op M, et al. The protease DDI2 regulates NRF1 activation in response to cadmium toxicity. iScience. 2022;25(10):105227.

168. Dirac-Svejstrup AB, Walker J, Faull P, Encheva V, Akimov V, Puglia M, et al. DDI2 Is a Ubiquitin-Directed Endoprotease Responsible for Cleavage of Transcription Factor NRF1. Mol Cell. 2020;79(2):332-41 e7.

169. Collins GA, Sha Z, Kuo CL, Erbil B, Goldberg AL. Mammalian Ddi2 is a shuttling factor containing a retroviral protease domain that influences binding of ubiquitylated proteins and proteasomal degradation. J Biol Chem. 2022;298(5):101875.

170. Kong J, Peng M, Ostrovsky J, Kwon YJ, Oretsky O, McCormick EM, et al. Mitochondrial function requires NGLY1. Mitochondrion. 2018;38:6-16.

171. Hou Y, Liu Z, Zuo Z, Gao T, Fu J, Wang H, et al. Adipocyte-specific deficiency of Nfe2l1 disrupts plasticity of white adipose tissues and metabolic homeostasis in mice. Biochem Biophys Res Commun. 2018;503(1):264-70.

172. Ren S, Hou Y, Zuo Z, Liu Z, Wang H, Xu Y, et al. Protracted rosiglitazone treatment exacerbates inflammation in white adipose tissues of adipocyte-specific Nfe2l1 knockout mice. Food Chem Toxicol. 2020;146:111836.

173. Wang Z, Hou Y, Ren S, Liu Z, Zuo Z, Huang S, et al. CL316243 treatment mitigates the inflammation in white adipose tissues of juvenile adipocyte-specific Nfe2l1 knockout mice. Free Radic Biol Med. 2021;165:289-98.

174. Willemsen N, Arigoni I, Studencka-Turski M, Kruger E, Bartelt A. Proteasome dysfunction disrupts adipogenesis and induces inflammation via ATF3. Mol Metab. 2022;62:101518.

175. Osswald C, Baumgarten K, Stumpel F, Gorboulev V, Akimjanova M, Knobeloch KP, et al. Mice without the regulator gene Rsc1A1 exhibit increased Na+-D-glucose cotransport in small intestine and develop obesity. Mol Cell Biol. 2005;25(1):78-87.

176. Yang L, Chen X, Yang Q, Chen J, Huang Q, Yao L, et al. Broad Spectrum Deubiquitinase Inhibition Induces Both Apoptosis and Ferroptosis in Cancer Cells. Front Oncol. 2020;10:949.

177. Yang Y, Luo M, Zhang K, Zhang J, Gao T, Connell DO, et al. Nedd4 ubiquitylates VDAC2/3 to suppress erastin-induced ferroptosis in melanoma. Nat Commun. 2020;11(1):433.

178. Hu X, Zou R, Zhang Z, Ji J, Li J, Huo XY, et al. UBE4A catalyzes NRF1 ubiquitination and facilitates DDI2-mediated NRF1 cleavage. Biochim Biophys Acta Gene Regul Mech. 2023;1866(2):194937.

Supplementary Figures

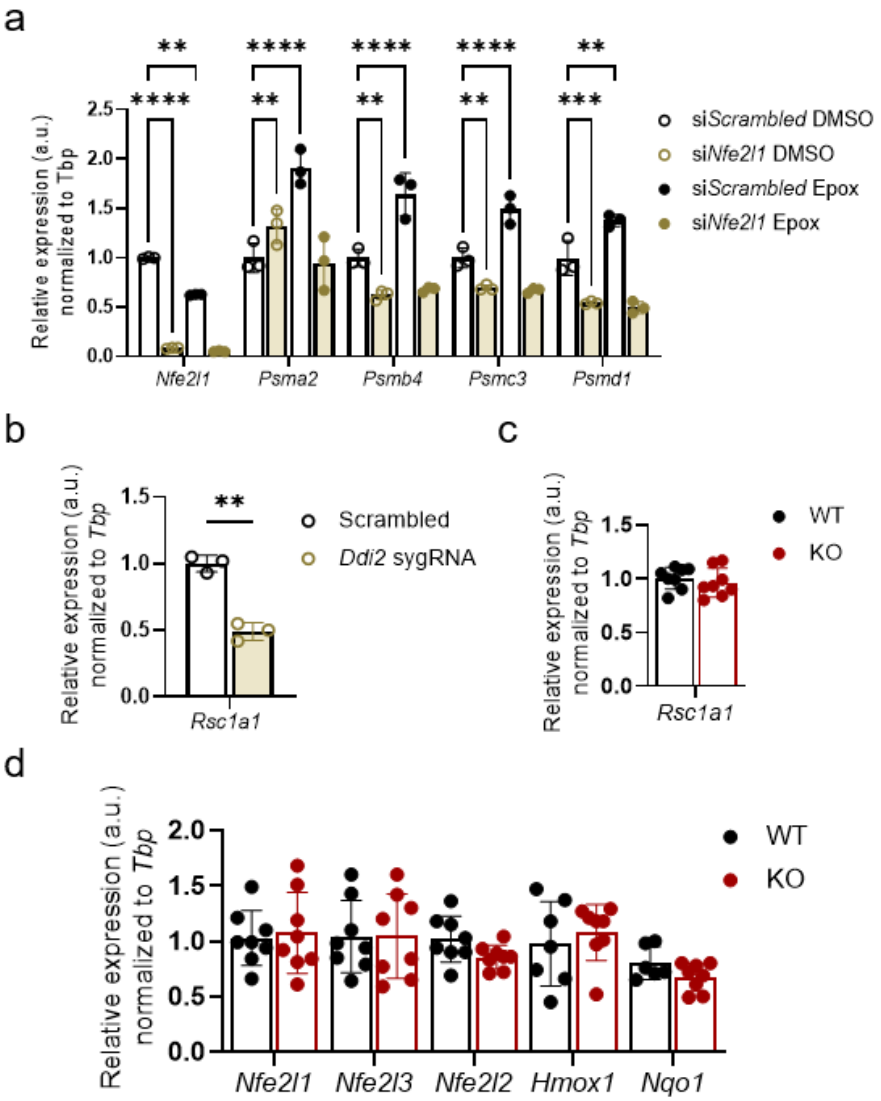

Supplementary Figure 1: Lack of Ddi2 does not activates Nfe2l1-dependent compensatory mechanisms. a) Expression of Stress marker and proteasome subunit genes after silencing of *Nfe2l1* with siRNA, followed by 100nM epoxomicin for 6h in differentiated WT-1 cells. b) Gene expression of *Rsc1a1* in differentiated WT-1 cells silenced with *Ddi2* siRNA. c) Gene expression of *Rsc1a1* in *Ddi2* KO and wild type mice. d) Gene expression in *Ddi2* KO and wild type mice. Data is presented as mean ± SD. Two-way analysis of variance (ANOVA) followed by Dunnett's multiple comparisons test was performed. *p < 0.05, **p < 0.01, ***p < 0.001 ****p < 0.0001. Thanks to Dr. Gökhan S. Hotamışlıgil, Karen Inouye, and Jilian Riveros from Sabri Ülker Center Harvard T.H. Chan School of Public Health for performing mouse experiments and providing tissue samples.

Acknowledgements

To my family.

No words can express how I feel about my PhD journey and all the great people I met and experiences I had. I would like to express my deepest gratitude to my supervisor Prof. Dr. Alexander Bartelt. Special thanks to Prof. Dr. Wolfgang Enard for his unbelievable support. Many thanks to every single member of the MLP30 that have a very special place in my heart and my memory.

Thanks to our collaborators:
Dr. Gökhan S. Hotamışlıgil, Karen Inouye, Jilian Riveros, and Mahsa Fardisi from Harvard T.H. Chan School of Public Health for kindly and professionally performing mice experiments and sending the tissue samples. Prof. Dr. Elke Krüger and Sophie Möller from Greifswald University and Dr. Scott Dixon from Stanford University for generously sharing cells and materials with us. Thanks to Dr. Natalie Krahmer and Daniel Haas from the Helmholtz Center for helping us with our proteomics and Ubiquitomics experiments.

Curriculum Vitae

Anahita Ofoghi

Education

Doctoral student [February 2020 - present]
Ludwig-Maximilian-University Munich (LMU), Germany
Supervisors: *Prof. Dr. Wolfgang Enard, Prof. Dr. Alexander Bartelt*
"The role of the protease Ddi2 in brown adipose tissue thermogenesis and ferroptosis"

Skills: cell RNA isolation, RT-qPCR, Immunoblotting, Immunofluorescent microscopy, FACS analysis, Maxiprep plasmid DNA purification, Mammalian cell culture, R-based Ubiquitomics analysis, Mouse handling, Indirect Calorimetry, Insulin Tolerance Test (ITT), Glucose Tolerance Test (GTT)

Master of Science (M.Sc.) [2016 - 2019]
Microbial Biotechnology, University of Science and Culture, Tehran, Iran
Supervisor: *Dr. Mahdi Behdani*, Venom and Biotherapeutics Molecules Lab, Pasteur Institute of Iran
"Cloning and expression of recombinant human T cell receptor CD3 protein"

Skills: Bacterial cloning and expression (*Ecoli, Staphylococcus aureus, Top10, BL21(DE3*) (Based on CLC Genomics Workbench), Primer design, PCR, Restriction analysis, Sequencing, Gel Electrophpresis and Gel extraction, Ni-NTA Affinity Chromatography and protein dialysis

Bachelor of Science (B.Sc.) [2010 - 2015]
Cellular and Molecular Biology, University of Tehran, Iran

Research experience

Research Assistant [December 2015- April 2018]
Supervisor: Dr. *Hamid Moghimi*, Department of Microbiology, University of Tehran, Iran

- Project-I: Anti-tumor activities of yeast exopolysaccharides
- Project-II: Engineered *Zymomonas mobilis* response to ethanol stress

Teacher Assistant in undergrad-students practical course and summer workshops: "Bacterial Transformation, Lymphocytes Cell Culture Microscopy, RNA Isolation, RT-PCR, Gel electrophoresis, Plasmid Extraction

Skills: Yeast culture medium preparation, cell counting, antioxidant/antimicrobial tests (such as MIC, DDPH, and MTT assay), Lymphocytes Cell Culture Microscopy, RNA Isolation, RT-PCR, Gel electrophoresis, Plasmid Extraction.

Activities

Co-Organizer Team Volunteer [September 2023]
European Lipoprotein Club, Evangelische Akademie in Tutzing, Germany

Volunteer biology teacher [2015-2017]
Yarigaran non-profit organization, Tehran, Iran
Biology instructor to all three high school grades, guiding and preparing them for university entrance exam over the course of two academic years

Member of Biology Students Scientific Association [2011-2013]
Department of Biological Sciences, University of Tehran, Tehran, Iran

Miscellaneous

Languages:

- Persian (Farsi): Native
- English: Advanced Proficiency

IELTS Score: Overall: 7 (Listening: 9, Reading: 7, Writing: 6 and Speaking: 6.5)
GRE General: Verbal Reasoning: 144, Quantitative Reasoning: 152, Analytical Writing: 2.5

- German: Elementary Proficiency (B1 level)

Softwares: MS Office, Excel, GraphPad Prism, R programming language (elementary)

Certificate: LAS – Laboratory animal science

Publications

Ofoghi A, Kotschi S, Lemmer I, Haas D, Willemsen N, Bayer B, Möller S, Haberecht-Müller S, Krüger E, Krahmer N, Bartelt A. *Activating the NFE2L1-ubiquitin-proteasome system by DDI2 protects from ferroptosis*. Under revision. Available on BioRxiv, https://doi.org/10.1101/2023.07.04.547652

Kotschi S, Jung A, Willemsen N, ***Ofoghi A***, Proneth B, Conrad M, Bartelt A. *NFE2L1-mediated proteasome function protects from ferroptosis*. Mol Metab. 2022 Mar; 57: 101436

Conference presentations (Talks)

- Annual Meeting of SPP 2306 Ferroptosis: From Molecular Basics to Clinical Applications, Dresden, Germany [November 2022]
  Title: “Adapting the ubiquitin-proteasome system by the protease DDI2 enhances ferroptosis protection”
- Annual Meeting of the European Lipoprotein Club, Tutzing, Germany [September 2022]
  Title: “Regulation of thermogenic capacity by posttranslational processing of NFE2L1 in adipocytes”
- EMBO Susan Lindquist School on Proteostasis (Flash talk) [December 2021]
  Title: “The role of Ddi2 in Posttranslational regulation of Nfe2l1 in adipocytes during non-shivering thermogenesis”

Conference presentations (Posters)

- Annual Meeting of the Society for Free Radical Research - Europe, "From Molecules to Tissues: Redox Biology in Action", Istanbul, Turkey [June 2024]
  Title: “Activating the NFE2L1-ubiquitin-proteasome system by DDI2 protects from ferroptosis” ***Anahita Ofoghi***, Stefan Kotschi, Imke Lemmer, Daniel Haas, Nienke Willemsen , Batoul Bayer, Sophie Möller, Stefanie Haberecht-Müller, Elke Krüger, Natalie Krahmer & Alexander Bartelt

- Brown and Beige Fat, organ crosstalk, signaling and energetics, Hamburg, Germany [May 2023]
  Title: “Posttranslational regulation of Nfe2l1 controls the ubiquitin-proteasome system in adipocytes during non-shivering thermogenesis” ***Anahita Ofoghi***, Stefan Kotschi, Imke Sajjad Khani, Alexander Bartelt
- Workshop São Paulo/Bavaria in Metabolism and Bioenergetics, Ribeirão Preto-SP, Brazil [May 2023]
  Title: “Posttranslational regulation of Nfe2l1 controls the ubiquitin-proteasome system in adipocytes during non-shivering thermogenesis” ***Anahita Ofoghi***, Stefan Kotschi, Sajjad Khani, Alexander Bartelt
- EMBO Workshop, Ferroptosis: When metabolism meets cell death, Seeon, Germany [April 2023]
  Title: “Activating the NFE2L1-ubiquitin-proteasome system by DDI2 protects from ferroptosis” ***Anahita Ofoghi***, Stefan Kotschi, Sajjad Khani, Alexander Bartelt
- Ubiquitin Biology and Targeted Protein Degradation, Vancouver, BC, Canada [November 2022]
  Title: “Calibrating the ubiquitin-proteasome system by the protease DDI2 enhances ferroptosis protection” ***Anahita Ofoghi***, Stefan Kotschi, Nienke Willemsen, Sophie Möller, Elke Krüger & Alexander Bartelt
- Iron, Reactive Oxygen Species and Ferroptosis Awaji Yumebutai conference center, Hyogo, Japan [Oct 2022]
  Title: “Adapting the ubiquitin-proteasome system by the protease DDI2 enhances ferroptosis protection” ***Anahita Ofoghi***, Stefan Kotschi, Nienke Willemsen, Sophie Möller, Elke Krüger & Alexander Bartelt
- Understanding Ubiquitylation: From Molecular Mechanisms to Diseases [Würzburg, Germany [May 2022]
  Title: “Posttranslational regulation of Nfe2l1 controls the ubiquitin-proteasome system in adipocyte” ***Anahita Ofoghi***, Stefan Kotschi, Sajjad Khani, Alexander Bartelt
- XXII Lipid Meeting Conference (Virtual) Leipzig, Germany [December 2021]
  Title: “Cold-induced protease Ddi2 is a novel regulator of adipocyte thermogenesis and lipogenesis” ***Anahita Ofoghi***, Stefan Kotschi, Sajjad Khani, Alexander Bartelt

Eigenständigkeitserklärung

Hiermit versichere ich an Eides statt, dass die vorliegende Dissertation mit dem Titel

The role of the protease Ddi2 in brown adipose tissue thermogenesis and ferroptosis

von mir selbstständig verfasst wurde und dass keine anderen als die angegebenen Quellen und Hilfsmittel benutzt wurden. Die Stellen der Arbeit, die anderen Werken dem Wortlaut oder dem Sinne nach entnommen sind, wurden in jedem Fall unter Angabe der Quellen (einschließlich des World Wide Web und anderer elektronischer Text- und Datensammlungen) kenntlich gemacht. Weiterhin wurden alle Teile der Arbeit, die mit Hilfe von Werkzeugen der künstlichen Intelligenz de novo generiert wurden, durch Fußnote/Anmerkung an den entsprechenden Stellen kenntlich gemacht und die verwendeten Werkzeuge der künstlichen Intelligenz gelistet. Die genutzten Prompts befinden sich im Anhang. Diese Erklärung gilt für alle in der Arbeit enthaltenen Texte, Graphiken, Zeichnungen, Kartenskizzen und bildliche Darstellungen.

München 23.04.2025

(Ort / Datum)

ANAHITA OFOGHI — (Vor und Nachname in Druckbuchstaben)

ANAHITA OFOGHI — (Unterschrift)

Affidavit

Herewith I certify under oath that I wrote the accompanying Dissertation myself.

Title: The role of the protease Ddi2 in brown adipose tissue thermogenesis and ferroptosis

In the thesis no other sources and aids have been used than those indicated. The passages of the thesis that are taken in wording or meaning from other sources have been marked with an indication of the sources (including the World Wide Web and other electronic text and data collections). Furthermore, all parts of the thesis that were de novo generated with the help of artificial intelligence tools were identified by footnotes/annotations at the appropriate places and the artificial intelligence tools used were listed. The prompts used were listed in the appendix. This statement applies to all text, graphics, drawings, sketch maps, and pictorial representations contained in the Work.

München 23.04.2025

(Location/date)

ANAHITA OFOGHI — (First and last name in block letters)

ANAHITA OFOGHI — (Signature)